AD-A111 663 JAYCOR ALEXANDRIA VA F/G 20/7
ION DIODE RESEARCH ON THE AURORA ACCELERATOR.(U)
JAN 82 R A MEGER N00014-81-C-2093
UNCLASSIFIED JAYCOR-J207-82-001FR NL

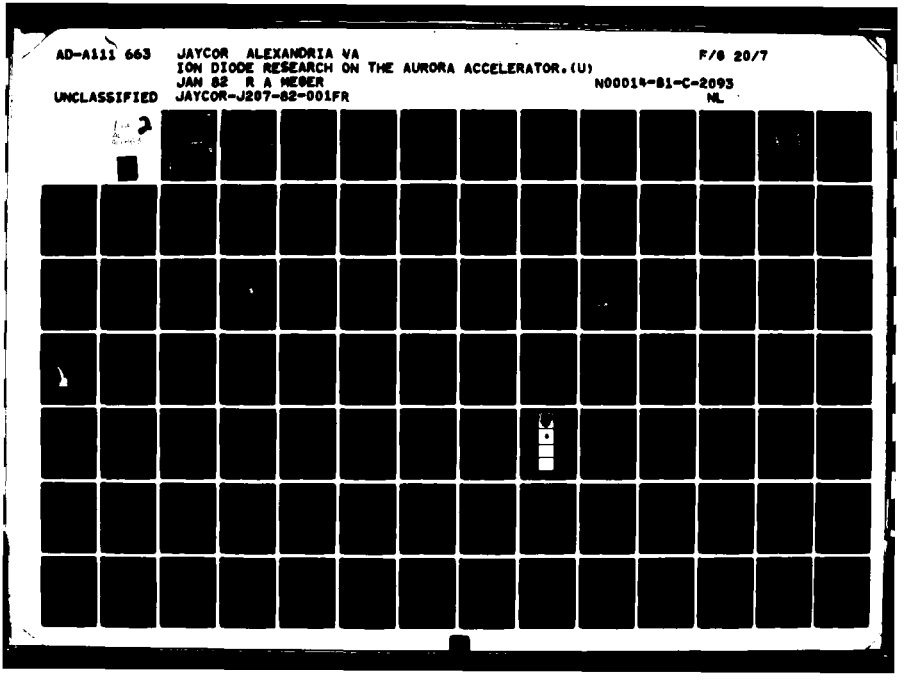

JAYCOR

205 South Whiting Street
Alexandria, Virginia 22304

(12)

ION DIODE RESEARCH ON THE AURORA ACCELERATOR

JAYCOR REPORT J207-82-001FR

FINAL REPORT

Robert A. Meger

Submitted to

Naval Research Laboratory
Washington, DC 20375

Under

Contract N00014-81-C-2093

January 1982

UNCLASSIFIED

SECURITY CLASSIFICATION OF THIS PAGE (When Data Entered)

REPORT DOCUMENTATION PAGE		READ INSTRUCTIONS BEFORE COMPLETING FORM
1. REPORT NUMBER J207-82-001FR	2. GOVT ACCESSION NO.	3. RECIPIENT'S CATALOG NUMBER
4. TITLE (and Subtitle) ION DIODE RESEARCH ON THE AURORA ACCELERATOR		5. TYPE OF REPORT & PERIOD COVERED Final Report 1/5/81 - 1/5/82
		6. PERFORMING ORG. REPORT NUMBER J207-82-001FR
7. AUTHOR(s) Robert A. Meger		8. CONTRACT OR GRANT NUMBER(s) N00014-81-C-2093
9. PERFORMING ORGANIZATION NAME AND ADDRESS JAYCOR 205 South Whiting Street Alexandria, VA 22314		10. PROGRAM ELEMENT, PROJECT, TASK AREA & WORK UNIT NUMBERS
11. CONTROLLING OFFICE NAME AND ADDRESS Naval Research Laboratory 4555 Overlook Avenue, SW Washington, DC 20375		12. REPORT DATE January 27, 1982 13. NUMBER OF PAGES 168
14. MONITORING AGENCY NAME & ADDRESS(if different from Controlling Office) Naval Research Laboratory 4555 Overlook Avenue, SW Washington, DC 20375		15. SECURITY CLASS. (of this report) UNCLASSIFIED 15a. DECLASSIFICATION/DOWNGRADING SCHEDULE

16. DISTRIBUTION STATEMENT (of this Report)

3 - Scientific Officer
1 - Administrative Contracting Officer
6 - Director, Naval Research Laboratory, Code 2627, Washington, DC
12 - Defense Technical Information, Bldg. 5, Cameron Station, Alexandria, VA

17. DISTRIBUTION STATEMENT (of the abstract entered in Block 20, if different from Report)

18. SUPPLEMENTARY NOTES

19. KEY WORDS (Continue on reverse side if necessary and ... ...eck number)

20. ABSTRACT (Continue on reverse side if necessary and identify by block number)

DD FORM 1 JAN 73 1473 EDITION OF 1 NOV 65 IS OBSOLETE
S/N 0102-LF-014-6601

UNCLASSIFIED
SECURITY CLASSIFICATION OF THIS PAGE (When Data Entered)

CONTENTS

Page

I. INTRODUCTION. 1

II. THEORETICAL SUPPORT 4

III. EXPERIMENTAL SUPPORT 8
1. Introduction. 8
2. Negative polarity results 9
3. Positive polarity results 9
4. Modified Aurora Ion Diode results 14

APPENDIX I High Impedance Ion Diode Experiment at Aurora

APPENDIX II Pinch-Reflex-Diode Scaling on the Aurora Pulser

APPENDIX III Modified Aurora Ion-Diode Experiments

APPENDIX IV The Use of Finite J_θ for Increasing the Ion Efficiency of High Impedance Diodes

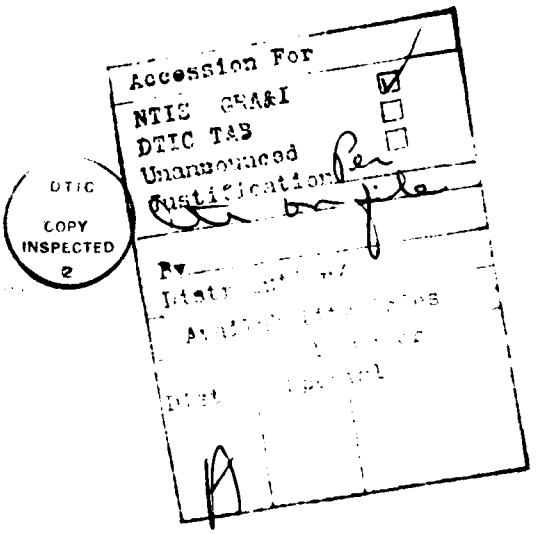

I. INTRODUCTION

Within the last few years interest in ion beams for inertial confinement fusion (ICF) applications has increased significantly. The Naval Research Laboratory (NRL), with support from JAYCOR, has been in the forefront of that research effort. The ion source which NRL has concentrated on is known as the pinch relfex diode (PRD). This type of ion diode was originated at NRL with JAYCOR assistance and is presently one of the few designs with application to ICF.

The PRD, shown schematically in Fig. 1, is comprised of a hollow cylindrical cathode of radius R separated from a plasma anode by a diode gap D. When a voltage is placed across the gap, electrons emitted from the cathode are accelerated toward the anode while being pinched toward the axis by their own magnetic field. The anode is normally made of a disk of thin dielectric material connected to a conducting backplate by a small conducting cylinder on axis. Electrons hitting the anode pass through and are reflexed back into the diode gap by the magnetic field from the current driven in the central button. Electrons undergo the combined reflexing and pinching motion until they are collected by the central button. Ions from the plasma formed on the front surface of the dielectric anode due to electron heating or flashover mechanisms are accelerated across the diode gap toward the cathode. The relative ion and electron current densities depend on the difference in crossing times of the two charge species. For diode voltages in the 1 - 10 MV range the ions move in nearly straight line trajectories at nonrelativistic velocities while the electrons are quickly accelerated to near the speed of light. The ions travel slowly but have only the diode gap, D, to cross while the electrons move at nearly the speed of light but must pinch to

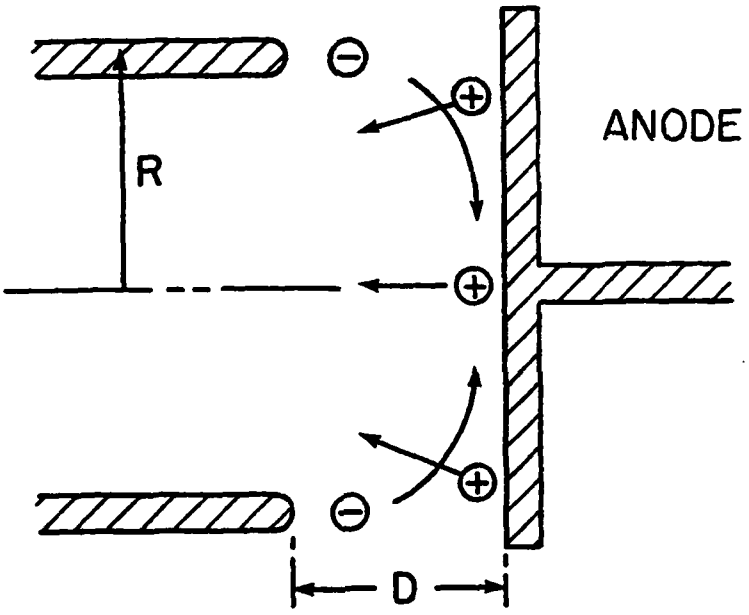

Figure 1. Schematic of a pinch reflex diode.

the axis before they are collected. Thus the longer path length of the electrons increases their time in the diode thereby enhancing the relative ion current. The ion generation efficiency ($\eta_i \equiv I_i/(I_e + I_i)$ where I_i and I_e are the ion and electron currents) will scale as R/D to first order. At the same time it has been shown that the diode impedance of such a pinched beam diode scales inversely with R/D, thus one would expect low impedance diodes to produce higher ion efficiencies.

Experiments on NRL's GAMBLE II generator have demonstrated the expected inverse scaling of ion efficiency with diode impedance. Diodes with 1.3 ohm impedance and 1.3 MV have produced 60% efficient ion beams while 4 ohm diodes have produced 40% efficient ion beams at 1.7 MV. To test this scaling further a higher impedance accelerator was necessary to drive > 4 ohm diodes at significant (~1TW) power levels.

The use of the Aurora accelerator at Harry Diamond Laboratories provided such an opportunity. This four-armed accelerator is normally a 35-ohm Bremsstrahlung producing weapons-effects simulator with up to 4 TW/arm delivered to the diode. An ion diode was designed by NRL, with JAYCOR support, to investigate the operation of PRD's in the 5-35 ohm range on this device. This experiment began in 1979 and has progressed through three distinct phases. JAYCOR has contributed to all aspects of this research effort from the outset including computer modeling of the experiment, design of apparatus and diagnostics, operation of the experiment and analysis of the data. This report summarizes the effort with emphasis on JAYCOR contributions over the contract reporting period.

II. THEORETICAL SUPPORT

Previous theoretical work on the application of Pinch Reflex Diodes (PRD) to high impedance accelerators suggested that significant ion generation efficiencies could be obtained. This work suggested a mechanism whereby small aspect ratio (ratio of cathode radius/diode gap) diodes could produce ion beams at up to 20% efficiencies when the diode current exceeded the Alfvén current (I_A = 17,000 $\beta\gamma$ amp where β and γ are the relativistic velocity and energy respectively). This mechanism results from the complicated trajectories that the electrons follow due to the self-pinching magnetic forces, the gradient drifts in the self-magnetic fields and the accelerating electric field which combine to lengthen the electron transit time across the diode gap. The Alfvén current represents the diode current level where the effect becomes significant. A more detailed diode simulation was performed by NRL for the negative polarity configuration used in the original diode experiments on Aurora. This work is reported in Appendix I, Section II. More recently in an effort to extend this work a new simulation was performed by JAYCOR in a positive polarity configuration. This work is discussed in detail in Appendix IV. The actual Aurora diode dimensions were used with a 5 MV voltage, 5 cm cathode radius and a 3.3 cm diode gap. The NRL DIODE2D code was used with 10^4 macro electron and ion particles in the simulation region. Electrons and ions were emitted from their respective electrodes according to local equilibrium with the fields in the diode. The code was run until an equilibrium condition was obtained. The results agreed well with the previous negative polarity simulation.

The simulation showed the diode to operate at 5 MV and 21 ohms with a total of 238 kA diode current and an ion efficiency of η_i = 0.235. Sample positions of electrons and ions in the diode at equilibrium are shown in Fig.

2 and Fig. 3 respectively. Figure 2 shows the positions of sample electrons at a given time after equilibriuim has been reached. Note that they show a pinching in toward the axis as well as fillng in the region inside the cathode. Very few electrons are on the opposite side of the anode. Figure 3 shows a similar snapshot of sample ions after equilibrium has been reached. The ions are being generated across the entire anode and are being accelerated inwards toward the axis. Figure 4 shows the radial ion current profile in the plane of the tip of the cathode. Note that the current density near the axis is ≥ 10 kA/cm^2 and is peaked on axis. The highly peaked current density on axis indicates some radial focusing of the ion beam.

This simulation was used as the benchmark for an effort to improve ion diode efficiency as presented in Appendix IV which was not covered by this contract.

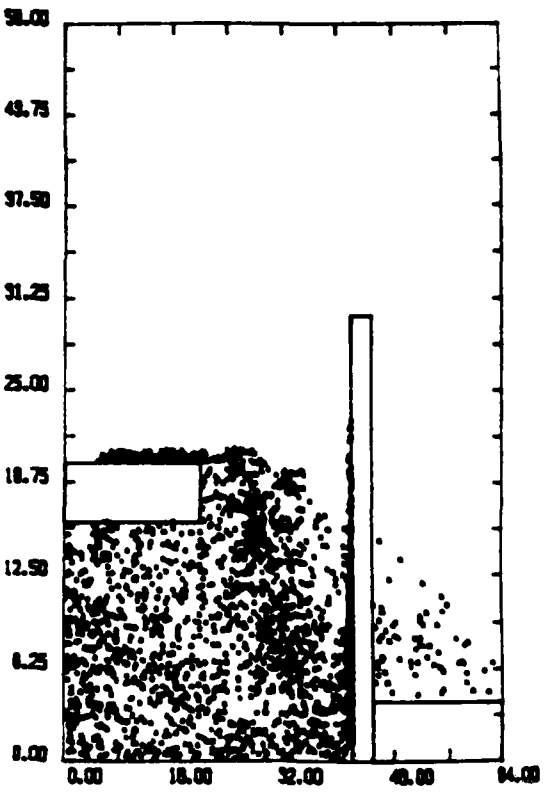

Figure 2. Sample electron positions at equilibrium for the Aurora diode simulation.

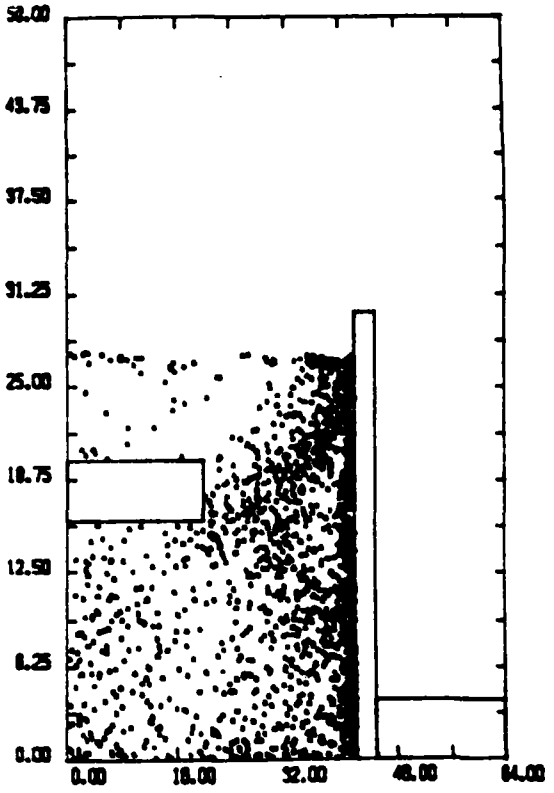

Figure 3. Sample ion positions at equilibrium for the Aurora diode simulation.

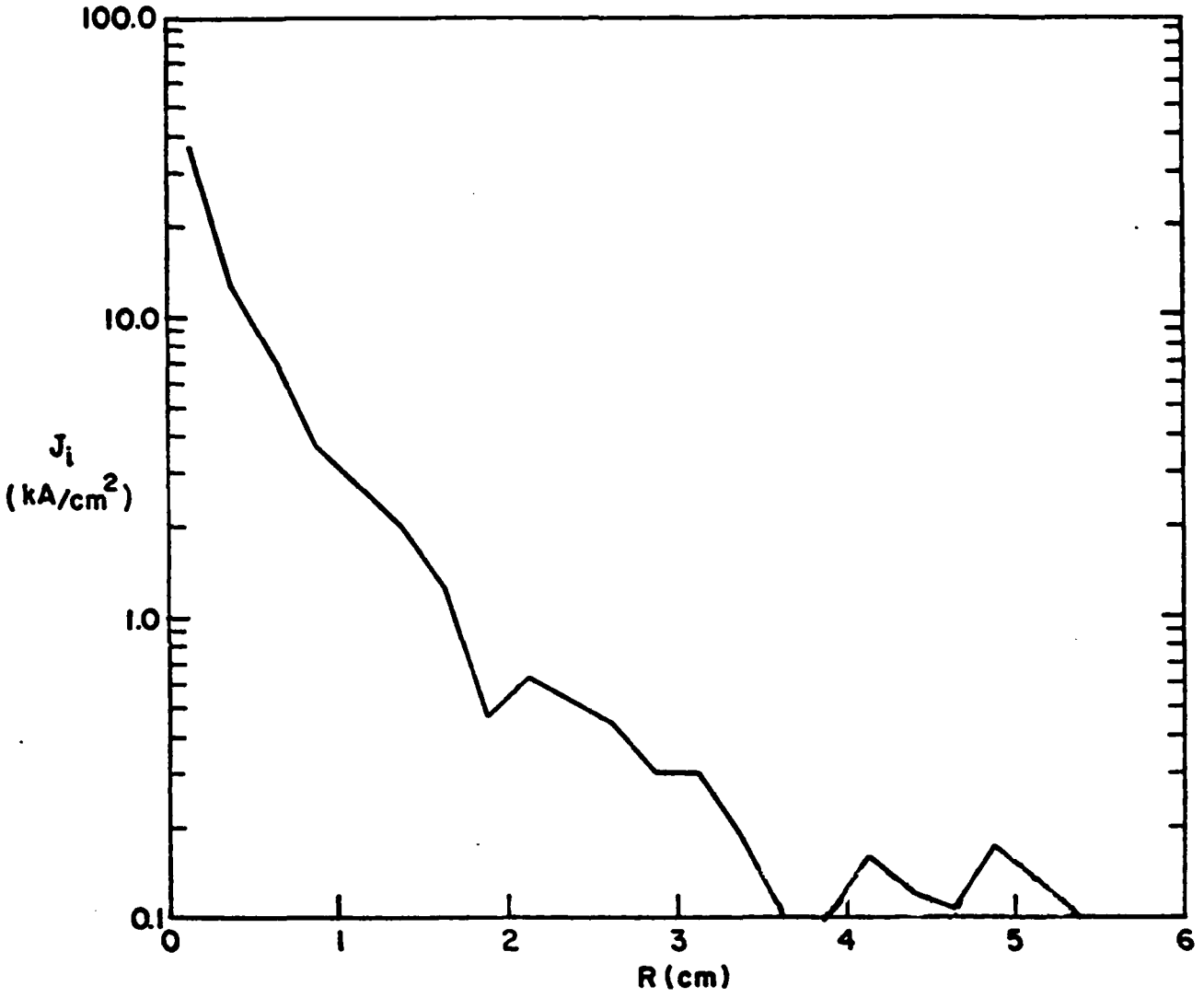

Figure 4. Ion current density at the plane of the cathode tip for the Aurora diode simulation.

III. EXPERIMENTAL RESEARCH

1. Introduction

The Aurora experimental program to date has spanned three different experimental configurations, each distinct from and embodying the knowldge gained from its predecessor. The first stage was carried out prior to the present contract and involved experiments on the Aurora pulse in negative polarity (the machine's normal polarity). The second stage involved reversing the machine polarity to allow direct access to the ion beam. This necessitated changes in redesigning the hardware and diagnostics. During this stage Plasma Erosion Switches (PES) were first introduced into the system to help control the machine prepulse. This contract spans the later efforts of the second state and the initial effort on the third stage. Stage 3 has produced the most radical changes to the diode and accelerator. In this stage the actual accelerator hardware was modified to increase power delivery in positive polarity to the ion diode. New diagnostics, including an inductive isolator for direct access to the high voltage end of the acclerator, were designed and installed. A new PES system was fielded and preliminary experiments have been performed. Several technical reports detailing the results of these experiments have been included as appendices to this report. Appendix I deals with background information and the original negative polarity experiments. Apendix II gives the results of the positive polarity work, a large fraction of which was performed under this contract. Appendix III deals with the Modified Aurora Ion Diode (MAID) experiment and presents the first results from the third stage of the experiment.

The principle results from the latter two stages of the experiment will be synopsized herein.

2. Negative Polarity Results.

The original negative polarity experiments produced the first experimental evidence that small-aspect-ratio (R/D) PRD's operate as predicted by computer simulations. Ion beams comprised of up to 5 x 10^{16} protons with energies of $\sim$ 5 Mev and 150 μsec pulse duration were generated. The ion efficiency was about 20% as predicted. All ion diagnostics were all indirect due to lack of access to the ion beam in negative polarity. Nuclear techniques including neutron detection and nuclear activation measurements were used to diagnose the ion beam. The experiments also showed that the accelerator prepulse caused diodes with less than 4 cm gaps to short out prematurely. This pointed out the need for suppressing the accelerator prepulse. More details are included in Appendix I.

3. Positive Polarity Diode Results

Inmmediately following the negative polarity experiments the machine polarity was reversed by the Harry Diamond Laboratories' staff. This had never been done previously. Testing with a high impedance Bremsstrahlung load at a reduced charging voltage was successful. The ion diode hardware was redesigned with the plasma producing anode foil on the high voltage inner conductor. Ions could then be extracted through the hollow cathode at ground potential. The polarity reversal made direct measuring ion current probes possible. These probes in conjunction with the previously used nuclear diagnostics gave independent and time resolved measurements of the ion beam parameters.

Initial experiments concentrated on varying the diode gap and observing the effects on impedance and ion generation efficiency. Diode gaps from 1.5 cm to 5.5 cm were used. Figures 5 and 6 show the peak ion current as measured

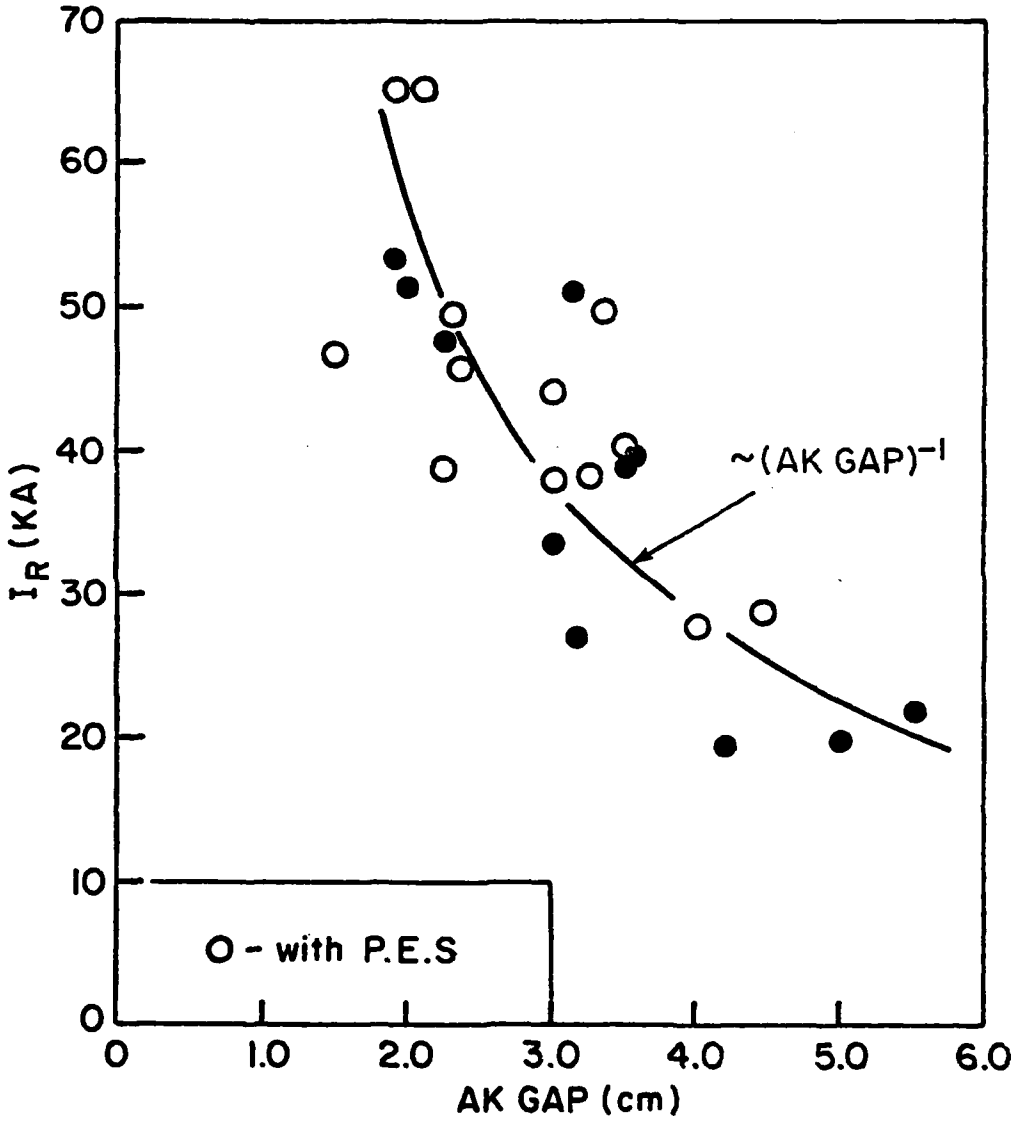

Figure 5. Peak ion current, I_R, measured for positive polarity shots on Aurora versus diode AK gap.

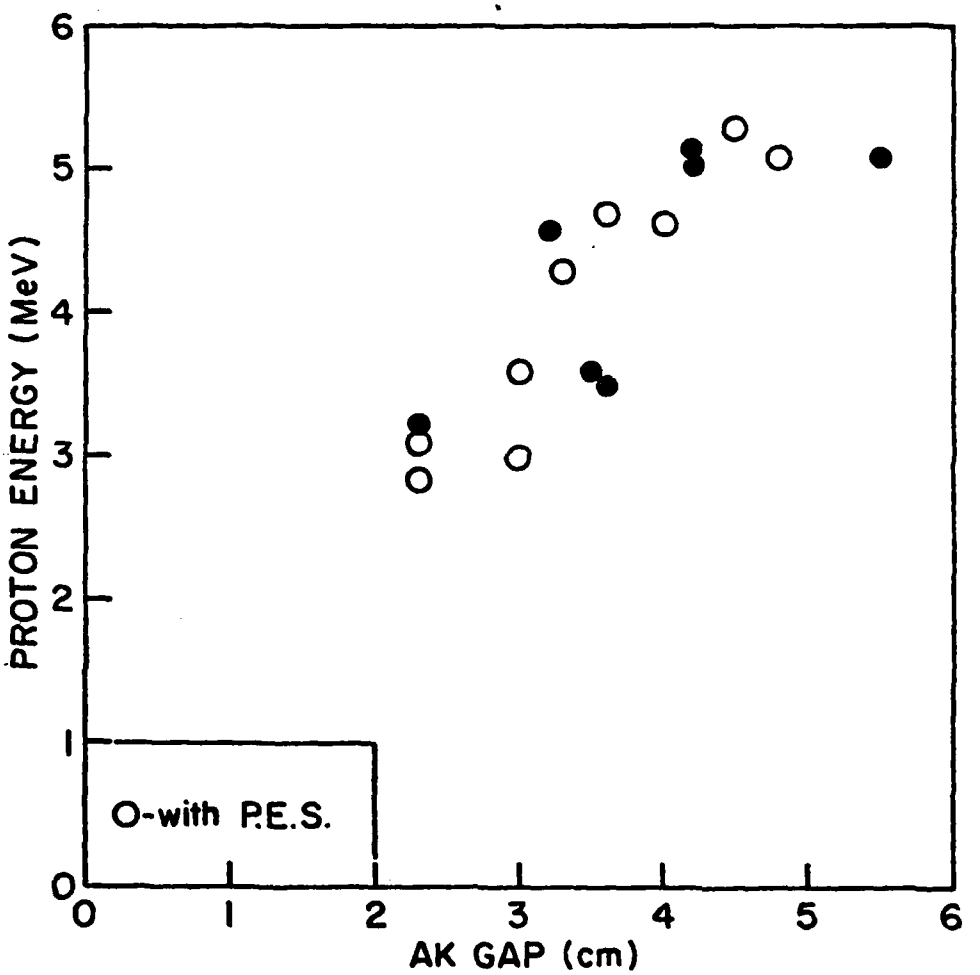

Figure 6. Average proton energies for positive polarity shots on Aurora versus the diode AK gap as measured by neutron-time-of-flight.

by a Rogowski coil and the ion voltage as measured by neutron-time-of-flight. At small diode gaps the voltage dropped toward the 2 MeV threshold for the neutron measurements and the ion current reached a peak of ~65 kA. The ion generation efficiency was ~20% over the entire range of parameters. A simple theory which is detailed in Appendix II suggests that the ion current should scale as $(\gamma + 1)^{1/2}$ R/D where γ is the electron relativistic factor, R is the cathode radius and D is the diode gap. Figure 7 shows this scaling at the peak value of the ion current. The inverse dependence on diode gap is consistent with the scaling.

In an attempt to minimize prepulse effects the data shown in Figs. 5, 6 and 7 was taken with and without the PES system turned on. This system consisted of three plasma guns mounted 30 cm upstream of the anode. Each gun injected a plasma column with density in the 10^{11} - 10^{12} cm^{-3} range radially between the outer and inner conductors of the vacuum feedline. The plasma guns are fired several microseconds before the beam arrives in order to allow the plasma which has a directed velocity ~10 cm/μs to flow from the guns into the coaxial region and short the inner and outer conductors. After a significant amount of charge is transmitted through the switches, the plasma columns would open up, suddenly switching the voltage onto the diode load. In this experiment the prepulse and some fraction of the rise of the main pulse were diverted through the plasma columns thereby shielding the ion diode from premature plasma formation on the anode or cathode. The open circles in Figs. 5, 6 and 7 were taken with the PES system turned on. On each shot the plasma was adjusted to erode only the leading edge of the main pulse. Figure 6 shows how the diode gap is affected by the prepulse. If each of the solid points were moved to the left by ~1 cm they would fall on the curve for shots with the PES. This could be accounted for by a gap closure of ~1 cm making the

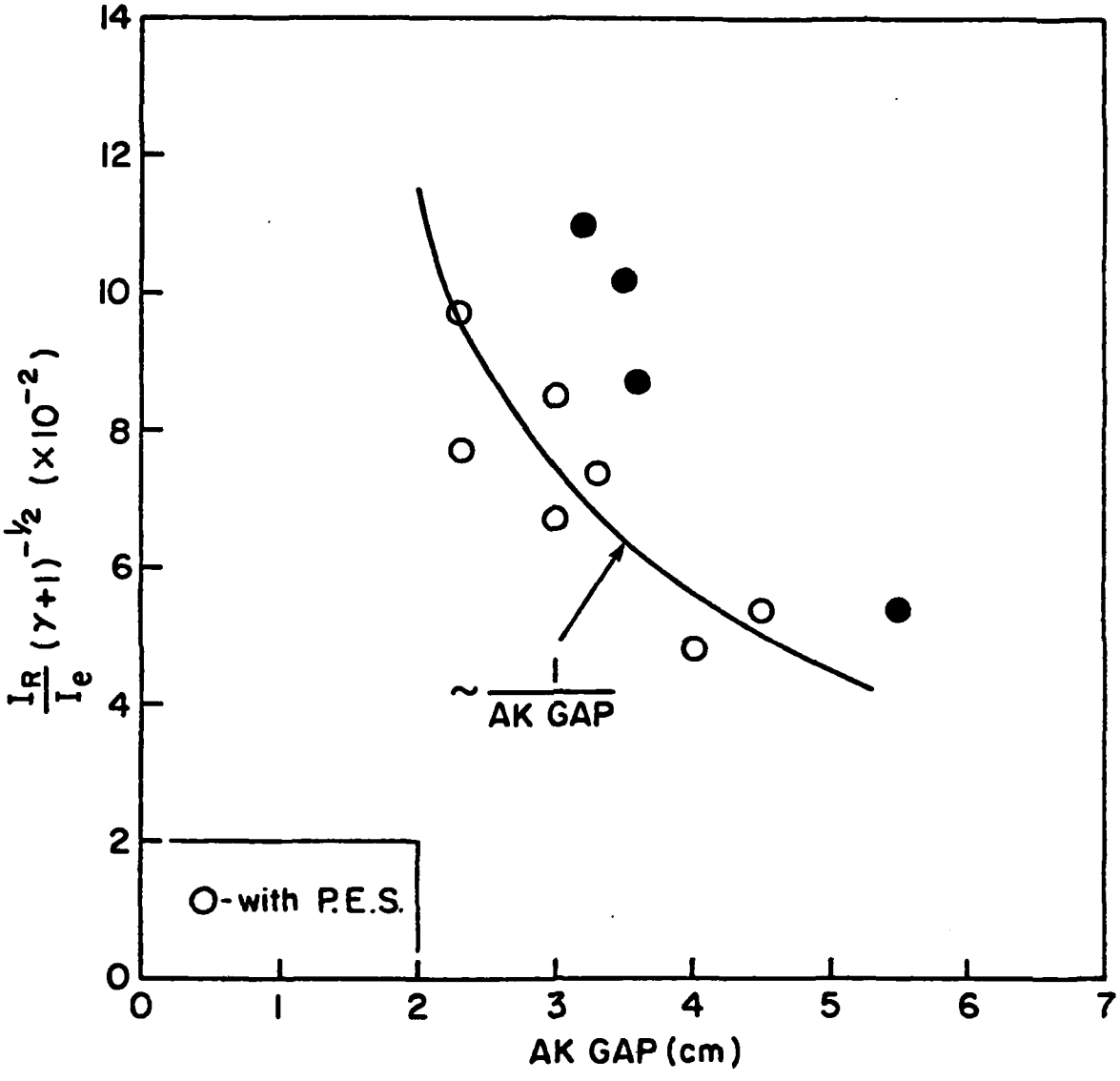

Figure 7. Peak ion current scaling as a function of diode AK gap.

effective gap on these shots smaller than the physical gap.

The diode produced ions with ion efficiency $\eta_i \sim 20\%$ over a wide range of diode gaps. This flat ion efficiency dependence was in part the result of the impedance mismatch between the ion diode and the accelerator. At small gaps the ion diode impedance dropped to < 10 ohms which lowered the accelerator voltage due to poor coupling with the 50 ohm accelerator driving impedance. Thus the voltage dependence and the R/D scaling in the ion efficiency approximately cancelled one another giving the $\sim 20\%$ efficiency over the entire range. The scaling shown in Fig. 7 implies that the diode operated as expected from PRD theory.

Another effect was observed dealing with the operation in positive polarity. The accelerator insulator appeared to flash over early in time when high voltages were placed across the insulator stack, thereby shorting the pulse measurably. This is believed to be due to the insulator design which was not built to withstand positive polarity voltage pulses.

4. Modified Aurora Ion Diode Results

The positive polarity experiments indicated the need for improved power flow into the ion diode. In order to accomplish this a 5 meter long section of magnetically insulated transmission line was removed and new diode hardware was designed and mounted near the insulator stack. This change was designed to reduce the voltage across the insulator stack and to improve power coupling to the ion diode load. Appendix III details the changes made in the experimental hardware. While modifying the diode region an inductive isolator was also installed in the oil behind the insulator stack. This permitted access for voltage and current diagnostics on the inner conductor near the ion diode. The ion diode hardware was significantly altered to mate to the new

accelerator output as shown in Fig. 8. The ion diode was mounted in a large diameter region making the power feed nearly radial in the vicinity of the diode. The PES's were mounted axially rather than radially, injecting their plasma onto the end of the center conductor. The cathode and anode hardware was designed to be modular for rapid turn around between shots. The diode was designed for maximum diagnostic access to both the anode and cathode regions.

The early data taken with this apparatus showed the expected improvement in power flow into the diode. Peak ion currents of 44 kA were measured with energies of 6 MeV. This represents a 50% increase in ion beam power over the previous positive polarity results. The ion efficiency remained at 20% for this 4 cm diode gap shot. The peak power delivered to the ion diode increased from 1 to 1.5 TW with the new configuration and pulse widths were observed to increase to $\sim$150 ns versus $\sim$110 ns for similar diode gap shots in the old configuration.

The new diode hardware also produced a higher voltage prepulse across the diode gap. This is partially due to better coupling of the accelerator to the load and to the lack of a flash over prepulse suppressor in the new configuration. Previous positive and negative polarity experiments had a series of flash over insulators on the inner conductor which capacitatively decreased the prepulse from a 200 kV peak down to about a 50 kV peak. Beam diagnostics on the inner conductor prohibit introduction of such a prepulse suppressor on the new diode. The prepulse may have affected the symmetry of the beam forcing the pinch to wander off axis on a shot to shot basis. The PES system was designed to counter this problem by again diverting the prepulse but as yet has been unable to force the beam to center properly. The prepulse may be producing an asymmetric flash over in the insulator stack which in turn affects the symmetry of power flow in the diode. Future experiments

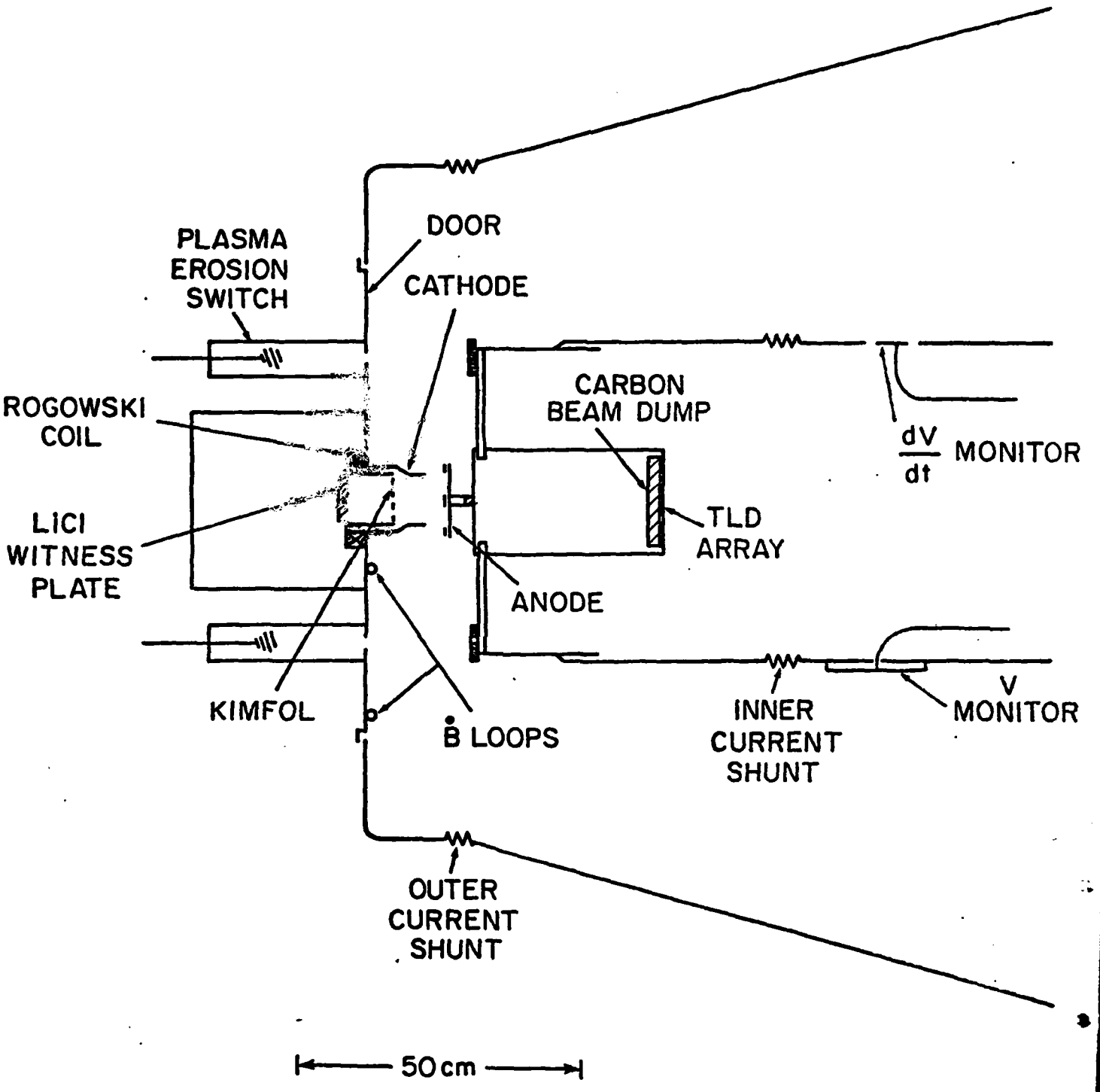

Figure 8. The Modified Aurora Ion Diode hardware.

are planned to lower the prepulse within the accelerator and to smooth the power flow in the insulator stack region.

APPENDIX I

HIGH IMPEDANCE ION DIODE EXPERIMENT ON AURORA

R. A. Meger*, F. C. Young, A. T. Drobot**,
G. Cooperstein, Shyke A. Goldstein*, and
D. Mosher

Plasma Technology Branch
Plasma Physics Division

S. E. Graybill, G. A. Huttlin, K. G. Kerris, and A. G. Stewart

Harry Diamond Laboratories
Adelphi, MD 20783

NRL Memorandum Report 4477

March 19, 1981

*JAYCOR
Alexandria, VA 22304

**Science Applications, Inc.
McLean, VA 22102

This research was sponsored in part by the Defense Nuclear Agency under Subtask T99QAXLA014, work unit 46, and work unit title "Ion Beam Generation."

CONTENTS

I. INTRODUCTION 1

II. THEORY AND SIMULATION 3

III. EXPERIMENTAL PROCEDURE 15

IV. EXPERIMENTAL RESULTS 31

V. SUMMARY OF RESULTS 56

ACKNOWLEDGMENTS 59

REFERENCES 60

I. INTRODUCTION

There is increasing interest in the development of intense light-ion beams as drivers for thermonuclear pellets in inertial-confinement-fusion (ICF) applications.[1,2] This approach requires the production of a number of intense beams of a few MeV/nucleon, focusing of each beam, then transport and overlapping of the beams onto a target with sufficient power density to ignite it. Experimental and theoretical research in these areas at the Naval Research Laboratory has been reviewed recently.[1]

The NRL studies have concentrated on the azimuthally-symmetric pinch-reflex diode for ion production. This diode uses the self-fields of the charged-particle flow to enhance ion production and aid in focusing. This diode operates most efficiently with a large aspect ratio (cathode radius/anode-cathode gap) and at low diode impedance ($Z \lesssim 2\Omega$).[3] Experiments on the 1.5-Ω NRL Gamble II generator have produced up to 700 kA of ion current at 1.3 MV with 60% ion efficiency (ion current/total current).[1] Using the 0.75-Ω line of the PITHON generator at Physics International, ion currents of 900 kA at 1.8 MV were achieved with comparable efficiency.[4,5] The high current density associated with these low-voltage, high-current ion beams puts limitations on the focusing and transport of such beams to ICF targets.[6,7]

Experiments at order-of-magnitude-higher impedance levels and at power levels comparable to Gamble II and PITHON experiments are now in progress on one line of the Harry Diamond Laboratories Aurora generator. In general, higher impedance generators are more efficient in delivering energy to the diode and can deliver higher power levels. Inductive losses in the vacuum diode are reduced. The increased stiffness of beams extracted from high-impedance diodes should improve focusability. Focused current densities required for pellet driving are reduced for higher-energy ion beams provided that the beam species is properly matched to pellet deposition requirements.

Manuscript submitted January 16, 1981.

These advantages must be weighed against theoretical predictions of lower ion production efficiencies for high impedance diodes.

The experiments described here employed a low-aspect-ratio modification of the conventional pinch-reflex diode in order to better match the high-impedance Aurora pulse-line. Computer simulation of the Aurora diode showed enhanced ion production when operating at diode currents exceeding the Alfven current. Aurora experiments have demonstrated similar enhanced ion production efficiencies ($\sim$ 25%). The ion diode was driven by a 200 nsec FWHM pulse from one of the 50-Ω vacuum transmission lines on the generator. The diode operated at $\simeq$ 5 MV and $\sim$ 200 kA ($Z \sim 25\ \Omega$). The mismatch of this ion diode to the 50-Ω driver limited the peak power to < 1.5 TW and the total diode energy to < 200 kJ. Average proton currents of 50 kA at 5 MeV were inferred from neutron activation and time-of-flight measurements using the $^{7}Li(p,n)^{7}Be$ reaction. A carbon ion component of >1% was also observed from the CH_2 foil anode. Ion imaging measurements indicated that the ion beam originated near the axis of the anode and was affected by an unknown focusing mechanism in the anode-cathode region. It was shown that the reflexing of electrons through the anode foil was not of primary importance to the enhanced ion production. The experimental results are consistent with computer simulations which indicate that the ion production is enhanced as a result of prolonged electron-lifetime in the diode due to the complicated trajectories of the electrons.

This paper will detail the theoretical simulations and experimental measurements of these ion-diode studies on the Aurora generator in negative polarity. Section II presents the results of the numerical simulations. Section III describes the experimental hardware and diagnostics.

The experimental results are presented in Section IV. Section V summarizes the experimental and theoretical studies.

II. THEORY AND SIMULATION

The high impedance diode used in the Aurora experiments exhibits an ion production efficiency much higher than the prediction from bi-polar Child-Langmuir flow. The most important aspect of the flow established in the diode is that the total current, I_{TOT}, exceeds the Alfvén current, $I_A = 17000\ \beta\gamma$, where I_A is in amps, β is the electron velocity normalized to the speed of light and γ is the relativistic factor calculated from the full diode voltage. When the total diode current exceeds the Alfvén current, the electron flow pinches in the region of the anode-cathode gap. The electrons no longer have trajectories which take them directly from the cathode to the anode; rather they appear to perform complicated figure-eight-like orbits through the diode's axis and drift across the gap due to a combination of $\bar{E}\times\bar{B}$ and $\bar{\nabla}B\times\bar{B}$ motion caused by the self-magnetic field arising from the electron and ion flow in the diode. As a result, the electron lifetime in the anode-cathode gap is enhanced. The ion production efficiency is determined by the total charge balance in the diode and the relative average lifetimes of electrons and ions in the gap. The ions travel in essentially straight lines and move more slowly than the relativistic electrons, but the longer path length of the electrons allows a larger fraction of the current than predicted by Child-Langmuir theory to be carried by the ions.

For the diode used in the Aurora experiments, it is difficult to calculate analytically the ion-generation efficiency. Therefore, numerical simulations were used to model the diode behavior. These simulations have

been carried out using the DIODEPR 2D-3V relativistic-quasistatic equilibrium code. The configuration used in the simulations is shown in Fig. 1. This figure also shows the equipotential lines in the empty diode under the assumption that the reflexing foil is a conducting surface. This geometry corresponds to a small-aspect-ratio, pinch-reflex-diode configuration. To limit the size of the simulation grid, only the region to the right of the cathode was simulated thus neglecting the effect of shank flow into the diode. The numerical model assumed a geometry close to that used in the Aurora experiments. The "reflexing foil" was modeled as an 0.175-cm thick CH_2 conducting disk acting as a space-charge-limited ion source on the cathode side. The on-axis rod and the anode support behind the foil were assumed to be perfectly absorbing surfaces for electrons. Simulations were conducted on a (64×50) R-Z mesh with $\Delta R = 0.25$ cm and $\Delta Z = 0.15$ cm. The time step was taken to be 2×10^{-12} sec, and the simulations were conducted until an average steady state was achieved. Electron emission was limited to the face of the cathode. Two simulations were completed, one at 3 MeV and another at 5 MeV, both with an anode-cathode gap of 3.3 cm.

In the simulation at 3 MeV, the steady-state diode current was calculated to be 114 kA with 14 kA of this current due to ions and the remaining 100 kA due to electrons. Of the electron current, 35 kA was absorbed by the sides of the supporting rod, while 50 kA was absorbed by the front surface of the anode at the center button where the anode foil is attached to the support rod. The remaining current was absorbed by the back plate behind the support stalk. The positions of the electrons projected on the R-Z plane are shown in Fig. 2 at time step 3000, well after a steady state has been achieved. The electron flow appears to be weakly pinched and there is evidence of some reflexing through the anode foil. The

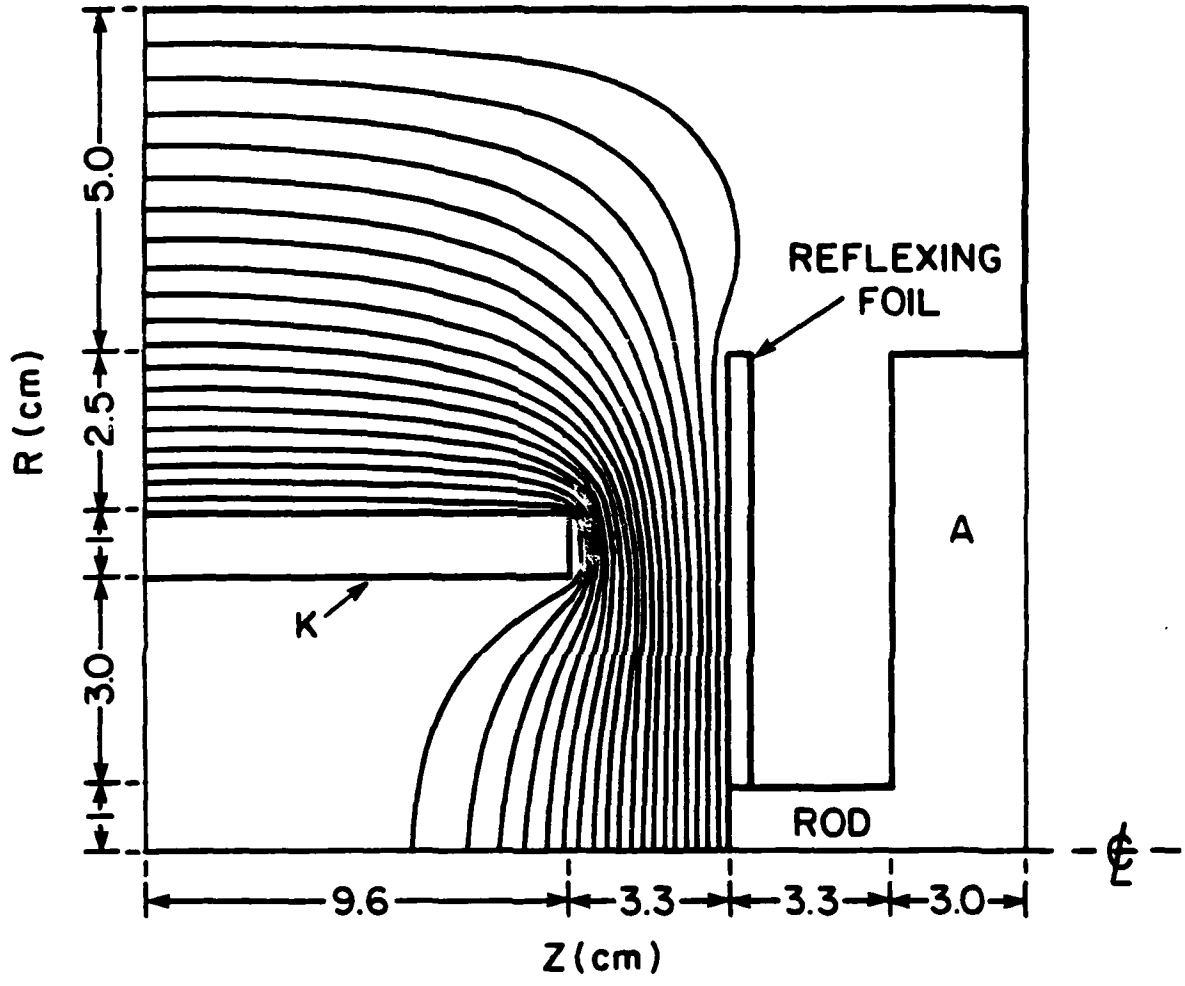

Fig. 1 — The pinch-reflex-diode geometry used for simulation of the Aurora experiments. The equipotential lines in the empty diode are shown. Only the region to the right of the hollow cathode was simulated.

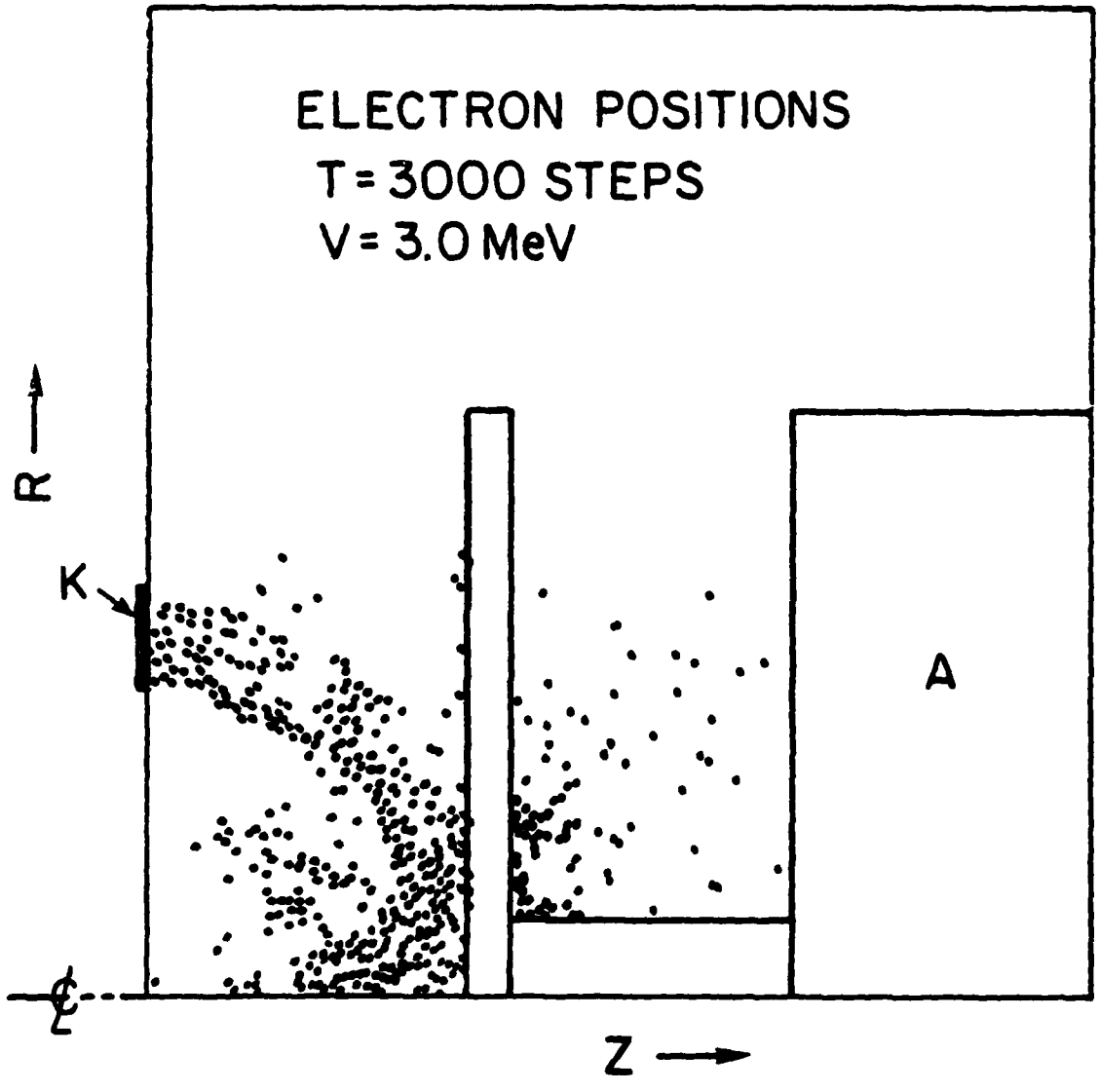

Fig. 2 — The positions of test electrons projected on the (R,Z) plane after 3000 timesteps. At this time the electron flow has reached steady state. This figure is for the 3-MeV case and shows a weak pinch of the electron flow.

corresponding ion positions appear in Fig. 3. The ion current density is peaked near the axis as can be seen from the radial profile for the ions at the cathode surface shown in Fig. 4. Within the resolution of the code, the peak ion density is $\sim$ 1 kA/cm^2. Ions arriving at the cathode face have an outward radial velocity with a maximum $v_R \sim 0.6$ cm/ns as shown in Fig. 5 compared to $v_Z \sim 2.3$ cm/ns indicating a defocusing of the ion orbits. The impedance of the diode was calculated to be 26 Ω with an ion efficiency of 12%, which is 2.5 times greater than the Child-Langmuir efficiency.

At the higher voltage of 5 MeV, the calculated ion-diode performance improves. Plots similar to those for 3 MeV show that the electron pinch is stronger at 5 MeV and that very few electrons reflex through the anode foil. The electron and ion maps are shown in Figs. 6 and 7, respectively, after 4000 time steps when the diode has achieved steady state. The electron flow appears to pinch toward the center of the anode face and very few electrons have passed through the foil. There also appears to be a sizeable electron flow in the direction of the ions which would contribute to space charge neutralization within the ion beam. The ion density on the cathode plane shown in Fig. 8 is strongly peaked on axis with a current density of at least 10 kA/cm^2 compared to 1 kA/cm^2 computed for 3-MeV operation. The total diode current for this case is 205 kA of which 40 kA is ion current and 165 kA is electron current. Of the electron current, 40 kA goes to the support rod and 125 kA to the center button. None of the electron current was absorbed by the back plate behind the anode stalk. In contrast to the 3-MeV case, this total current now exceeds the Alfvén current of 188 kA. The diode impedance of 24 Ω was not significantly different from the 3-MeV case, but the ion efficiency increased to $\sim$ 20%. The maximum radial velocity component, v_R, shown in Fig. 9, is somewhat

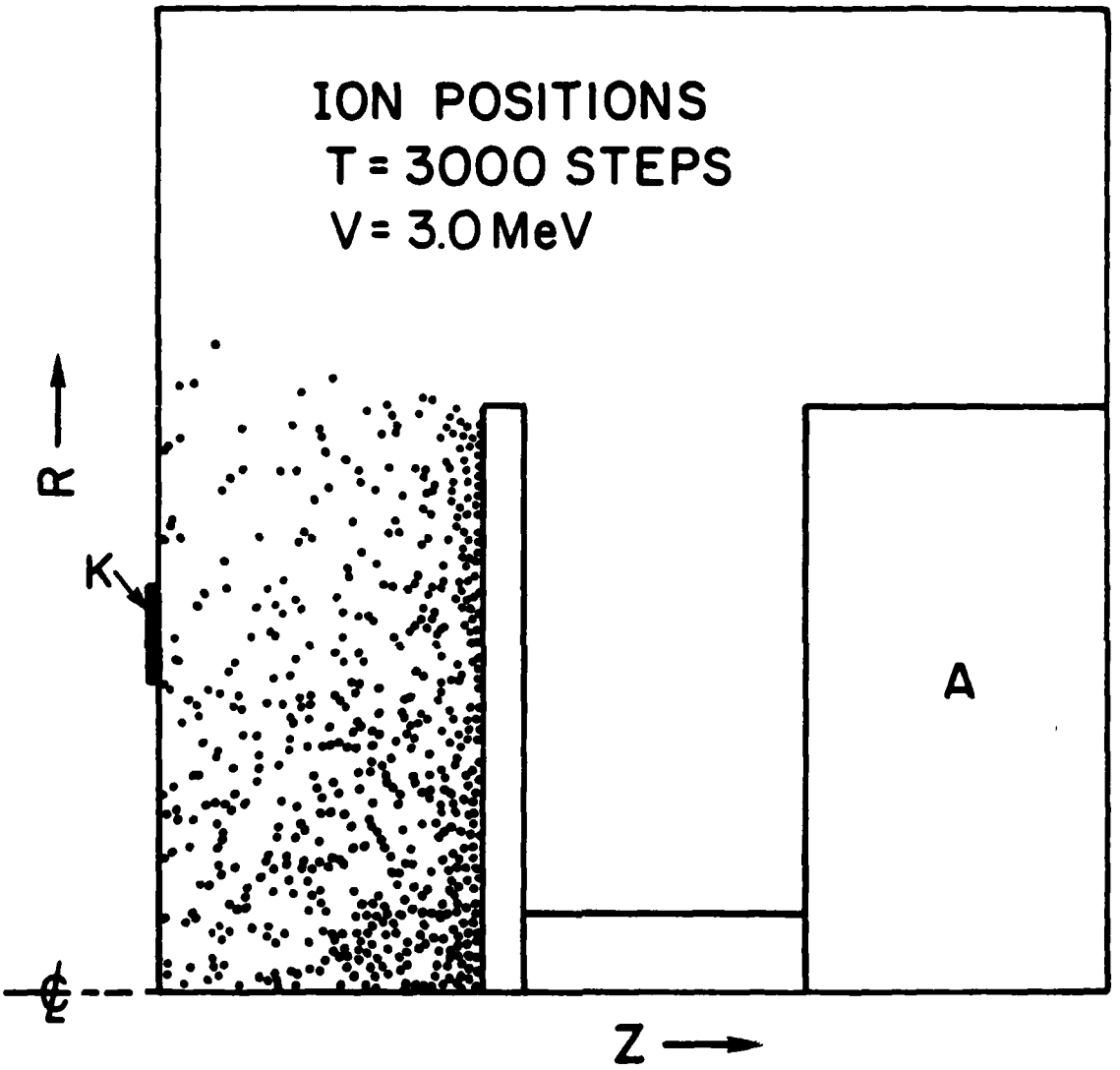

Fig. 3 — The positions of test ions projected onto the (R,Z) plane for the case shown in Fig. 2

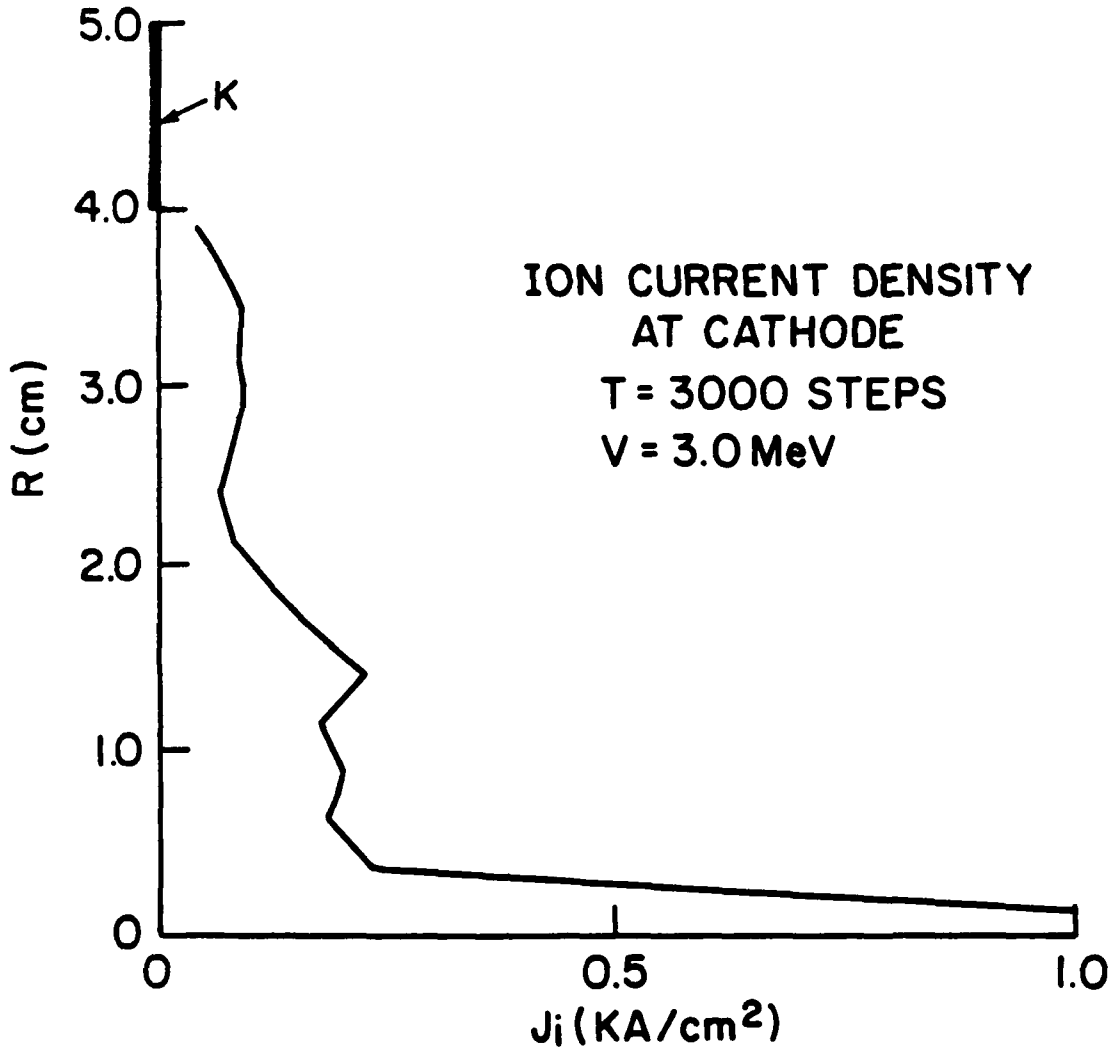

Fig. 4 — The radial profile of the ion-current density at the plane of the front surface of the cathode for the 3-MeV case

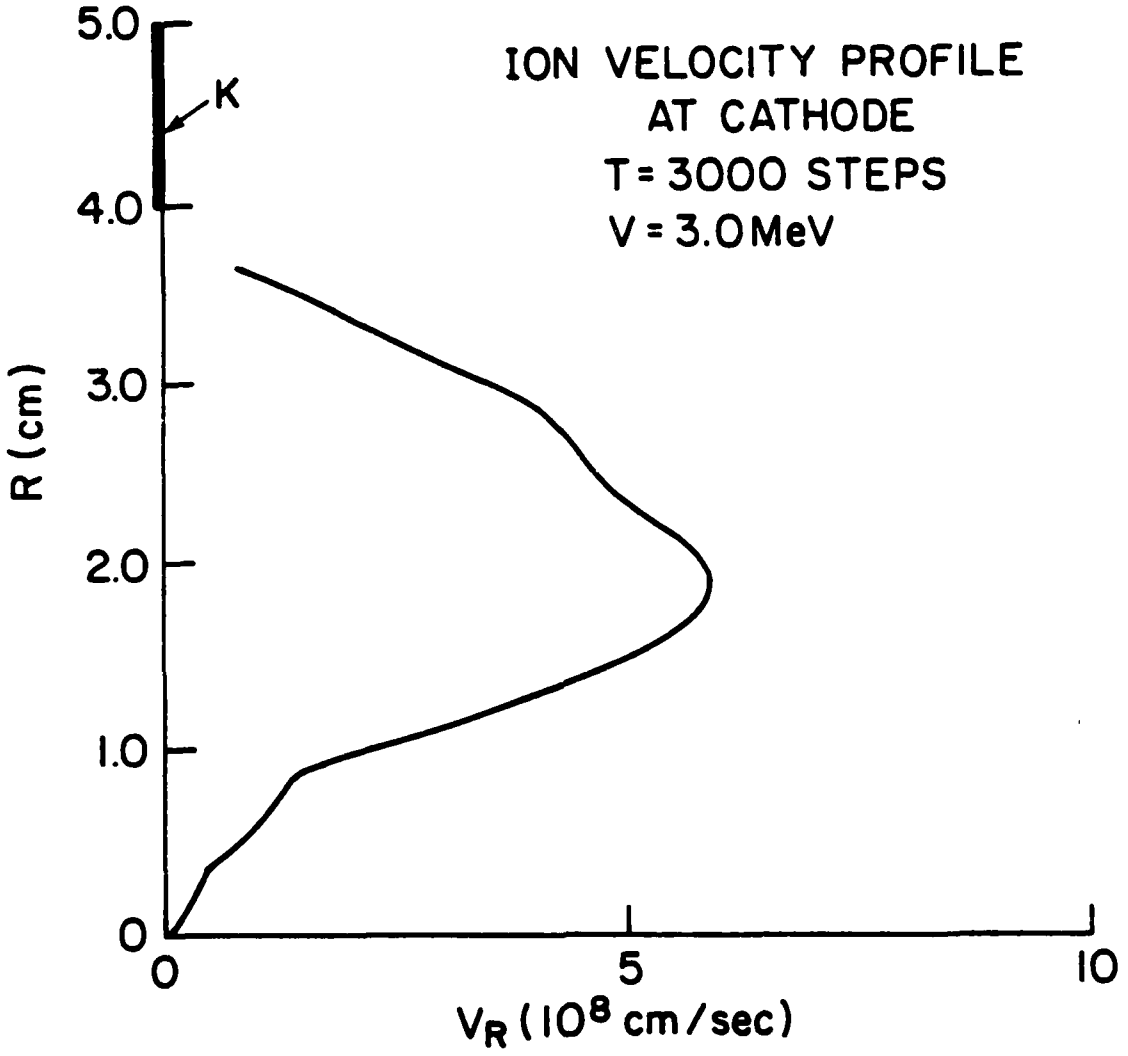

Fig. 5 — The radial velocity profile of ions at the cathode plane for the 3-MeV case

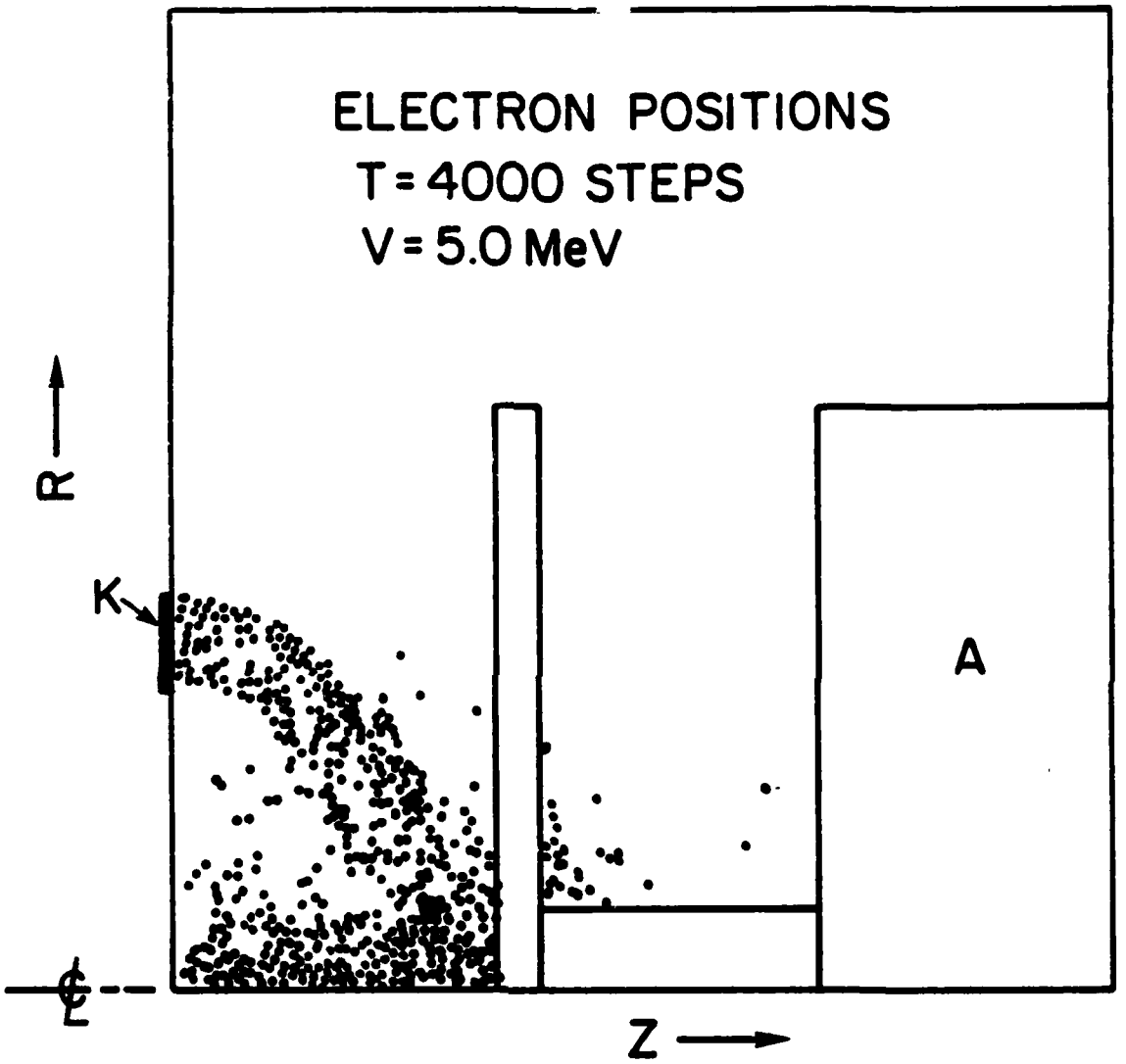

Fig. 6 — The projection of test electrons onto the (R,Z) plane for the 5-MeV case after steady state has been reached. The figure shows a focused pinch for the electrons flowing back towards the cathode plane at small radii.

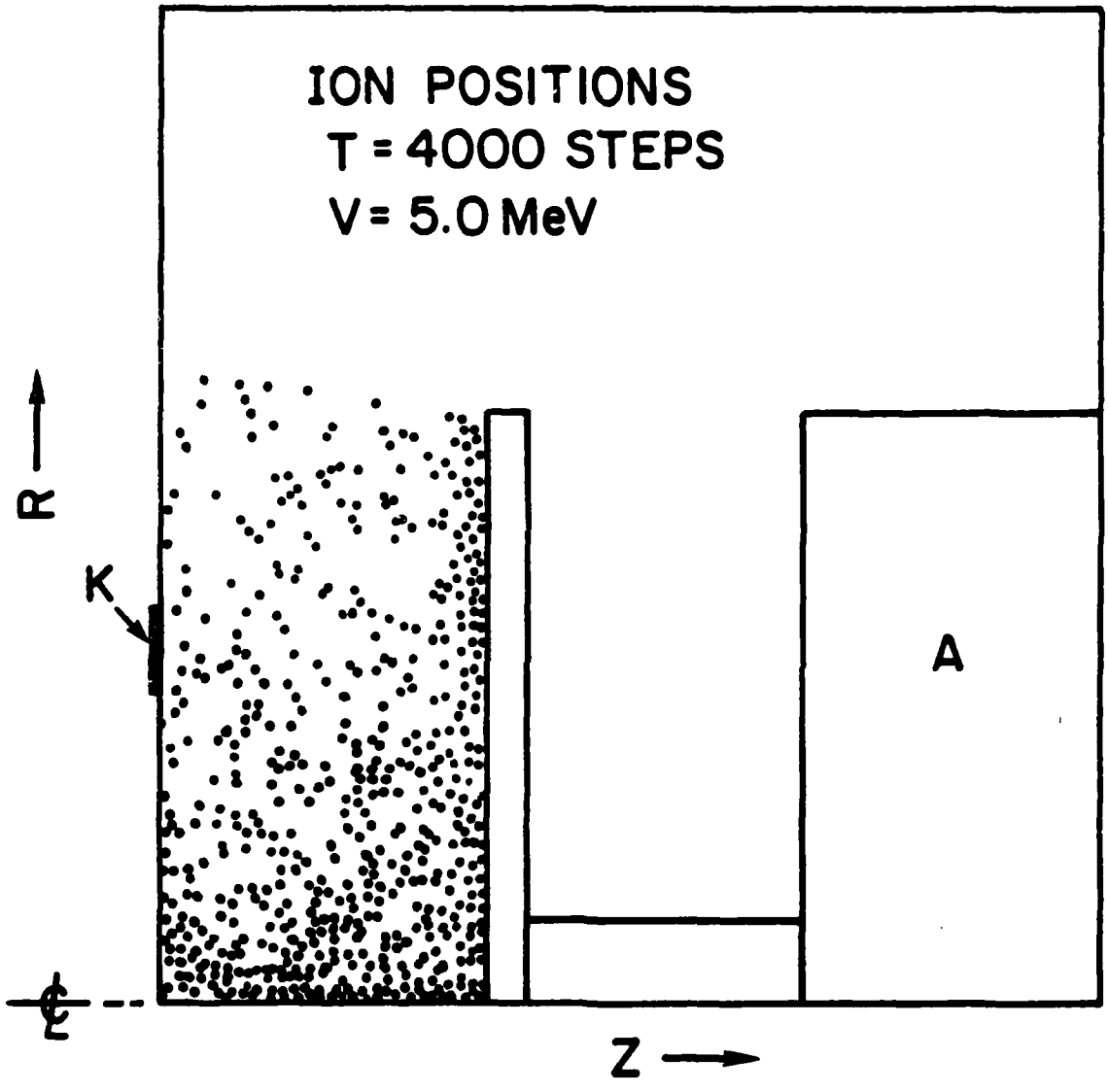

Fig. 7 — The positions of test ions projected onto the (R,Z) plane for the case shown in Fig. 6

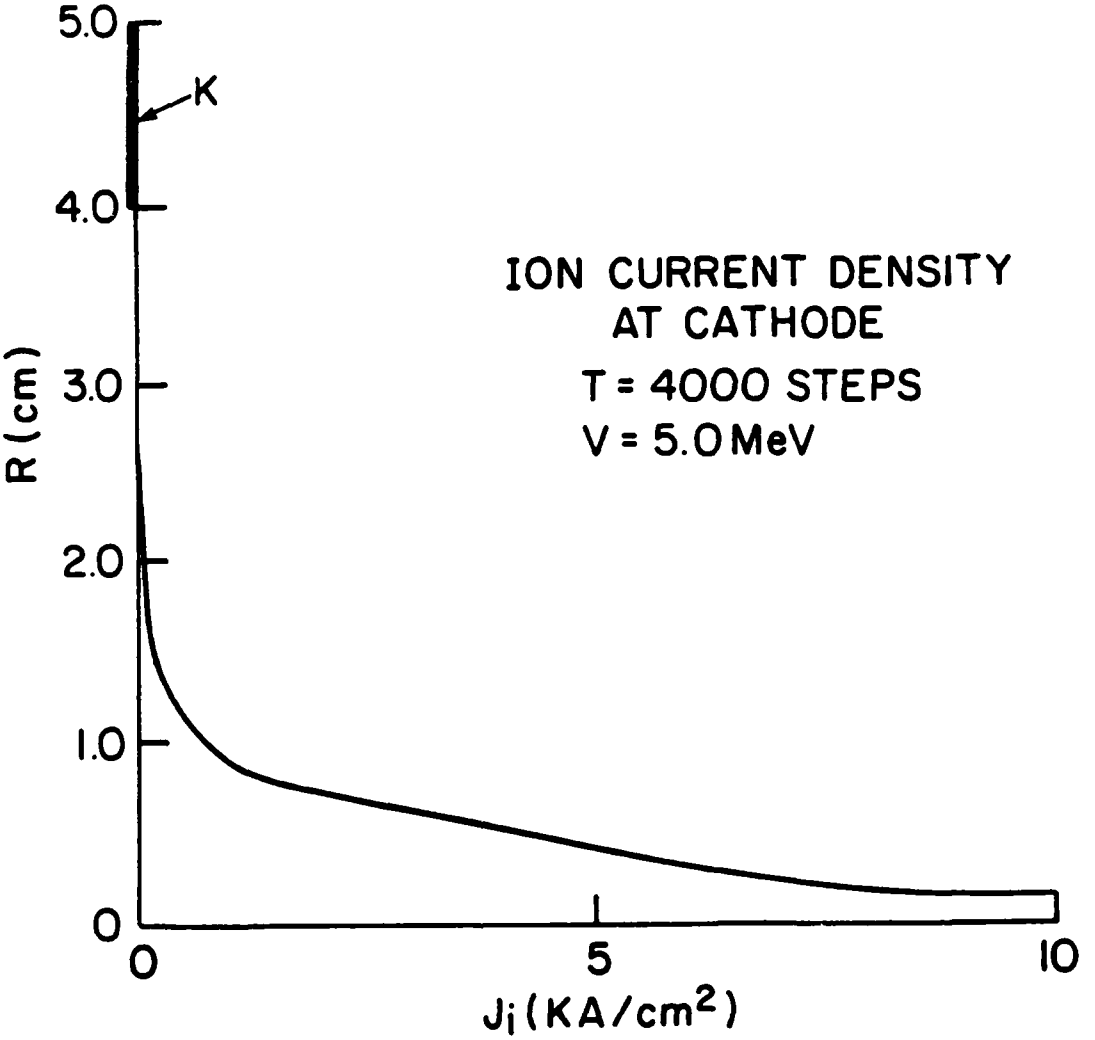

Fig. 8 — The ion-current-density profile at the cathode plane for the 5-MeV case. A strong peak on axis is observed.

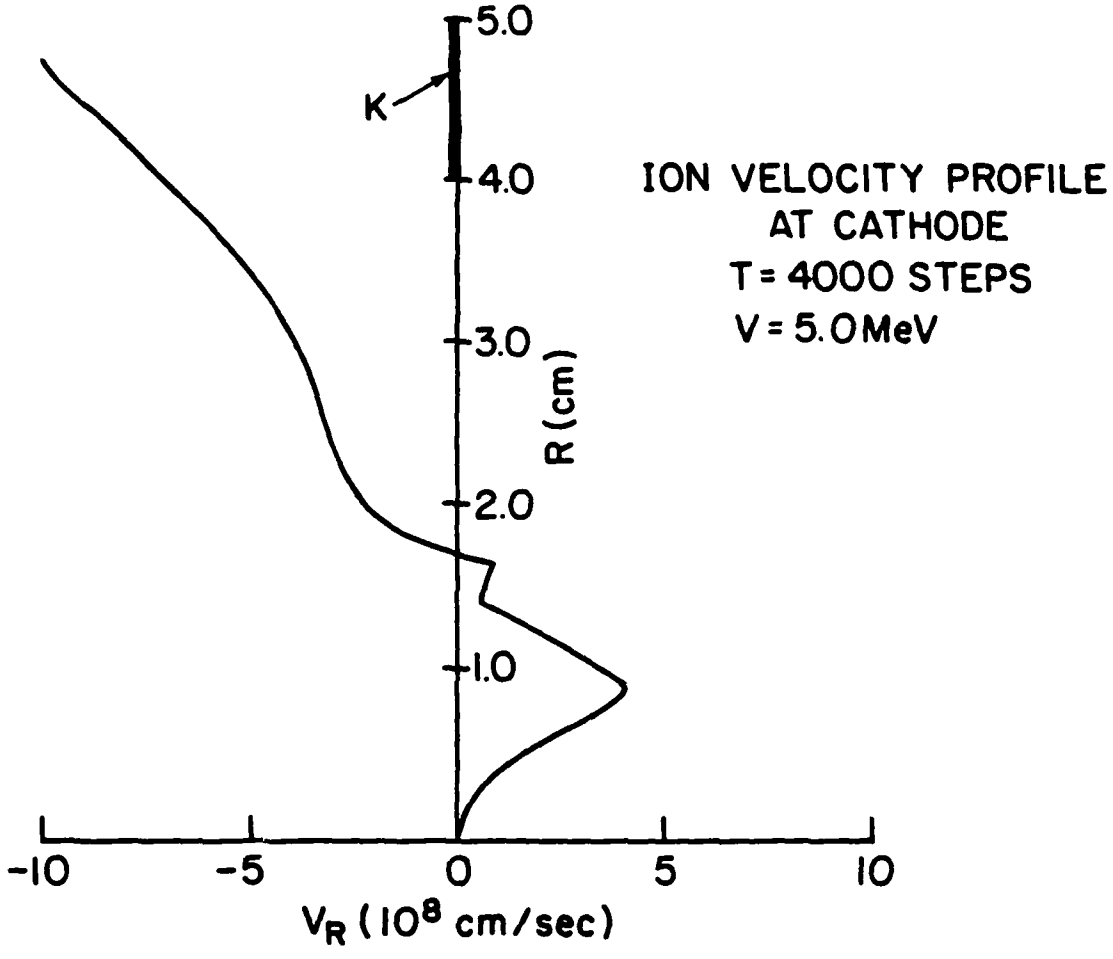

Fig. 9 — The radial velocity profile of ions at the cathode plane for the 5-MeV case. This velocity profile when compared to the 3-MeV case suggests some ion focusing is taking place in the diode. Some of the ions may even have crossed the axis.

smaller near the axis than for the 3 MeV case while the v_z component is larger due to the higher voltage ($v_z \sim 3.1$ cm/ns). Note also that the ion velocity goes negative for R >1.6 cm suggesting the outer ions are being focused.

The electron orbits for the 5-MeV-diode-voltage case are shown in Fig. 10. The pinching effect on the electrons can be seen clearly as well as the "figure-eight" like drift motion of the electrons toward the anode. Such electron motion is characteristic of the ∇B drift of primary electrons in this diode.

III. EXPERIMENTAL PROCEDURE

I. Experimental Hardware

The Aurora Simulator has been described in detail elsewhere.[9] In this experiment, a single arm of the accelerator was used with a second elbow and extension section in place to bring the beam out in the horizontal plane.[8] The Marx generator was operated in negative polarity at the 90-kV charge level, well below the maximum 120-kV charge available. The Marx charges a Blumlein pulse-forming line which is discharged through an oil prepulse switch onto the diode insulator oil-vacuum interface. The pulse is transmitted through a 10-meter long, magnetically-insulated coaxial transmission line to the ion diode. The geometric impedance of the nominal 1.2-m O.D., 0.53-m I.D. transmission line is 50 Ω. Figure 11 shows the location of voltage and current probes along the transmission line. A single resistive-divider voltage monitor was located in the oil, and three capacitive dividers were located along the line. Current measurements were made with three 7-mΩ resistive current monitors spaced along the outer coax. The resistive voltage monitor measured a peak of 10 to 11 MV for a 90-kV Marx charge while the capacitive voltage monitor (V_B) and current shunt (I_T) measured ~ 6 MV and ~ 190 kA, respectively. These values suggest that

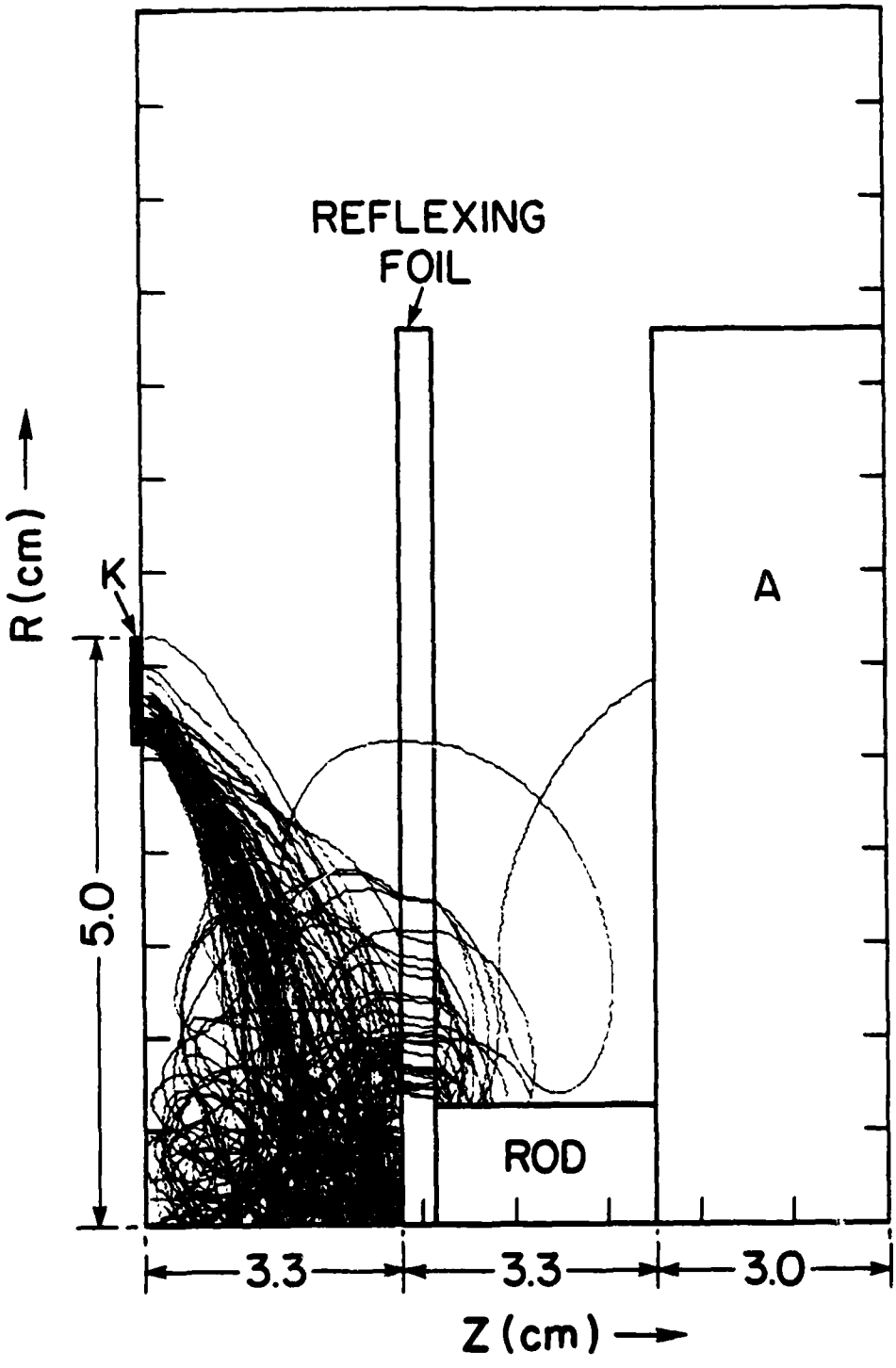

Fig. 10 — Test electron orbits for the 5-MeV case showing the complicated trajectories that are responsible for the enhanced electron lifetime. The orbits are projected onto the (R,Z) plane.

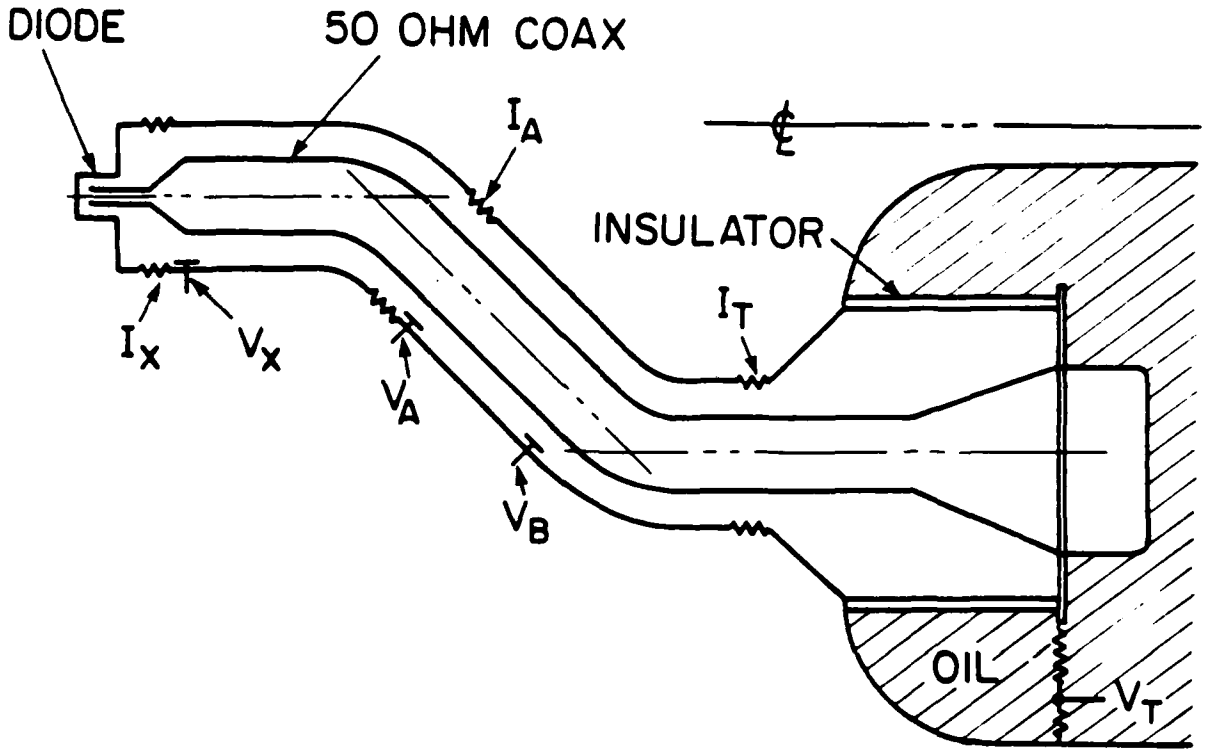

Fig. 11 — One arm of the Aurora accelerator from the oil region to the ion diode. The resistive voltage divider in the oil is shown as well as various resistive current shunts and capacitive voltage monitors in the vacuum coax.

the diode was operating somewhat below the geometric 50-Ω impedance. A prepulse of 150-200 kV peak and ~ 300 ns FWHM was measured on the vacuum coax 1.5 μsec before the main pulse.

An enlarged view of the ion diode end of the coaxial transmission line is shown in Fig. 12. The 53-cm diameter center stalk tapers to 10 cm while still in the 1.2-m diameter chamber. After a 50-cm long section, the outer conductor is reduced to 25 cm to recover the 50-Ω line impedance. A prepulse switch is located on the center stalk just downstream of the large-diameter transition as shown in Fig. 12. The switch consists of a series of acrylic insulators and field grading rings. The insulator was designed to capacitively divide the prepulse down below 50 kV depending on the number of insulators in place. The cathode was mounted on the 10-cm diameter inner stalk and was aligned with the anode mounted on an aluminum plate in the 25-cm I.D. vacuum region. A 35-cm long vacuum chamber with a carbon beam dump was located downstream of the anode.

The cathode and anode used in these experiments are illustrated in Fig. 13. The cathode consisted of a 10-cm diameter, 6-mm thick wall aluminum tube with a rounded edge. An aluminum witness plate was recessed inside the cathode. On most shots, lithium chloride (LiCl) was deposited on the witness plate to provide a neutron source through the $^{7}Li(p,n)^{7}Be$ reaction. The anode consisted of 100-μm thick polyethylene (CH_2) foil stretched between a 0.8-mm thick, 15-cm diameter aluminum ring and a 2.5-cm diameter central aluminum disk. The outer edge of the center disk and the inner edge of the ring were sharp to enhance surface breakdown of the CH_2 foil. The center disk was covered with various thicknesses of CH_2. An aluminum round-head screw clamped the anode onto a 1.9-cm diameter, 0.17-mm thick, 6-cm long aluminum tube. The entire anode was bolted onto a 1.5-mm

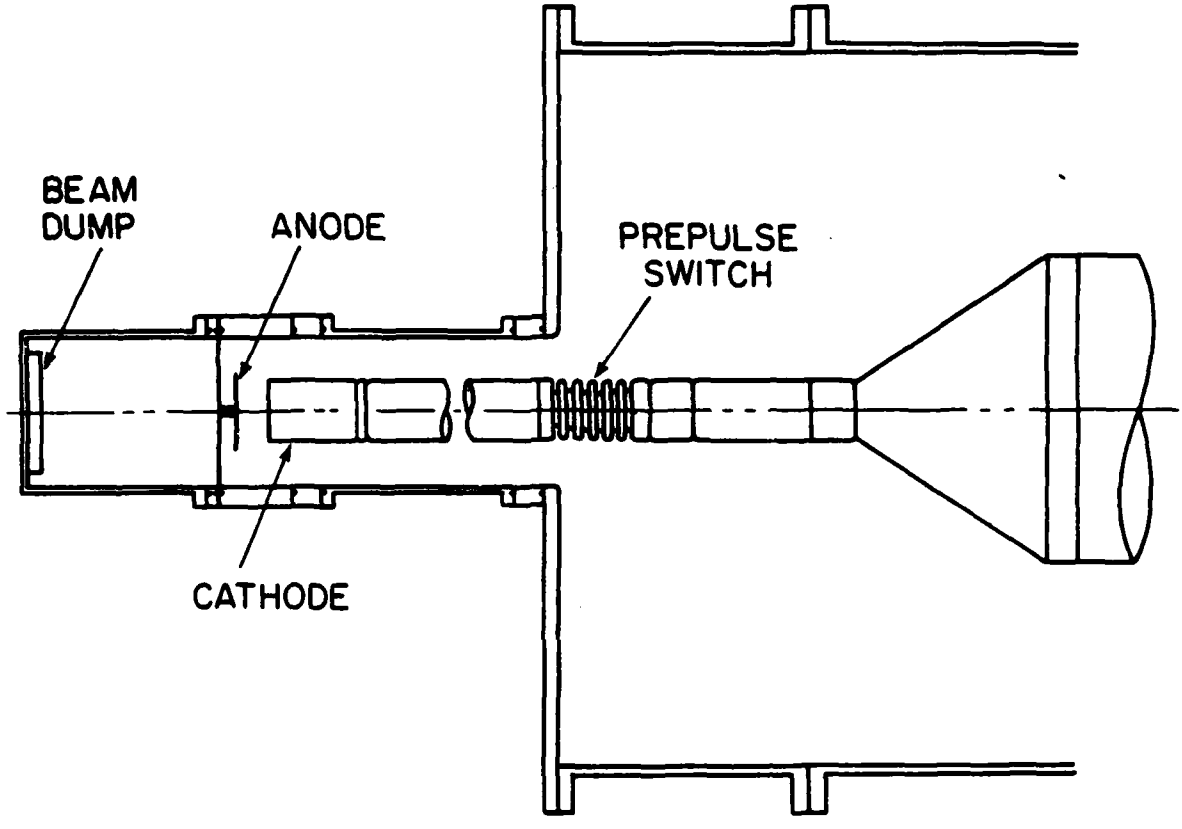

Fig. 12 — The diode end of the vacuum coax as used in the ion-diode experiments

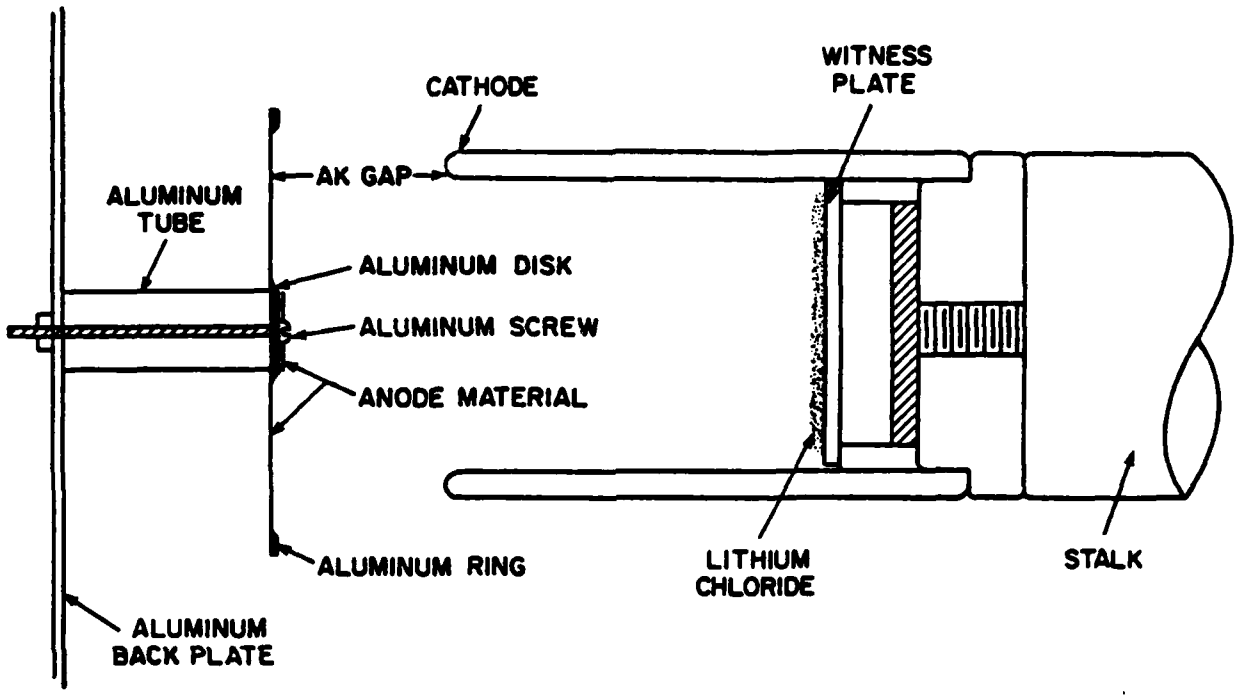

Fig. 13 — Details of the cathode and anode used in the negative-polarity, ion-diode experiments

thick aluminum plate. The anode structure was made of thin aluminum to limit debris from the shot as well as to allow many reflexes of electrons through the structure (the range of 5-MeV electrons in aluminum is 1.1 cm).

2. Diagnostics

a. X-Ray

X-ray and neutron diagnostics used in this experiment are indicated schematically in Fig. 14. Because the machine was operated in negative polarity and there was no access to the center stalk, all ion diagnostics were, of necessity, remote or delayed. X-ray diagnostics consisted of a collimated photodiode and a pinhole camera, both directed at the diode region, and TLD's placed at various locations to provide gross x-ray fluxes. The pinhole camera had a demagnification factor of 1/3.5.

b. Neutron Time of Flight

The neutron time-of-flight (TOF) technique was used to determine the proton energy in the diode. The TOF detector consisted of a 6.7-cm diameter by 5.6-cm cylindrical plastic scintillator coupled to a photomultiplier tube and mounted within a 7.6-cm thick lead shield. This detector was deployed at 10° to the anode-to-cathode axis and at 13.8 m from the LiCl target. At this angle the proton energy for the $^{7}Li(p,n)^{7}Be$ reaction is a sensitive function of the neutron energy as shown in Fig. 15. Also, in this figure is shown the dependence of proton energy on neutron flight time, which is the quantity directly measured by the TOF technique. The neutron energies are small enough so that the TOF signal is well separated from the bremsstrahlung signal. For 5-MeV protons, the neutron energy is about 3 MeV and the flight time is $\sim$ 0.5 μsec. The bremsstrahlung

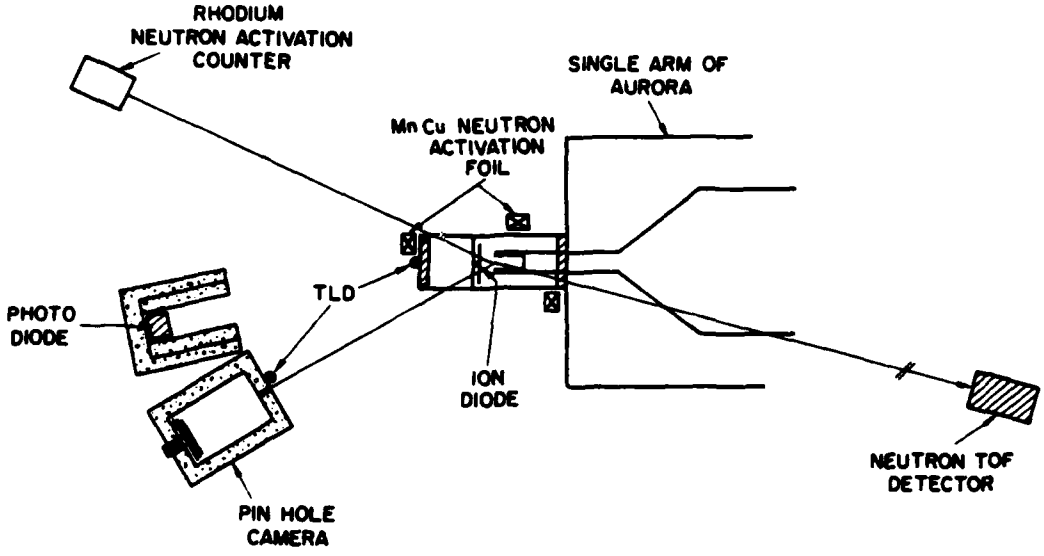

Fig. 14 — A schematic arrangement of the x-ray and neutron diagnostics

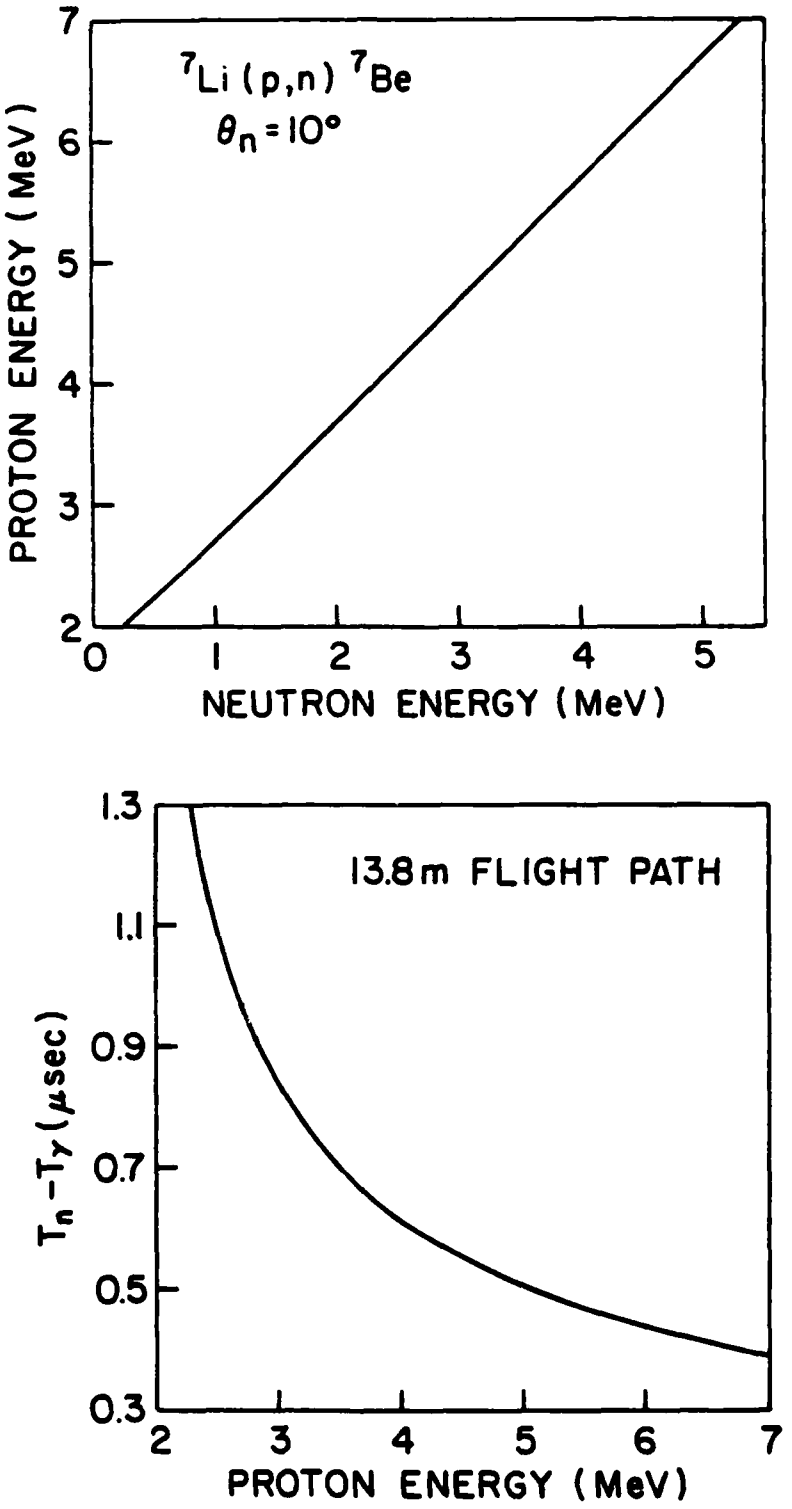

Fig. 15 — The dependence of the energy of protons in the ^{7}Li(p,n)^{7}Be reaction on the energy of the outgoing neutrons and on the neutron flight time (T_n) for a neutron TOF detector at 10° and 13.8 meters. The x-ray flight time (T_γ) has been subtracted from the neutron flight time.

acts as a time marker on the TOF traces, and its flight time, T_γ, has been subtracted from the neutron flight time.

c. Shadowbox

The trajectories of ions emitted from the diode were diagnosed by measurements with a pinhole shadowbox placed within the cathode.[1] The shadowbox is illustrated in Fig. 16. It consists of a 6-mm thick stainless-steel plate which contains an array of countersunk holes and is mounted 2.6 cm in front of a polished aluminum witness plate. The stainless steel plate is masked by a thin aluminum disk which has a matching array of 1-mm diameter apertures. The aluminum witness plate will melt if >100 A/cm^2 of 5-MeV protons are deposited, and it will vaporize for >1.4 kA/cm^2. The front aperture plate was coated with LiCl for neutron diagnostics.

d. Cathode Activations

Measurements of residual radioactivity on the cathode were made after each shot to provide additional information about the ion beam. The γ-ray activity of the cathode stalk was measured with a cylindrical 7.6-cm diameter by 7.6-cm NaI detector. Counting of the cathode could be initiated 15 minutes after a shot. Pulse-height spectroscopy was used to determine γ-rays due to radioactive species produced by ion bombardment of the cathode.

e. Neutron Activation Techniques

Neutron intensities were determined with a Rh-activation detector[10] and an array of Mn-activatic foils. The Rh detector was deployed at 155° to the ion-beam direction, and Mn-foil samples were positioned at several different angles as noted in Fig. 14. The Rh-detector consisted of a 5-cm diameter Rh-foil mounted against a plastic scintillator and enclosed in a polyethylene moderator.[11] Due to the intense neutron yields in this

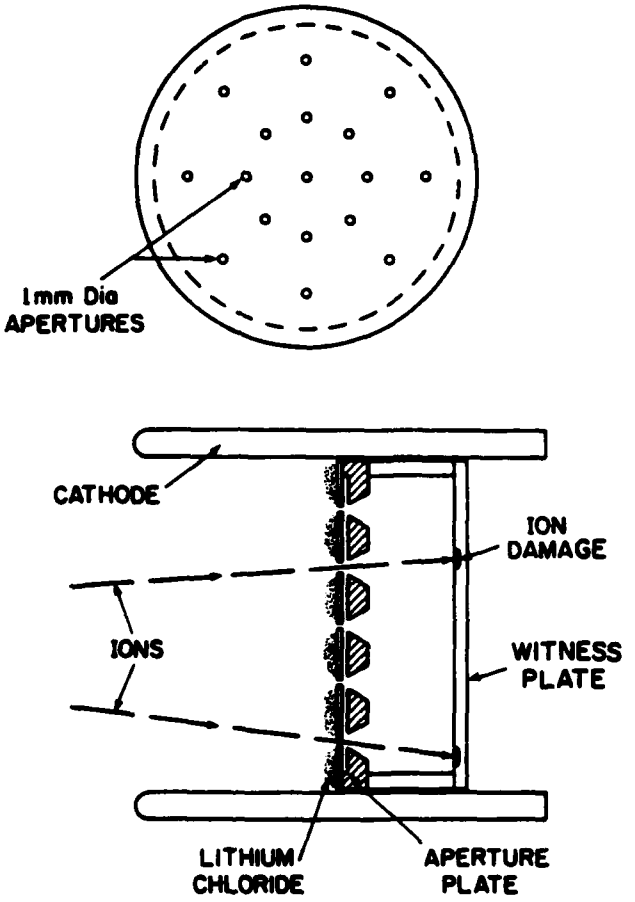

Fig. 16 — A schematic of the shadowbox used in these experiments. The aluminum mask with 1-mm diameter apertures allows LiCl to be deposited on its front surface for neutron diagnostics while protecting the stainless steel aperture plate. Ion damage is observed on the aluminum witness plate.

experiment a foil thickness of only 25 μm was used in this detector. Even so, it was necessary to locate this detector several meters from the LiCl target to prevent pileup effects.

Measurements with Mn-foil activations were used to provide neutron intensities at different angles and distances from the target on a single shot. This activation technique is illustrated in Fig. 17. Foils of Mn-Cu (81% Mn) 2.5 cm in diameter and 50-μm thick were placed in the center of a cylindrical 7.6-cm diameter by 7.6-cm CH_2 moderator. After this assembly was exposed to neutrons on a shot, the Mn foil was removed and its activity was measured with a cylindrical 7.6-cm diameter by 7.6-cm NaI detector. A γ-ray pulse-height spectrum of the induced activity is presented in Fig. 17. Gamma rays of 0.847, 1.81 and 2.11 MeV are observed. The higher-energy gamma lines (2.66 MeV and 2.96 MeV) result from summing of lower energy γ-lines. To simplify the measurement, the output count of an integral discriminator located just below the 0.847-MeV γ-ray peak was used to measure the activity. This activity decays with a 156-min half-life, as shown in Fig. 17. The combination of measured γ-ray energies and half-life is consistent with the ^{56}Mn activity expected from neutron activation via the $^{55}Mn(n,\gamma)^{56}Mn$ reaction. This measurement technique is 10^3 less sensitive than the Rh-activation detector.

Absolute calibration of these neutron detectors is based upon a calibration of the Rh counter with a Cf-252 neutron source. Calibrations with similar neutron sources have been described previously.[10] This source was used because its neutron energies are similar to those expected from the $^{7}Li(p,n)^{7}Be$ reaction. Even so, the neutron moderator on these detectors makes their response relatively insensitive to the neutron energy. For this

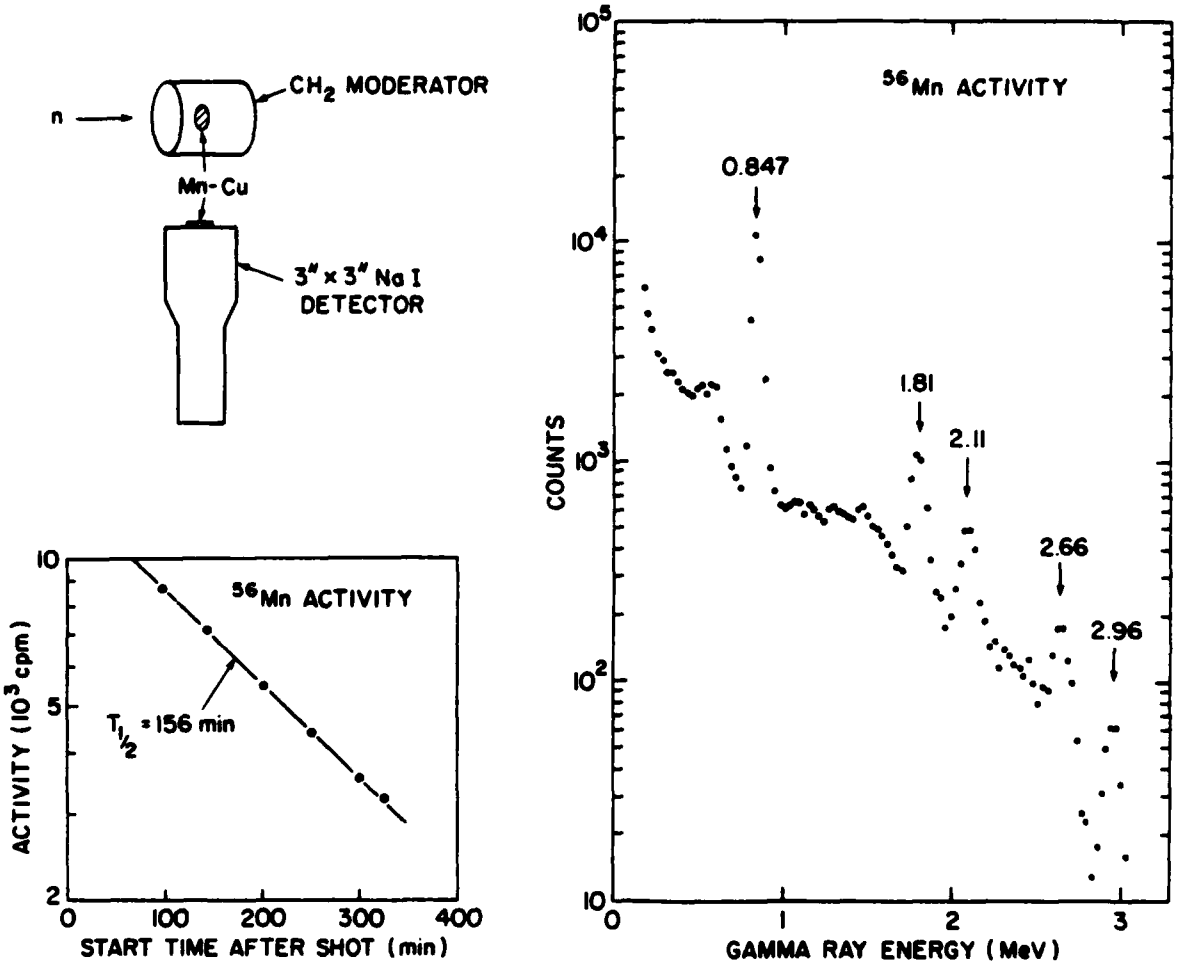

Fig. 17 — Neutron intensity determinations by Mn-foil activations. The apparatus for activating the Mn-foil and counting them is shown on the top left. A gamma-ray spectrum of the activity induced in a Mn-foil by moderated neutrons, as measured with a NaI detector, is shown at the right. This activity decays with a 156-min half-life corresponding to ^{56}Mn as shown on the lower left.

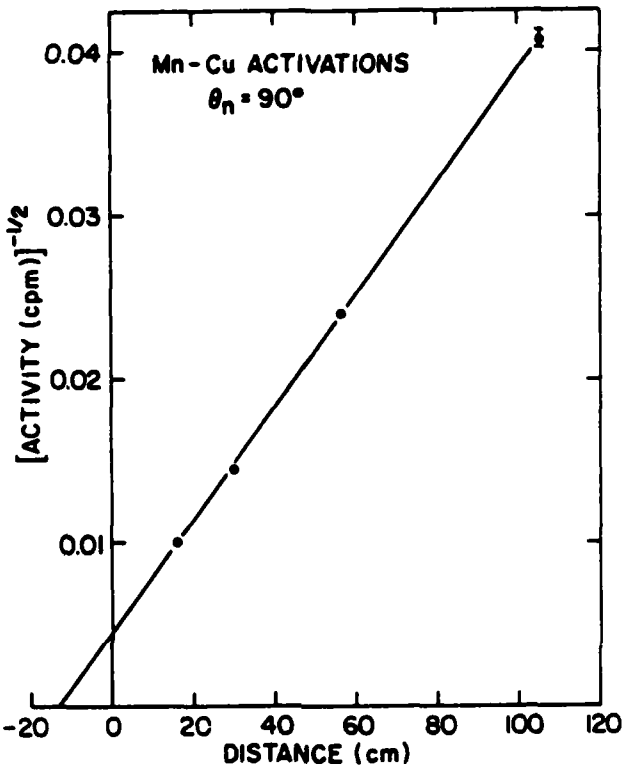

Fig. 18 — The dependence of Mn-foil activations on the distance from the LiCl target is shown for an array of four Mn-samples located at 90° from the ion beam direction in the plane of the target for a single shot. The plot demonstrates the inverse-square scaling of the neutron emission with distance out to ~ 1 meter.

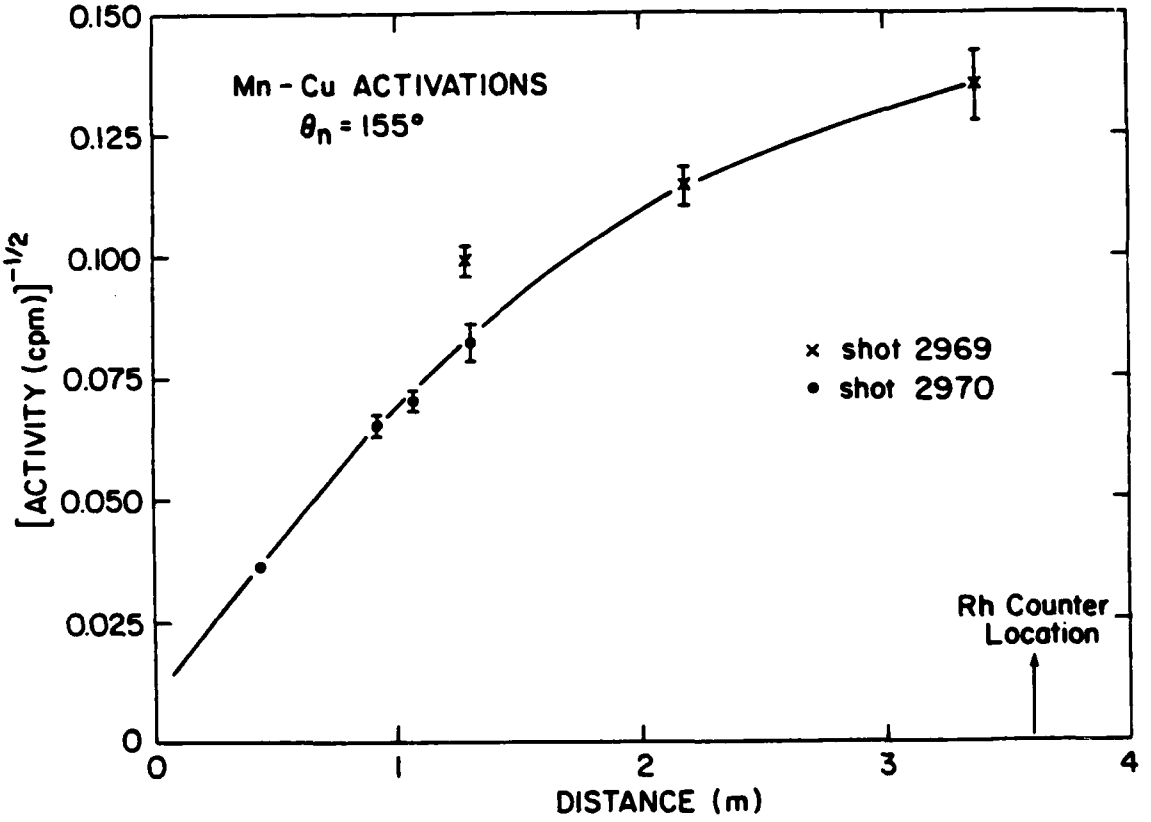

Fig. 19 — The dependence of Mn-foil activations on the distance from the LiCl target to the Rh-counter. The nonlinearity indicates that inverse-square scaling with distance is not obeyed for distances greater than one meter.

calibration, the detector response was observed to scale inversely with the square of the distance. The calibration factor, F, in neutrons/sr/cpm is

$$F = \frac{83}{4\pi} (d + 6.5)^2$$

where d is the source-to-detector distance in cm. This factor was used to convert the measured activity into neutron intensity. This Rh-detector calibration is three times smaller than a previous calibration[10] of the detector with a d-d neutron source because the Rh foil is of smaller thickness.

To apply this absolute calibration to the ion diode experiments, the scaling of neutron intensity with distance from the target was determined with the Mn-activation technique. The activation of an array of four Mn-Cu samples positioned from 0.16 to 1 meter from the LiCl target is shown in Fig. 18. The samples were located at 90° to the anode-cathode axis. In this figure, the square root of initial activity induced in each foil has been plotted against the target-to-detector distance. The linearity of these data demonstrates the inverse-square scaling of the neutron emission out to a distance of one meter. Similar measurements with arrays of Mn-Cu samples positioned along the direction of the Rh counter are shown in Fig. 19 for two different shots. The activities on these shots are normalized to each other by using measurements from the Rh detector and a Mn-Cu sample at 20°. The normalizations determined by these two independent neutron monitors were in agreement within 5%. The nonlinearity of the data in Fig. 19 indicates that the neutron intensity no longer obeys inverse-square scaling at distances greater than one meter. This deviation is attributed to room scattering of neutrons. Clearly, inverse-square scaling with distance is not appropriate for the Rh-counter positioned at 3.6 meters.

In order to use the Cf-252 calibration where the neutron emission obeyed inverse-square scaling, the Rh-counter was positioned 0.76 m from the LiCl target. For each shot the Rh-counter activity was measured for several minutes to identify the two decay components expected from Rh activation. With the detector located closer to the target, pulse pileup of the detector output at early time was observed as indicated by the data points in Fig. 20. To correct for this problem, the shape of the decay curve at early time was determined from a shot where the counter was 3.6 m from the target and did not suffer pulse pileup. The solid line in Fig. 20 is such a decay which has been normalized to the late-time measured activity. Then an absolute neutron-intensity determination could be performed by combining the Cf-252 absolute calibration with the first minute count implied by the solid line in Fig. 20.

IV. EXPERIMENTAL RESULTS

1. Results from a Typical Shot

Experimental results will be presented by discussing a single shot (No. 2978) in detail. In most aspects this shot typifies all the shots for this ion-diode experiment. The Marx generator was charged to -90 KV producing a 8.3-MV peak voltage on the Blumlein before being discharged across the insulator stack and onto the vacuum coax transmission line. Figure 21 shows a plot of the tube voltage (V_T) in the oil just before the insulator stack. The peak value of 11 MV is slightly higher than the 10.3-MV average peak value for the entire run (25 shots). The voltage risetime of ~ 100 ns with ~ 150 ns FWHM is typical. Figure 21 also shows the capacitive voltage monitor signal (V_B). Its peak of 6.3 MV is typical. The 40% drop in peak voltage between V_T and V_B is consistent with computer

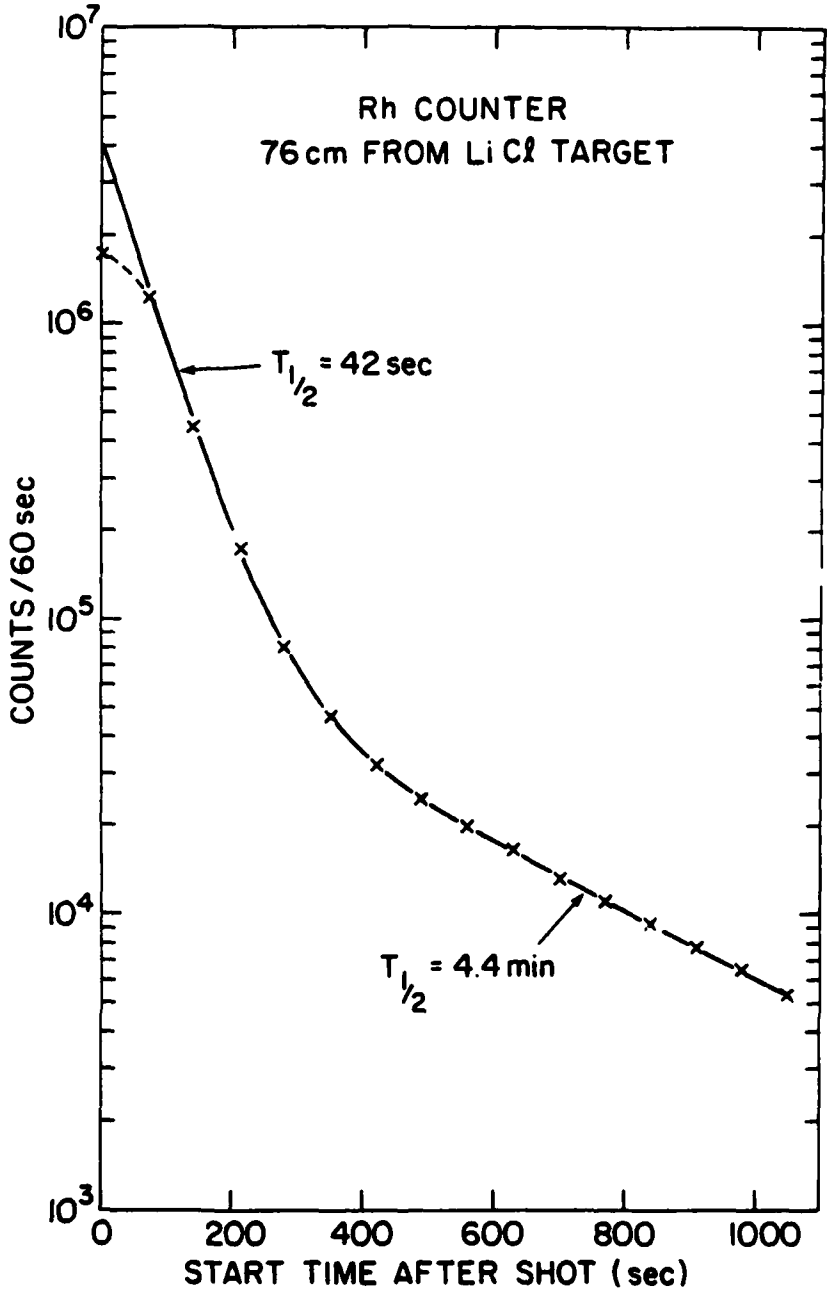

Fig. 20 — The measured decay of the activity induced in a Rh-counter by an intense burst of neutrons. The data points are for an intense pulse resulting in pulse pileup at early times. The solid line is the decay curve resulting from a less intense burst of neutrons and has been normalized to the late-time data points.

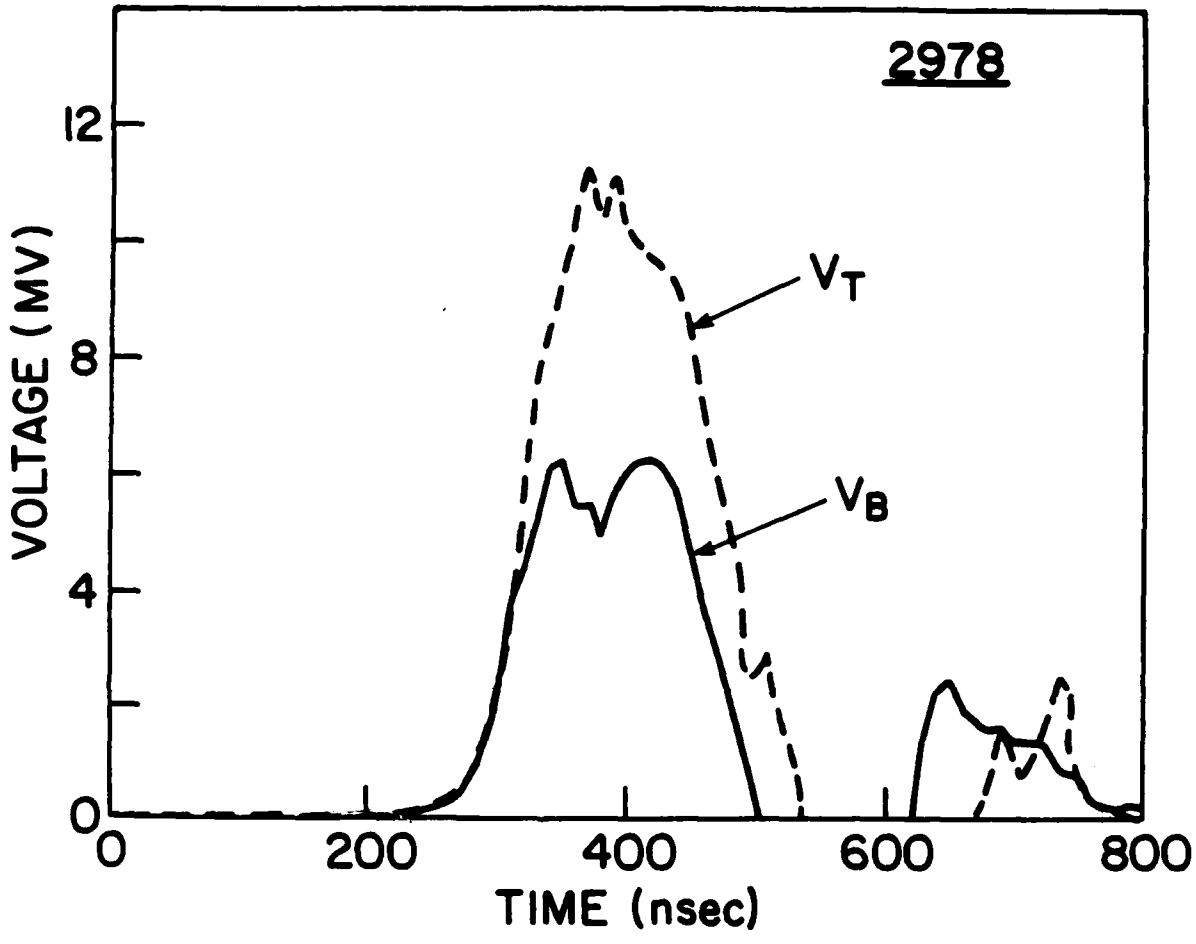

Fig. 21 — Two voltage wave shapes are shown, namely the copper sulphate voltage divider located in the oil (V_T) and a capacitive monitor located in the vacuum transmission line (V_B)

modeling of the generator and is the result of the impedance mismatch between the Blumlein and the vacuum coax. Voltages measured closer to the ion diode have wave shapes similar to V_B. No direct measurement of the cathode voltage was made. A diode voltage of ~5 MV is inferred from neutron TOF measurements to be discussed below.

Figure 22 compares the voltage, V_B, the current, I_T, just downstream of the diode insulator, and the effective line impedance $Z = V_B/I_T$. This current rises in ~120 nsec to a peak value of ~190 kA and plateaus for the remainder of the voltage pulse. The value agrees with the average peak current of 25 shots which ranges from 210 kA to 170 kA depending on the diode configuration. The calculated impedance at this location has a plateau of ~30 Ω for ~100 nsec during the useful portion of the diode pulse. Figure 23 shows the power and energy derived from V_B and I_T. The peak power of ~1.2 TW is typical for this run. At the end of the voltage pulse, these probes have measured ~160 kJ. The diode voltage will be lower than V_B and the diode current higher than I_T due to the impedance mismatch between the transmission line and the ion diode. Transmission line computer code studies[12] indicate that the current is ~250 kA in the diode region. This result coupled with the ~5-MV diode voltage implied from the TOF measurements suggests that the diode was operating close to 20-Ω impedance.

The ion diode used on this shot had a 4.9-cm anode-cathode (AK) gap. The anode consisted of a 86-μm thick CH_2 foil on the outer section and a 0.43-mm thick CH_2 foil on top of the center field-enhancing disk and aluminum screw head. This anode was supported by a 6.0-cm long stalk mounted on a 1.5-mm thick aluminum diaphragm. A shadowbox was recessed

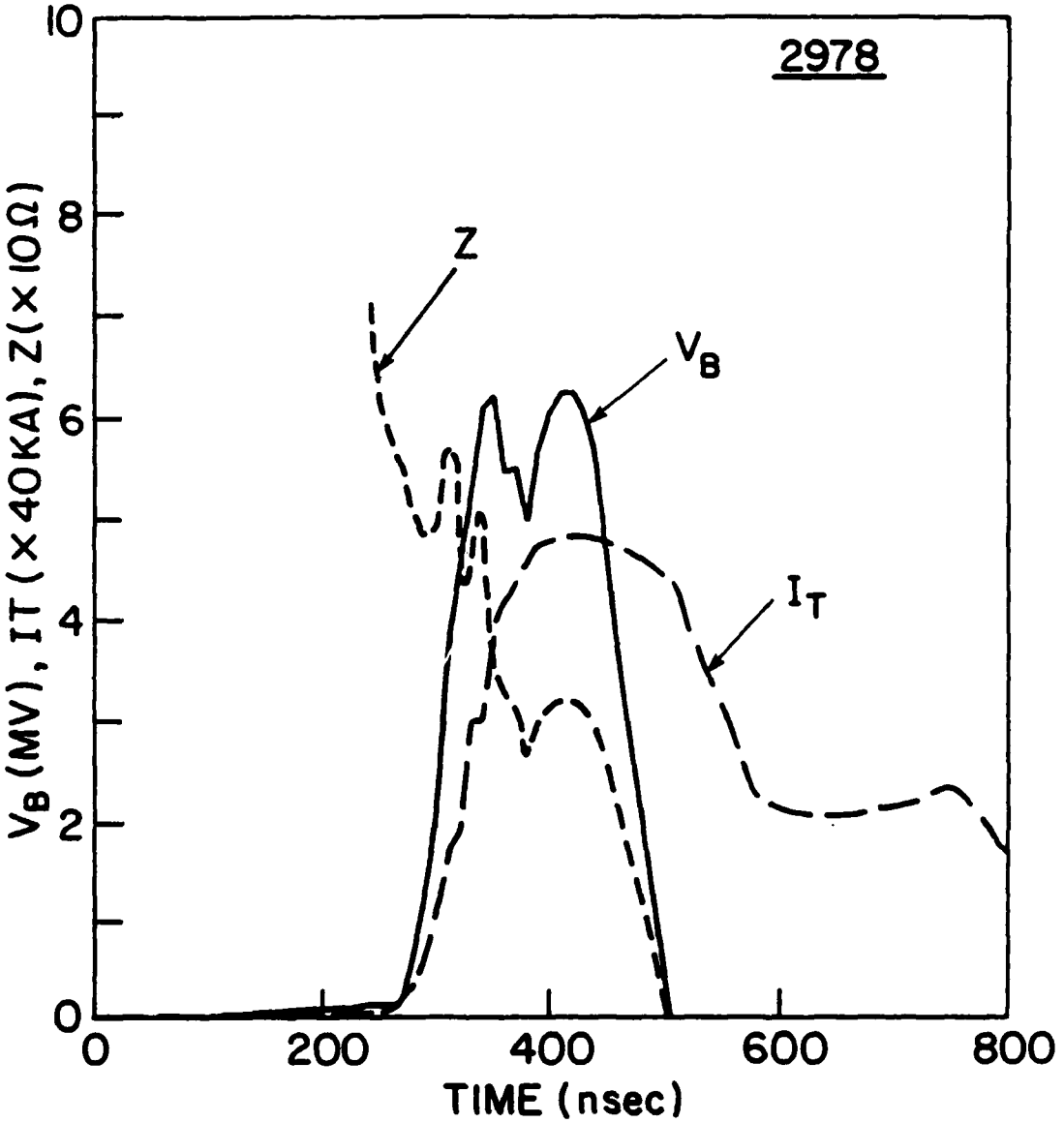

Fig. 22 — The voltage on the vacuum transmission line, V_B, is shown relative to the current I_T. The effective impedance, Z, computed from V_B and I_T is also shown. This impedance represents the combination of the vacuum transmission line downstream of the monitors and the actual ion-diode load impedance. The line impedance appears to be ~ 30 ohms during the latter half of the pulse when the diode is fully turned on.

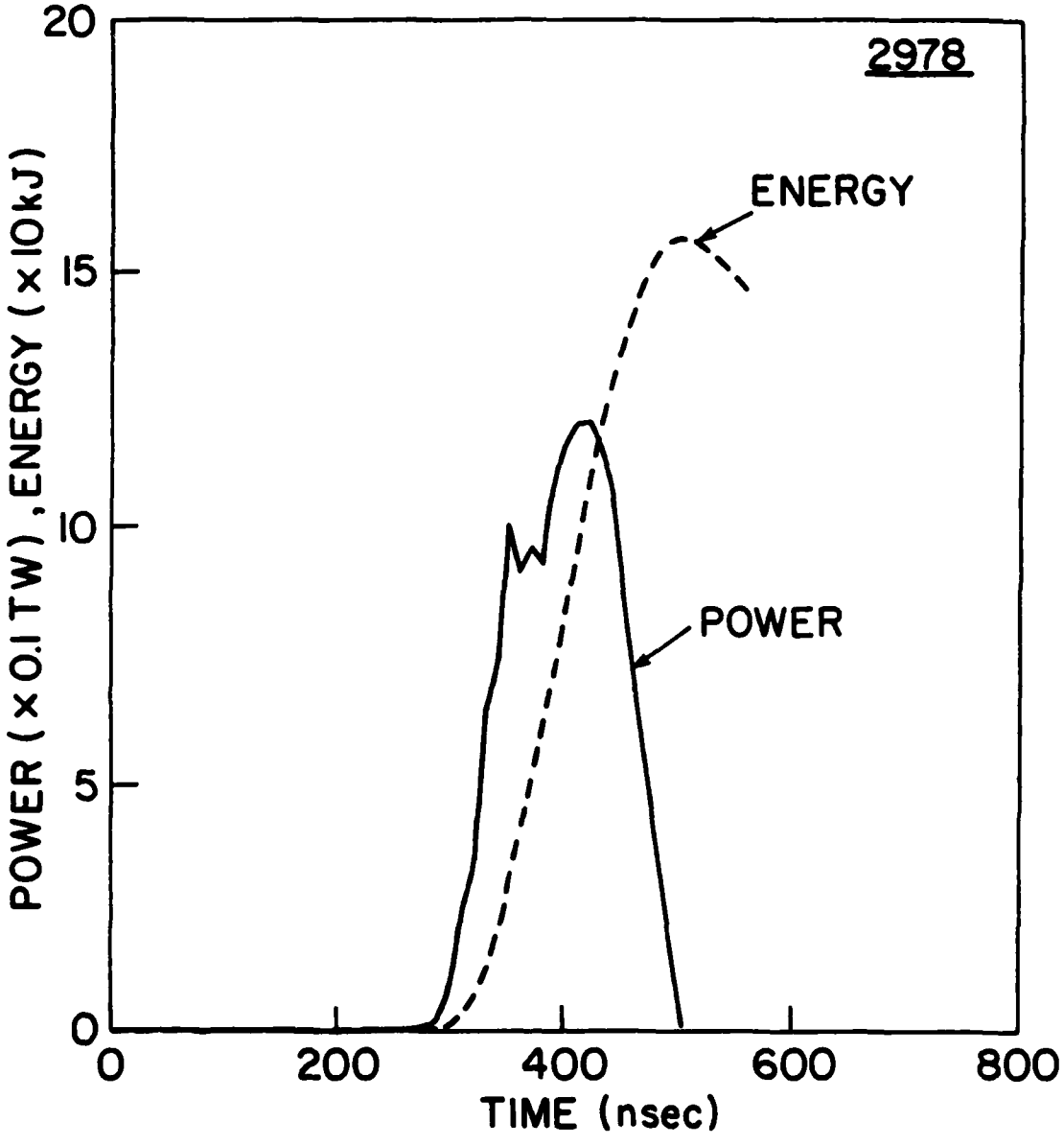

Fig. 23 — The power and energy delivered to the transmission line at the location corresponding to probes V_B and I_T as calculated using these traces

10.5 cm inside the cylindrical aluminum cathode and had a LiCl target mounted on its front surface. A four-insulator-section prepulse switch was located behind the cathode.

The results of x-ray measurements with the pinhole camera are shown in Fig. 24. Images were recorded with four different film sensitivities through a 1.9-mm diameter pinhole. These pictures are typical of the experiment. The pinch was well centered on all shots, seemingly striking the central disk or screw head. The intensity of the x-ray images depended on the diode impedance with lower impedance shots showing weaker images. In no case were bright regions observed from the aluminum back plate except near the center.

The signal measured by the x-ray photodiode for this shot is shown in Fig. 25. The shape of this signal is compared with a theoretical scaling[13] for x-ray production from e-beams given by $I_T(V_B)^{2.8}$. The calculated signal was normalized in magnitude and positioned in time for comparison with the measured signal. The shapes of the two signals agree reasonably well. This agreement provides an independent check on how well the measured voltage and current wave shapes agree with the actual wave shapes across the diode. In general, the peak intensity from the photodiode depended on the diode configuration. Intensities observed with the x-ray pinhole camera were consistent with the intensities recorded by this photodiode.

Ion diagnostics on this shot included measurements of neutrons resulting from proton bombardment of the LiCl target, pulse-height analysis of residual gamma activity from the cathode, and a shadowbox to observe the ion trajectories. Neutron diagnostics and cathode activation analyses were used on most shots, but the shadowbox diagnostic was used on only two shots.

Fig. 24 — X-ray pinhole photographs at four different film sensitivities for a single shot (2978). Film sensitivity increases from left to right. On the left, only the aluminum screw head on the front of the anode (see Fig. 13) is seen. Next, some of the thin aluminum anode-supporting tube and more of the central aluminum anode disk are apparent. The outer aluminum anode ring is evident in the third image. The last image indicates that the aluminum back-plate was irradiated by a diffuse spray of electrons.

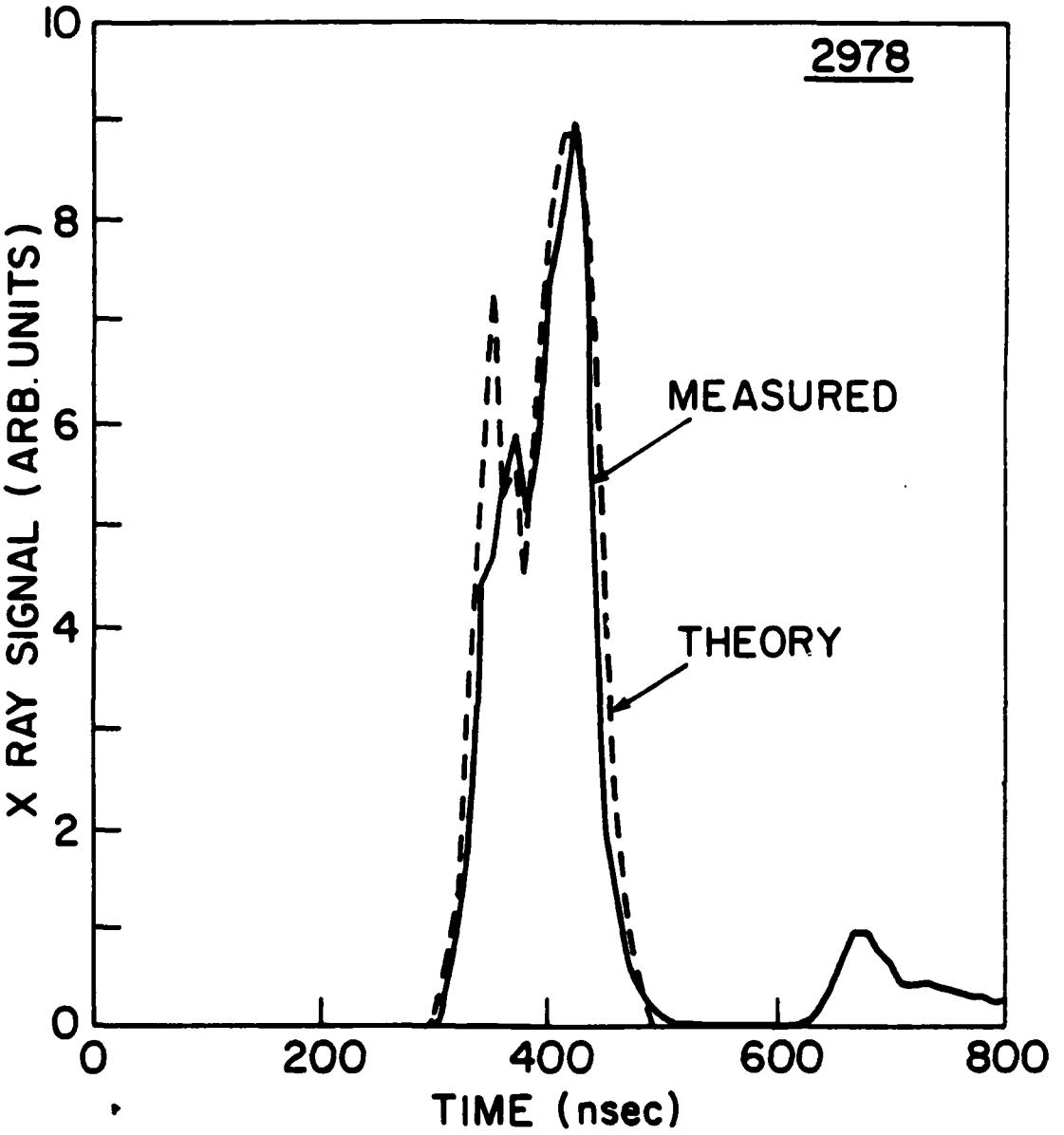

Fig. 25 — The measured signal from an x-ray photodiode collimated to see only the anode-cathode region. The dashed line represents the calculated x-ray production with the $I_T(V_B)^{2.8}$ scaling and has been normalized to the peak of the measured signal.

Neutron TOF measurements for this shot and for a shot without a LiCl target are compared in Fig. 26. The neutron pulse is readily detected above the bremsstrahlung tail. The onset of the neutron pulse is ~ 400 nsec after the peak of the bremsstrahlung and the ~ 150 nsec risetime followed by a rounded peak and long tail is characteristic of the neutron TOF data. The width of this pulse is due primarily to the duration of proton emission from the diode and the energy loss of protons in the thick LiCl target. Proton energies were extracted in two ways. First, the time interval from the peak of the x-ray pulse to the peak of the neutron pulse gives a measure of the average proton energy. Second, the time interval from the peak of the x-ray pulse to the 50% point on the leading edge of the neutron pulse gives an estimate of the maximum proton energy. Proton energies were extracted from these time measurements by using the curve given in Fig. 15. The results for this shot are compared with averages for 12 shots in Table 1. We conclude that a proton energy of 5 MeV is characteristic of this experiment.

The Rh-activation detector measurement for shot 2978 indicated a neutron yield of 4.3×10^{11} neut/sr at 155^{o}. This shot gave the largest yield, which can be compared to an average of 2.8×10^{11} neut/sr for 18 shots. The larger yield may be due in part to the higher than average proton energy on this shot. With no LiCl, the neutron yield was only $0.5 - 1.0\times10^{10}$ neut/sr. In this case, neutron production presumably results from ion bombardment of the aluminum witness plate and cathode.

Proton intensities were determined from the neutron intensities using known nuclear reaction yields. Thick-target yields for $^{7}Li(p,n)^{7}Be$ reaction on a LiCl target were calculated using published cross sections[14] and stopping powers.[15] The results are displayed in Fig. 27. These curves

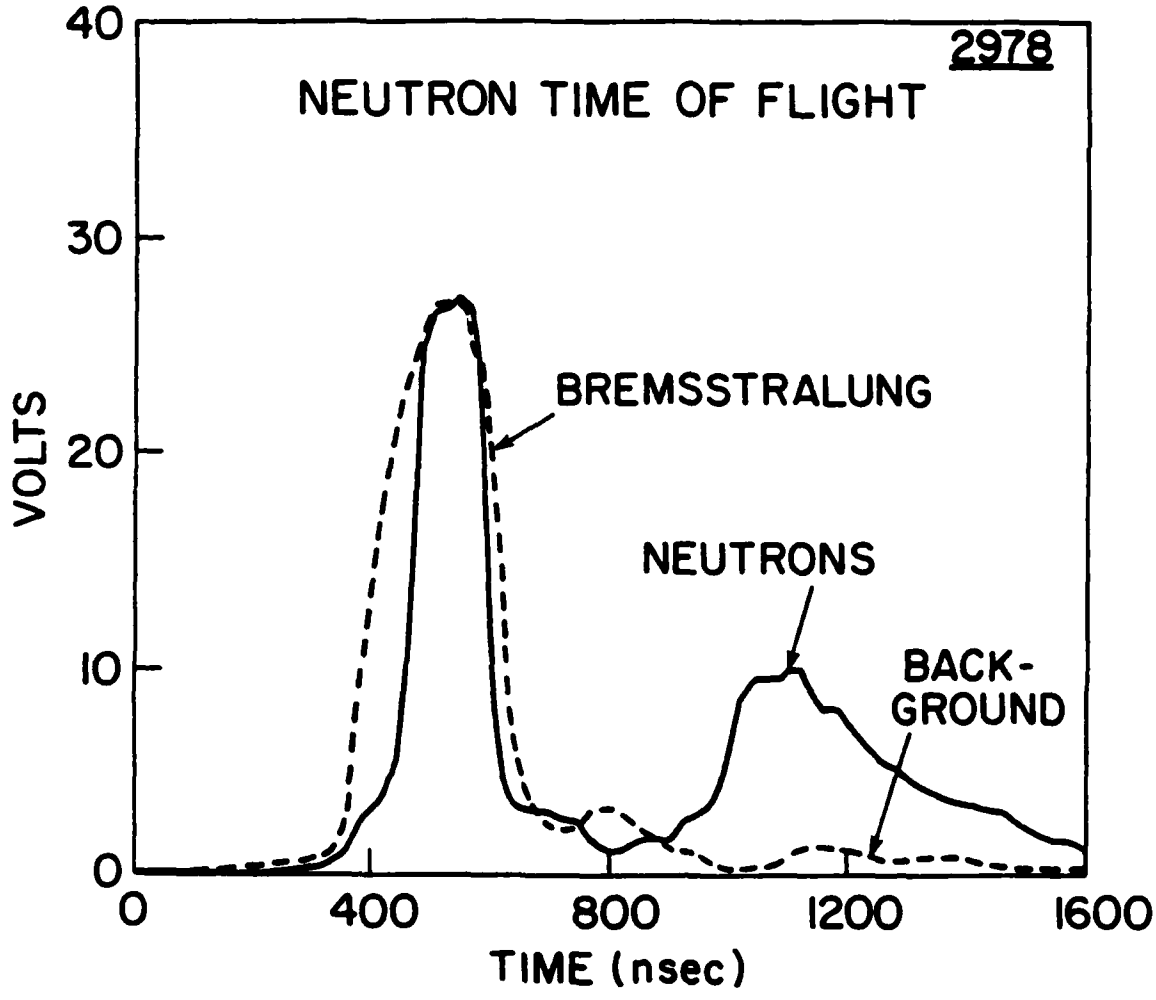

Fig. 26 — Neutron time-of-flight traces measured for shot 2978 and for a shot without a LiCl target

TABLE 1

PROTON ENERGIES FROM NEUTRON TOF

TIMING PROCEDURE	SHOT 2978	AVG OF 12 SHOTS	
	E MeV	E MeV	RANGE MeV
Peak to Peak	4.6	4.4	4.0 - 5.5
Peak to 50% Rise	5.9	5.2	4.6 - 5.9

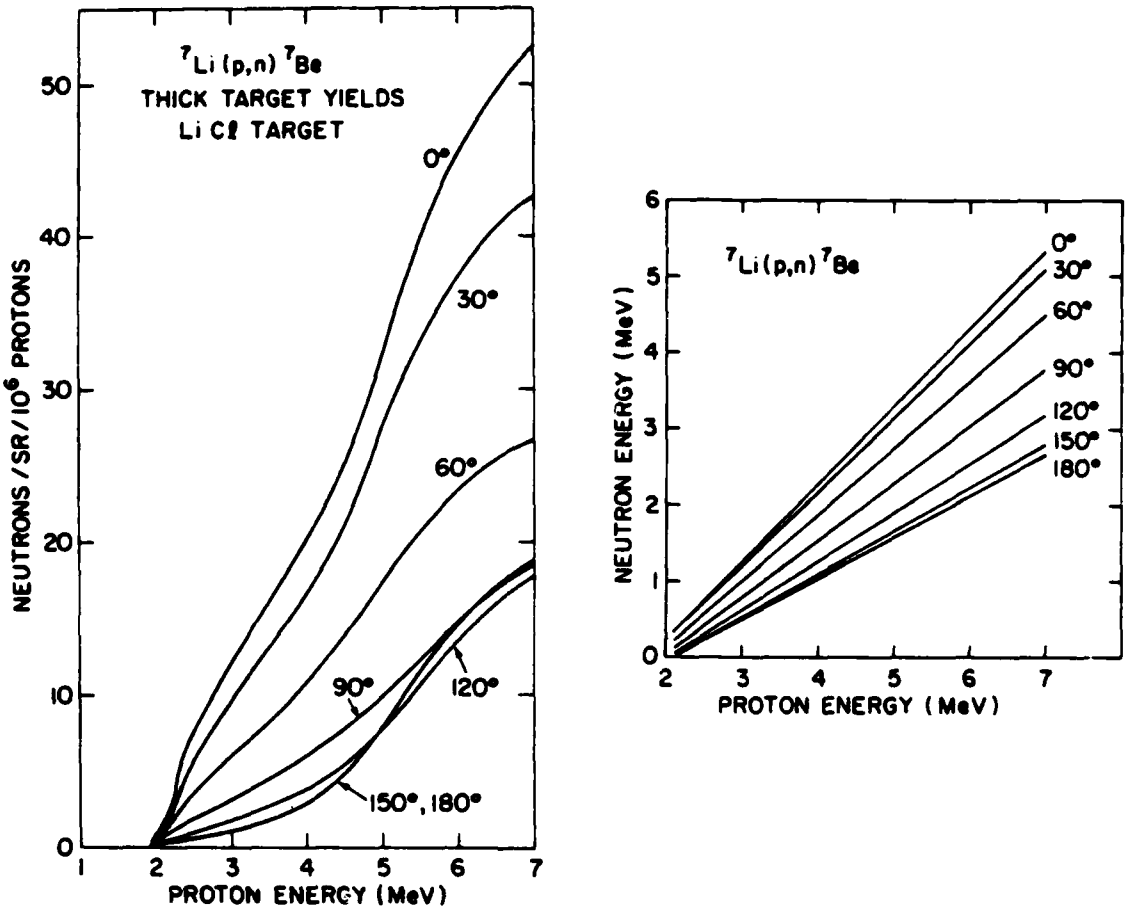

Fig. 27 — Thick target yields for the ^{7}Li(p,n)^{7}Be reaction on a LiCl target (left) and reaction kinematics for the ^{7}Li(p,n)^{7}Be reaction (right)

include only the ground-state reaction. The contribution from the first excited state is less than 10% at these energies. Note that this reaction has a threshold at 1.9 MeV and that the reaction yield is forwarded peaked. The kinematics for this reaction are also displayed in Fig. 27. For 5-MeV protons, neutron energies ranging from 1.6 to 3.3 MeV can be expected depending on the angle of the detector. For shot 2978, the observed neutron output corresponds to 5.4×10^{16} protons at 5 MeV. This result is relatively sensitive to the proton energy and ranges from 3.1×10^{16} protons at 5.9 MeV (maximum energy from TOF) to 8.1×10^{16} protons at 4.6 MeV (average energy from TOF). For all 18 shots, the average number of protons is 3.7×10^{16}. We conclude that up to $\sim 5\times10^{16}$ protons are produced with energies of $\sim$ 5 MeV.

Results from the shadowbox recessed 10.5 cm inside the cathode are shown in Fig. 28. The damage patterns produced by ions on the witness plate are outlined. These images are projected by straight-line trajectories through the corresponding witness plate apertures back toward the anode-cathode region. Ions observed at larger radii in the shadowbox appear to come from a common source which is nearer the anode than that for ions observed at smaller radii. The ions appear to come from the central region of the anode. The projections at different radii suggest that ion-focusing is going on within the anode-cathode gap with a significant fraction of the ions crossing the axis several centimeters in front of the anode.

2. Cathode Activations

Radioactivity induced on the cathode after a shot could not be understood solely by proton bombardment, but required the presence of an energetic carbon component in the beam. A pulse-height spectrum of the delayed γ-ray activity measured on the aluminum cathode with a cylindrical 7.6-cm diameter by 7.6-cm NaI detector is shown in Fig. 29. Invariably,

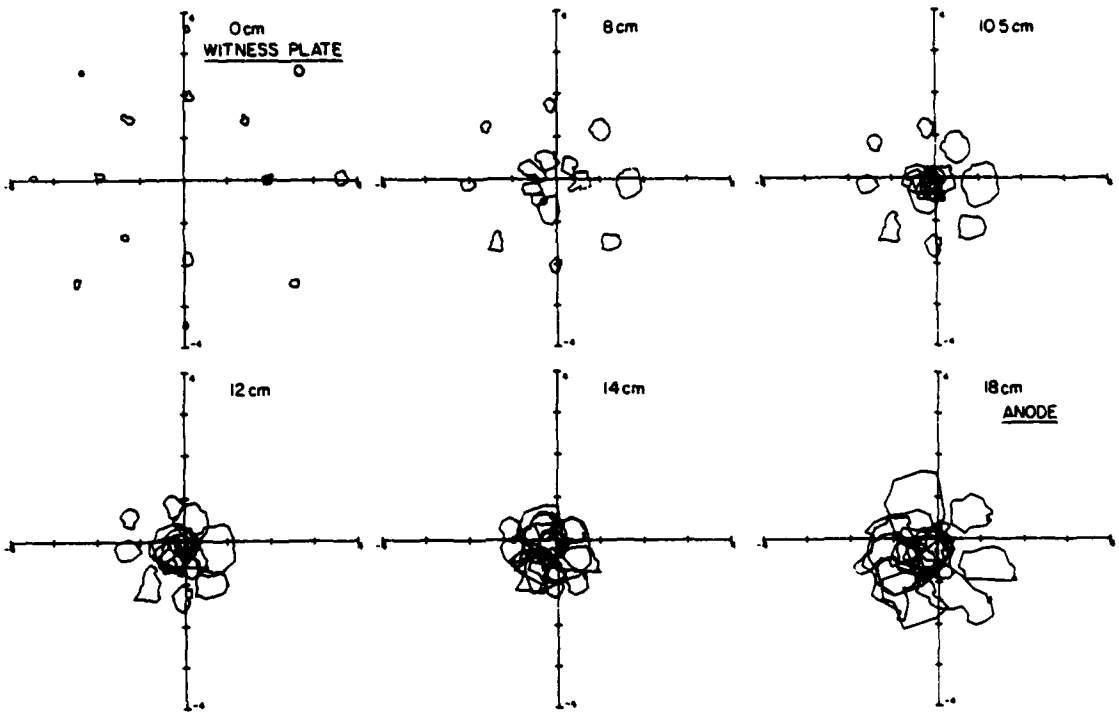

Fig. 28 — Projections of the ion damage observed on a shadowbox witness plate back through the shadowbox apertures toward the anode. The observed witness-plate damage is outlined at 0 cm. The projections at 8 cm and 10.5 cm from the witness plate indicate that ions at the smaller radius are converging faster than ions at the larger radius. The inner-radius projections pass through an apparent best focus at 10.5 cm and begin to diverge as one approaches the anode located at 18 cm. The outer-radius projections have an apparent best focus very near the anode plane.

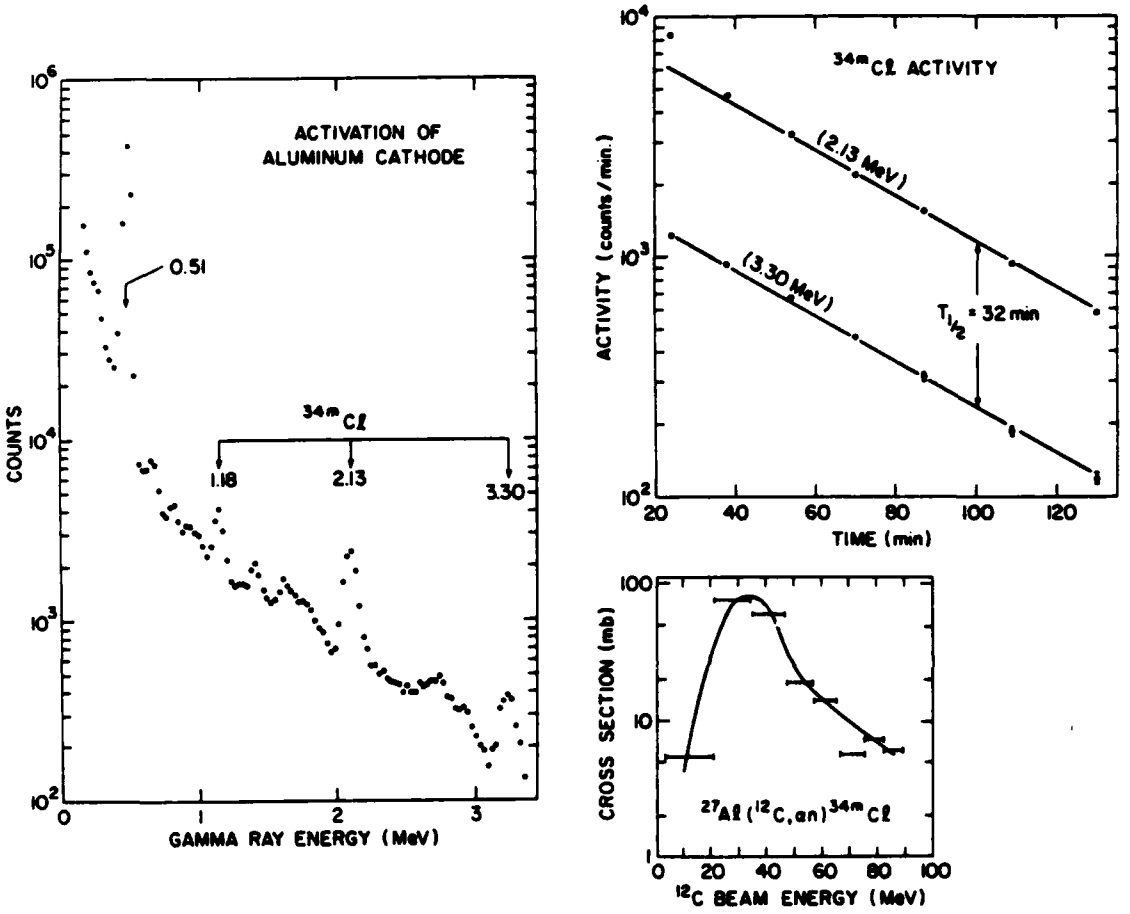

Fig. 29 — A spectrum (left) of the delayed γ-lines of 2.13 and 3.30 MeV which are observed to decay with a half-life of 32 min characteristic of ^{34m}Cl (top right). This activity can be produced by carbon-ion bombardment of the aluminum cathode as indicated by the cross section for the ^{27}Al(^{12}C,αn)^{34}Cl reaction (lower right).

the most intense γ-ray observed was annihilation radiation (0.51 MeV) resulting from positron activity produced by a variety of nuclear reactions. The decay of this γ-ray could not be characterized by a single half-life. The γ-rays at 1.18, 2.13 and 3.30 MeV dominate the high energy region of this spectrum. A half-life of 32 min. was measured for the decay of 2.13 and 3.30 MeV γ-rays, as shown in Fig. 29. These results indicate that this activity is ^{34m}Cl. This identification was confirmed by Ge-spectroscopy of the cathode activity, as summarized in Table 2. Gamma-ray energies were measured to a precision of ± 1 keV, and the values agree with those recommended from the literature for ^{34m}Cl. Note that the intense 146-keV γ-ray from ^{34m}Cl was observed by Ge-spectroscopy, but not in the NaI spectrum (see Fig. 29). In addition, γ-rays associated with ^{63}Zn and ^{7}Be were also observed. The ^{7}Be activity results from the ^{7}Li(p,n)^{7}Be reaction in the LiCl target. The ^{63}Zn activity results from the ^{63}Cu(p,n)^{63}Zn reaction on a copper impurity in the aluminum cathode. No other γ-activities were observed in these measurements. The ^{34m}Cl activity cannot be accounted for by a proton-induced reaction but can result from the ^{27}Al(^{12}C,αn)^{34m}Cl reaction due to a carbon component in the ion beam. The cross section[16] for this reaction is given in Fig. 29. If the carbon ions were produced in the 6+ charge state and accelerated through 5 MV to give an energy of 30 MeV, the number of ions required to account for the maximum observed activity would be 3×10^{14}. For lower energy ions, the number increases because the cross section for this reaction decreases with energy. Also, this value represents a lower limit because activity blown off the cathode during the shot is not measured. We conclude that more than 3×10^{14} carbon ions per shot are generated in these experiments.

TABLE 2

Ge - Spectroscopy of Aluminum Cathode

Observed Gamma Lines (keV)	Recommended Gamma Energies (keV)	Radionuclide	Source Reaction	Threshold Energy (MeV)
3303	3303.5[a]	^{34m}Cl	$^{27}Al(^{12}C,\alpha n)^{34m}Cl$	4.9
2127	2127.5[a]			
1176	1175.8[a]			
510	511.0[b]			
145.7	145.7[c]			
669	669.6[d]	^{63}Zn	$^{63}Cu(p,n)^{63}Zn$	4.2
961	961.9[d]			
477	477.6[b]	^{7}Be	$^{7}Li(p,n)^{7}Be$	1.9

[a] R. W. Kavanagh, A. Gallmann, E. Aslanides, F. Jundt, and E. Jacobs, Phys. Rev. 175, 1426 (1968).

[b] J. B. Marion, Nuclear Data A4, 301 (1968).

[c] T. F. Ward and P. K. Kuroda, J. Inorg. Nucl. Chem. 33, 609 (1971).

[d] R. Colle, R. Kishore, and J. B. Cumming, Phys. Rev. C9, 1819 (1974).

The activation of the cathode was also measured on a shot where the aluminum cathode was replaced by a stainless steel cathode. The γ-ray pulse-height spectrum obtained in this case is shown in Fig. 30. There is no evidence for the ^{34m}Cl activity when the aluminum cathode is removed. This observation supports the previous conclusion that the ^{34m}Cl activity results from the bombardment of aluminum by energetic carbon ions. The only prominent feature in the spectrum in Fig. 30, except for annihilation radiation, is a 1.43-MeV γ-ray which decays with a half-life of 22 min. This activity is characteristic of ^{52m}Mn which can be produced by the $^{52}Cr(p,n)^{52m}Mn$ reaction on the 18% chromium component in the stainless steel. The thick-target yield[17] for this reaction, which has a threshold at 5.9 MeV, is shown in Fig. 31. The presence of this activity indicates that protons exceeded 5.9 MeV on this shot. For a proton energy of 6.5 MeV, only $\sim 5\times10^{14}$ protons are required to account for the measured ^{52m}Mn activity. This is only ~ 2% of the number of protons measured on this shot by the $^{7}Li(p,n)^{7}Be$ diagnostic. Therefore, the ^{52m}Mn activity can be accounted for by a small fraction of the proton beam exceeding the 5.9-MeV threshold for producing this activity.

3. Variation of Diode Parameters

In the course of the 25 shots comprising this experiment, the behavior of the diode was studied for several different variations of diode parameters. These studies included variations of the anode-cathode gap, the number of prepulse insulators, and the anode structure.

The AK gap study consisted of 5 shots with gaps ranging from 2.8 cm to 7.0 cm. For gaps >4.8 cm, the voltage and current traces did not change significantly with the gap spacing. For gaps <4 cm the voltage risetime and peak value did not change, but the voltage decayed more rapidly after

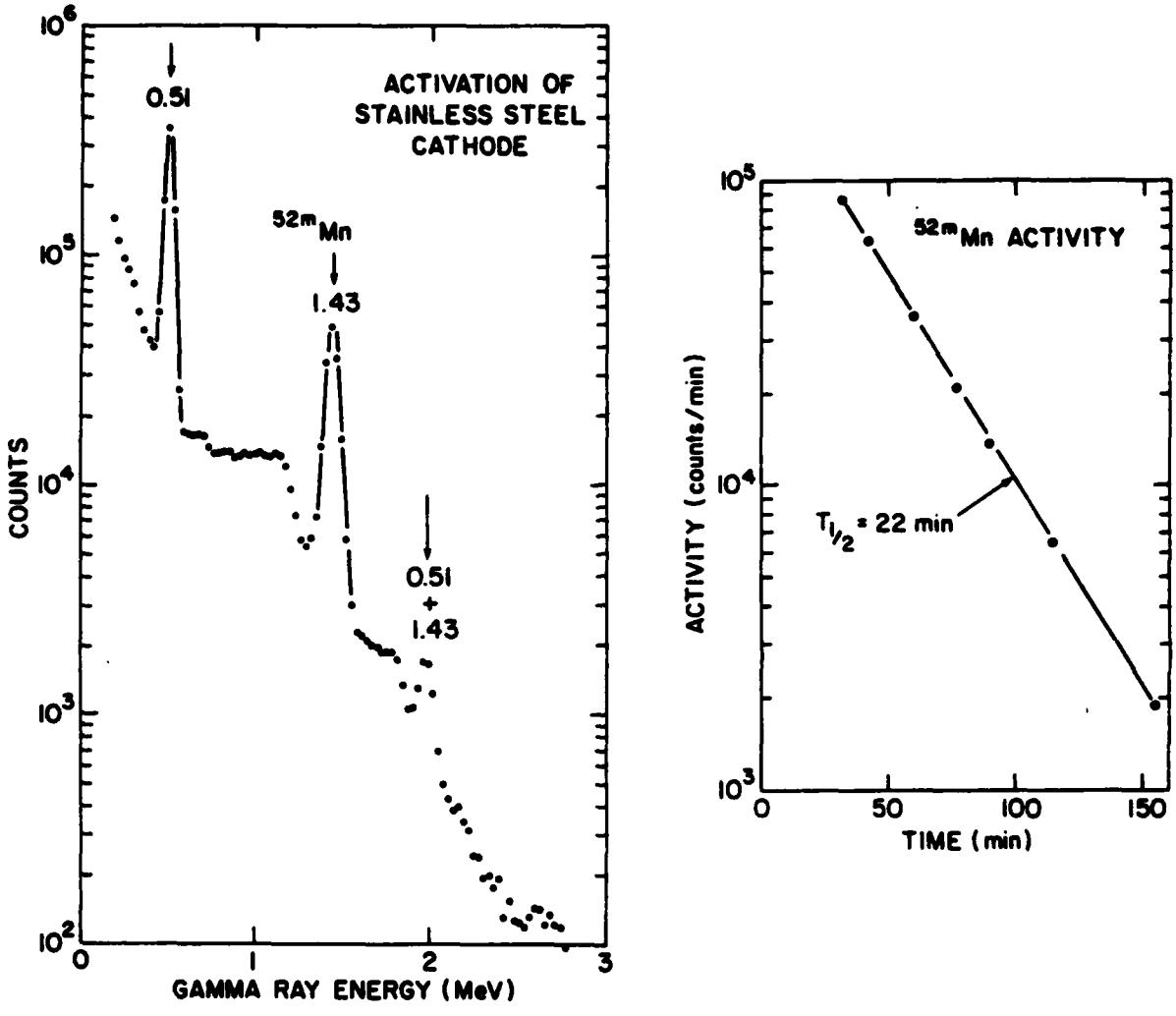

Fig. 30 — A spectrum of the delayed γ-ray activity (left) measured on a stainless steel cathode shows a 1.43-MeV γ-line which decays with a 22-min half-life characteristic of ^{52m}Mn (right)

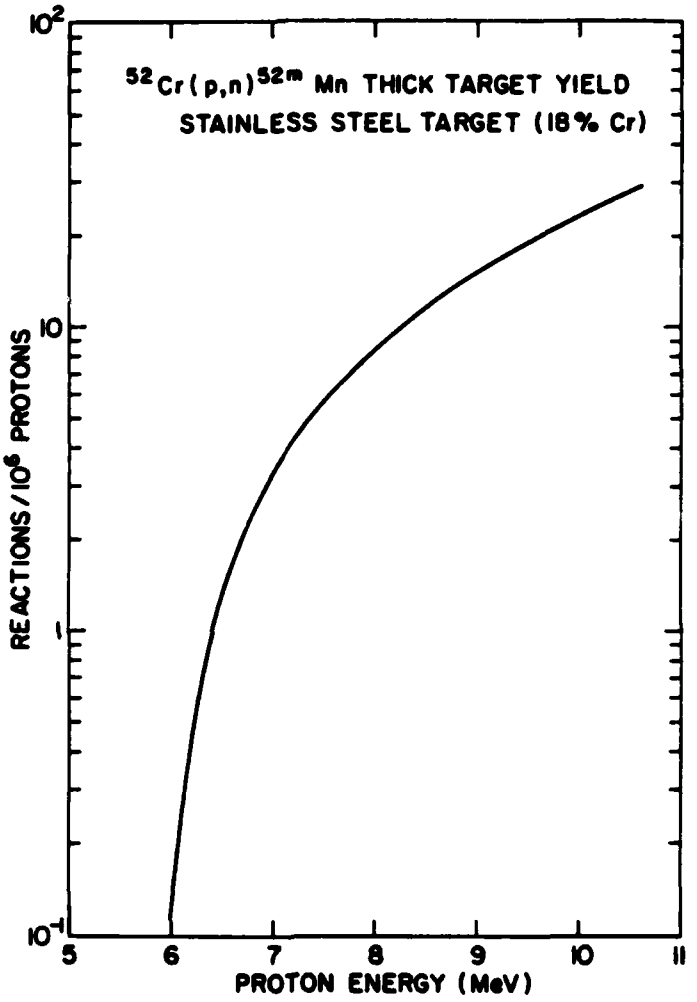

Fig. 31 — The thick target yield for the ^{52}Cr(p,n)^{52m}Mn reaction on a stainless steel target

the peak. For example, the full width at half maximum of voltage V_B dropped from ~ 160 ns for gaps ≥4.8 cm to ~ 100 ns for a 2.8-cm gap. Likewise the peak current as measured by I_T was 30 kA higher for the small gap. These observations indicate that the diode impedance is falling rapidly during the latter half of the pulse. The ion diagnostics showed a decrease in the number of neutrons and ^{34m}Cl nuclei produced for smaller gaps as indicated in Fig. 32. The decrease in neutron and ^{34m}Cl production may be due to either the production of fewer ions or to a reduced voltage across the diode. In the latter case, the strong energy dependence of the cross sections for these diagnostics causes the reduced outputs. The ion intensity cannot be unfolded from these diagnostics until better voltage and current measurements are available and direct ion current measurements are made.

One constraint on the efficient coupling of a low impedance diode to the Aurora generator is the presence of a diode prepulse. A prepulse can cause anode and cathode plasmas to form and begin to close the diode gap. As a consequence, the diode may short out prematurely when the main pulse is impressed on the diode. A 300-nsec long prepulse of ~ 100-kV peak voltage appears on the vacuum transmission line 1.5 μsec before the main voltage pulse. This prepulse could be a source of premature plasma formation in the diode region. To minimize this effect, an insulator flashover switch was located behind the cathode to capacitively attenuate the prepulse level at the diode. By changing the number of insulators, the prepulse voltage could be decreased by an order of magnitude. Shots were taken with 0, 2, 4 and 6 insulators in this switch, for a 5-cm AK gap. The diode behavior showed no difference between four to six insulators. For 2 insulators, the rise of the voltage to its peak did not change

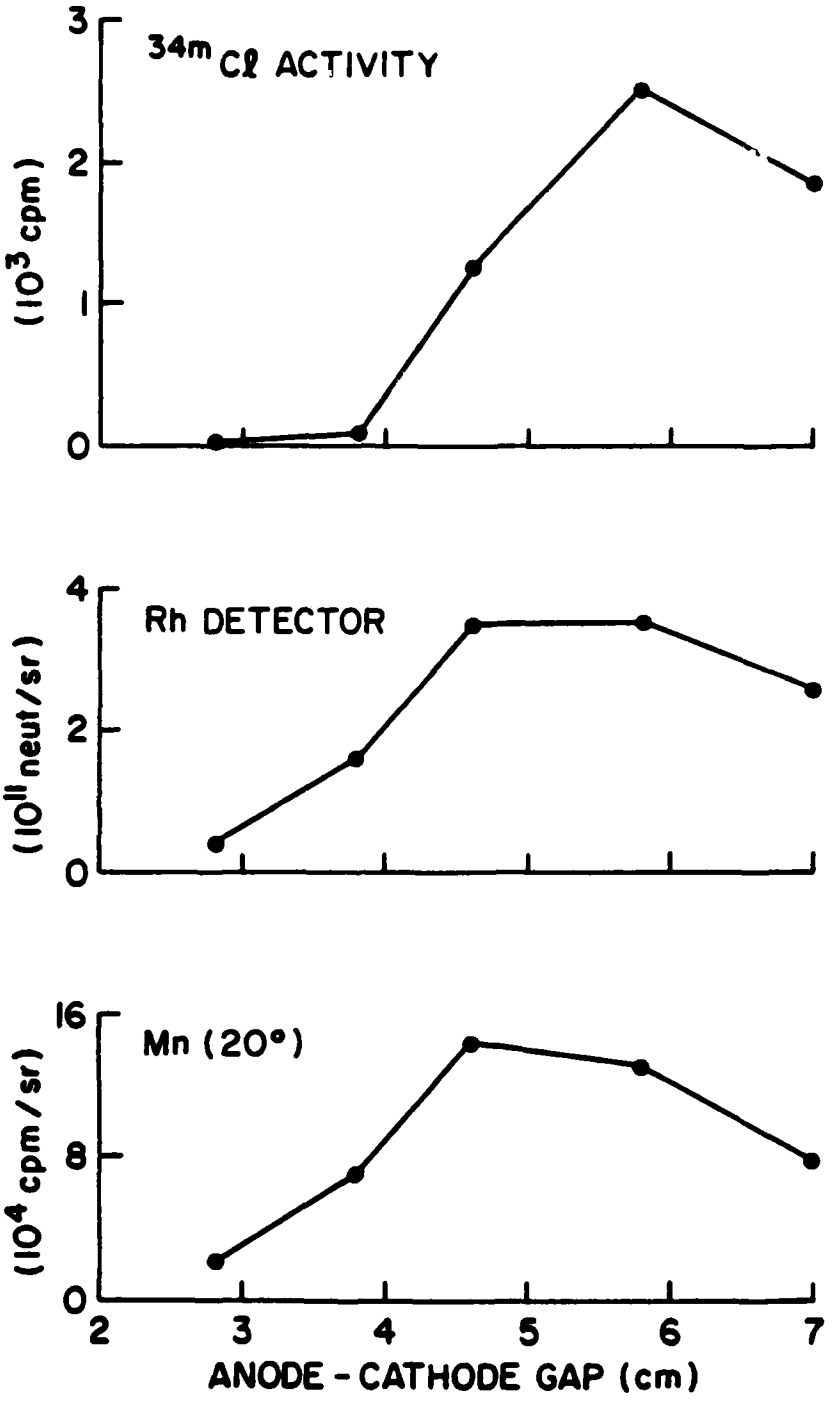

Fig. 32 — Dependence of the cathode activation (^{34m}Cl) and the ^{7}Li(p,n)^{7}Be neutron production (Rh and Mn detectors) on the anode-to-cathode gap.

significantly, but after the peak, the voltage collapsed rapidly. For zero insulators (no prepulse switch), the voltage risetime increased, the peak voltage decreased by ~ 1 MV and a rapid decay followed the peak and shortened the pulses to 135 nsec (FWHM). For the configurations with zero and two insulators, peak diode currents of ~ 230 kA were well above the average of 190 kA for the entire run, indicating lower impedance operation of the diode. The dependence of the ion diagnostics on the number of insulators in the prepulse switch is shown in Fig. 33. The decrease in neutron and Cl^{34m} production is consistent with gap closure due to plasma production lowering the diode voltage.

Ion production in these experiments depends on the interaction of electrons with the anode foil. Reflexing of electrons through the anode foil may enhance ion production. In these negative-polarity experiments, the CH_2 anode foil acts as a ground plane as well as a plasma source for ions (see Fig. 13). Electrons from the cathode may reflex through the anode foil due to the magnetic field produced by current in the anode stalk. The gyroradius of 5-MeV electrons in the magnetic field at the cathode radius resulting from a 150-kA current is ~ 3 cm. For an anode stalk longer than 3 cm, electrons can reflex through the anode without interacting with the aluminum plate supporting the anode. In addition, a virtual cathode may be formed in the vacuum region behind the support plate and reflect electrons back toward the anode. These two potential reflexing mechanisms complement one another.

Several shots with different anode structures were made to examine the role of electron reflexing in the diode. First, a series of shots with anode stalk lengths ranging from 3 to 12.8 cm was made for AK gaps of 5 cm. No significant differences in the voltage, current, neutron

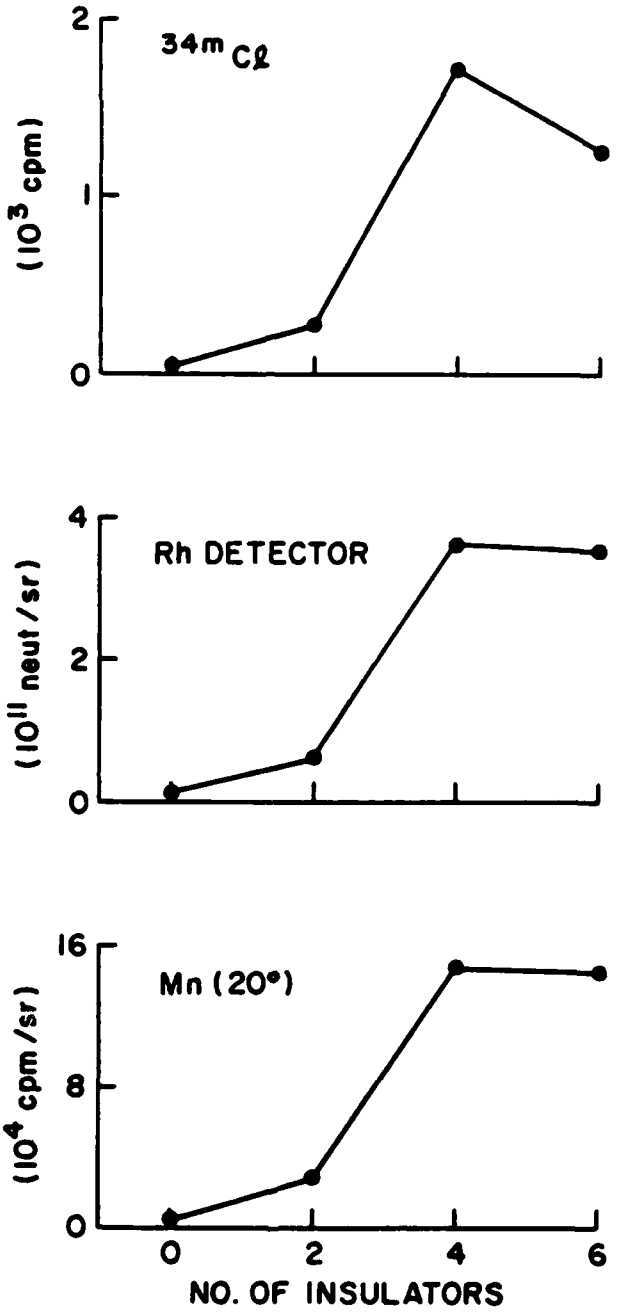

Fig. 33 — Dependence of the cathode activation (^{34m}Cl) and the $^{7}Li(p,n)^{7}Be$ neutron production (Rh and Mn detectors) on the number of prepulse insulators.

output and ^{34m}Cl production were observed. X-ray pinhole images indicated that the longer stalks were radiating along almost their entire length. This suggests that current is being conducted along the anode stalk to the aluminum support plate. Finally, three shots were taken with the anode foil placed directly on the support plate as indicated in Fig. 34. Shot 1 is identical to the previous shots except it has no anode stalk. Shot 2 has a CH_2 foil with no aluminum backing plate. Electron reflexing through the anode is possible in these two shots. Shot 3 has a 13-mm thick carbon plate behind a 3-mm thick aluminum support plate to suppress electron reflexing. The neutron yield on shot 3 is about one-half of that on shots 1 and 2 as indicated by the Mn activity at 90° and 20°. The Rh-counter activity scales with the 90° Mn-foil activity. The thicker anode on shot 3 attenuates the neutron intensity toward the Rh counter by about 20%. A comparison of the neutron yields at 20° and 90° indicates that the angular distribution is forward-peaked, as expected from the yield curves see Fig. 27. These shots indicate that if electron reflexing is enhancing the ion production, it is not the dominant effect.

V. SUMMARY OF RESULTS

The ion diode experiments on Aurora described in this paper have produced up to 5×10^{16} protons with energies of ~ 5 MeV and pulse durations of ≤ 150 ns. The corresponding average proton current exceeds 50 kA or 20% of the total current. These numbers give ~ 40-kJ energy in the proton beam. The ~ 20% ion generation efficiency compares favorably with computer simulations. In addition to protons, a carbon-ion component of greater than 3×10^{14} ions was extracted from the CH_2 anode foil. The energy of these ions was not determined, but their number may be larger depending on their charge-state and hence their energy.

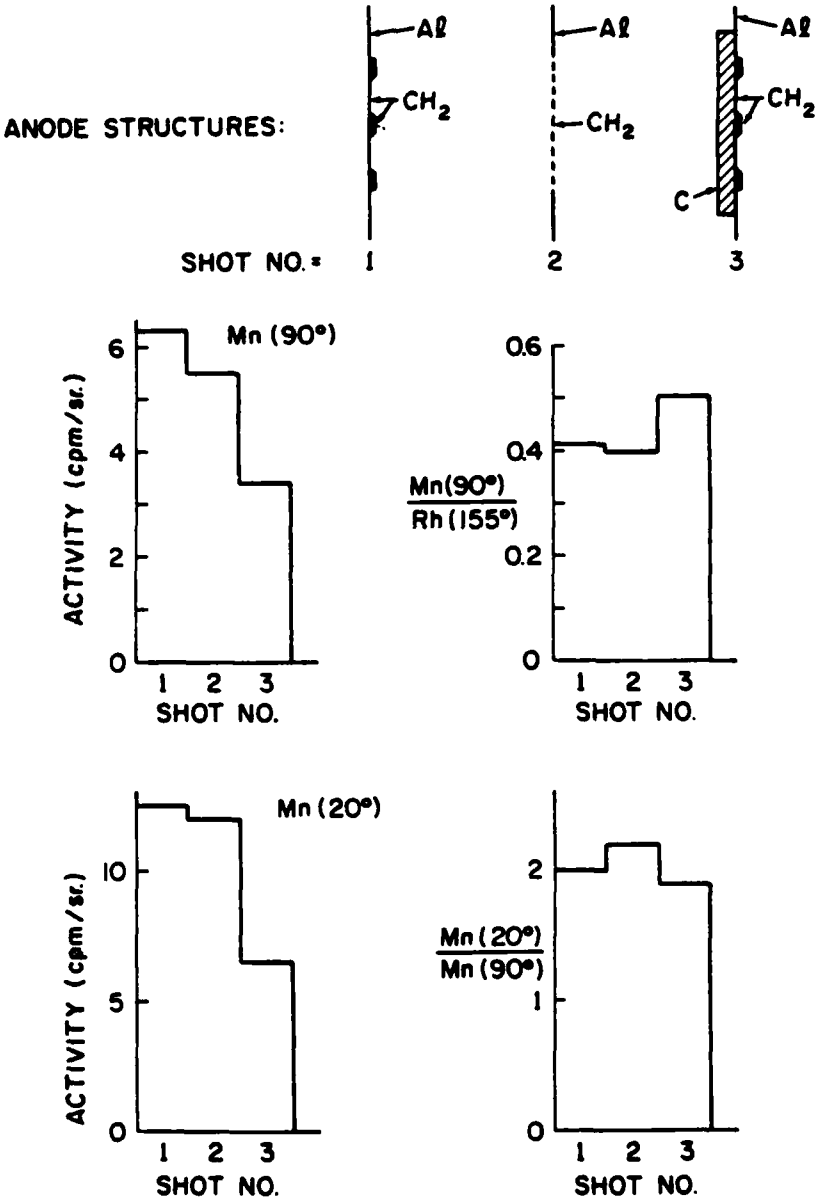

Fig. 34 — Comparisons of neutron measurements for three shots (1, 2 and 3) with different anode structures.

The enhancement of the ion production efficiency over the child-Langmuir limit may be due to increased electron lifetime in the diode. Previous experiments[1] with pinch reflex diodes have indicated enhanced ion production can result from electron reflexing through an anode foil. However, it was demonstrated that electron reflexing is not the dominant effect in the present experiments. Experimentally, the electron beam pinches on the anode, and the ions appear to originate primarily from a small area (2-4 cm^2) on the anode axis. Both of these results are supported by the computer simulation. Moreover, the simulation indicates that electrons in the diode undergo complicated figure-eight-like orbits. The relatively slow gap crossing due to electron ∇B drift motion is consistent with the observed ion efficiency.

Ion images and trajectories from the shadowbox measurements suggest that the ions have a relatively large divergence from a localized region on axis within the anode-cathode gap. This result suggests some focusing mechanism at work in the diode. These observations are consistent with the computer simulation.

Experiments with various prepulse switches and AK gaps indicate that the diode is sensitive to the prepulse voltage level (25 kV < Vpp < 200 kV). There was some indication that gap closure may have occurred late in the pulse for small AK gaps (< 4 cm) or for large prepulse levels. Such closure may be caused by anode or cathode plasmas produced by the prepulse which occurs ~ 1.5 μs before the main voltage pulse.

Several new diagnostic techniques were developed and applied successfully in the course of these experiments. The use of the $^7Li(p,n)^7Be$ reaction with LiCl targets as a neutron source for protons of ~ 5 MeV was demonstrated. Neutron intensity measurements by Mn-activation proved to

be a viable technique. An independent absolute calibration of this detection technique would be very useful. A nuclear reaction for detecting carbon ions, namely $^{27}Al(^{12}C,\alpha n)^{34m}Cl$, was used successfully. Additional measurements of the cross section for this reaction below 30 MeV are needed.

The continuing experimental program has focused on reversing the accelerator polarity to permit ion beam extraction, improvements of the ion and accelerator diagnostics, and improvement of power flow to the diode.

ACKNOWLEDGMENTS:

The authors would like to acknowledge a preliminary computer simulation performed by Roswel Lee which provided the impetus for performing the initial experiments as well as the invaluable technical assistance of J. Negri and T. Robinson at the Naval Research Laboratory and D. Whittaker, C. Casaers, T. Cassidy, A. Pourier and the entire Operations and Maintenance crew at the Harry Diamond Laboratories.

REFERENCES

1. G. Cooperstein, Shyke A. Goldstein, D. Mosher, R. J. Barker, J. R. Boller, D. G. Colombant, A. Drobot, R. A. Meger, W. F. Oliphant, P. F. Ottinger, F. L. Sandel, S. J. Stephanakis and F. C. Young, "NRL Light Ion Beam Research for Inertial Confinement Fusion", Fifth Workshop on Laser Interaction and Related Plasma Phenomena, Laboratory for Laser Energetics, Rochester, New York, November 5-9, 1979.

2. P. A. Miller, D. J. Johnson, T. P. Wright, and G. W. Kuswa, Comments Plasma Phys. 5, 95 (1979).

3. Shyke A. Goldstein and R. Lee, Phys. Rev. Lett. 35, 1079 (1975).

4. S. Stephanakis, J. R. Boller, G. Cooperstein, Shyke A. Goldstein, D. D. Hinshelwood, D. Mosher, W. F. Oliphant and F. C. Young, Bull. Am. Phys. Soc. 24, 1031, (1979).

5. G. Cooperstein, J. R. Boller, Shyke A. Goldstein, D. Mosher, W. F. Oliphant, S. J. Stephanakis, F. C. Young, R. D. Genuario and J. E. Maenchen, IEEE Conference Record-Abstract, 1980 Intl. Conf. on Plasma Science, Madison, Wisconsin (1980), p. 97.

6. D. G. Colombant, Shyke A. Goldstein, D. Mosher, Phys. Rev. Lett. 45, 1253 (1980).

7. D. Mosher, D. G. Colombant, Shyke A. Goldstein, to be published in Comments on Plasma Physics and Controlled Fusion, 1980.

8. S. E. Graybill, Harry Diamond Laboratories Technical Report No. 1862, (1978).

9. B. Bernstein and I. Smith, IEEE Trans. Nucl. Sci. 20, 294 (1973).

10. F. C. Young, IEEE Trans. on Nucl. Sci. NS-22, 718 (1975).

11. F. C. Young and S. J. Stephanakis, NRL Memorandum Report No. 3104, August 1975.

12. G. Huttlin, Harry Diamond Laboratories Technical Report No. 22900-80-1.

13. H. W. Koch and J. W. Motz, Rev. Mod. Phys. 31, 4 (1959).

14. H. Liskien and A. Paulsen, Atomic and Nuclear Data Tables 15, 57 (1975).

15. H. H. Andersen and J. F. Ziegler, The Stopping and Ranges of Ions in Matter, Vol. 3 (Pergamon Press, NY, 1977).

16. I. Landenbauer-Bellis, I. L. Preiss and C. E. Anderson, Phys. Rev. 125, 606 (1962).

17. F. C. Young, S. J. Stephanakis, and D. Mosher, J. Appl. Phys. 48, 3642 (1977).

APPENDIX II

This appendix has been submitted to the Journal of Applied Physics

PINCH-REFLEX-DIODE SCALING ON THE AURORA PULSER

R.A. Meger* and F.C. Young

Naval Research Laboratory

Washington, DC 20375

Abstract

A pinch-reflex ion diode has been operated on the Aurora pulser in positive polarity at impedances ranging from 10 to 35 Ω. Ion-generation efficiencies of 20% were observed with ion energies ranging from 2.5 to 5 MeV. The ion current scaled inversely with the anode-cathode gap, and a peak value of 65 kA was measured for the smallest gap. A plasma erosion switch was used to decrease prepulse and gap closure in the diode.

*JAYCOR, Alexandria, VA 22304.

I. Introduction

Progress in the field of intense pulsed light ion beam generation has been rapid over the last few years and high power ion beams are being investigated at several laboratories.[1] The Naval Research Laboratory (NRL) has concentrated its efforts on the pinch-reflex type of ion diode.[2] Experiments with this diode have been performed on the Gamble I and Gamble II accelerators at NRL,[3] the PITHON accelerator at Physics International,[4] and the Aurora accelerator at the Harry Diamond Laboratories.[5] With these machines a large range of diode impedances and ion energies have been investigated. Ion beams have been produced with diodes operating at impedances of 1 to 35 Ω. Ion-generation efficiencies (ion current/diode current) of up to 60% have been achieved at the lower-impedance level. For higher-impedance diodes, efficiencies of up to 20% at 20 Ω and 5 MV have been measured. The dependance of the ion-beam output on various pinch-reflex-diode parameters is being studied in order to understand the scaling of such diodes with impedance and voltage.

The Aurora pulser is normally operated at high impedance (35 Ω) in negative polarity for bremsstrahlung production.[6] Ion-diode experiments in negative polarity on this machine have been reported.[5] Since then the accelerator has been modified to operate in positive-polarity. In this paper experiments on Aurora in positive polarity using a pinch-reflex-diode geometry are reported with emphasis on scaling of the ion-generation efficiency in the 10 to 35 Ω impedance regime. First, a simple scaling relationship for the ion efficiency of pinch-reflex diodes is presented. Then the experimental measurements and results are described. In particular, it is shown that the diode

efficiency is 20% at 10 Ω and 2.5 MV. Finally, the experimental results are compared with the expected scaling of the ion-beam-generation efficiency.

II. Ion-Generation-Efficiency Scaling

If a steady-state voltage is placed across a diode where electrons and ions are freely emitted from the cathode and anode surfaces, an equilibrium charge flow is established. This so called Child-Langmuir bipolar current scales as $V^{3/2}/D^2$ at nonrelativistic electron voltages where V is the diode voltage and D is the diode gap. The current is made up of electrons and ions streaming in opposite directions. In a planar diode most of the current is due to electron flow while the fraction of the current carried by ions depends on the electron to ion mass ratio. In the non-relativistic limit the relative current densities are given by

$$\frac{J_i}{J_e} = \left(\frac{M_e}{M_i}\right)^{1/2} \tag{1}$$

where J_i and J_e are the ion and electron current densities and M_e and M_i are the electron and ion masses. This calculation has been extended by Poukey to bipolar flow with relativistic electrons.[7] It shows that the relative ion flux density should increase with diode voltage according to

$$\frac{J_i}{J_e} = \left(\frac{M_e}{2M_i}\right)^{1/2} (\gamma + 1)^{1/2}, \tag{2}$$

where γ is the relativistic factor for electrons at the full diode

voltage. Physically the γ dependence is due to electron-velocity saturation at relativistic energies. This means that for a bipolar diode ~2.3% of the diode current would be in protons for non-relativistic voltages versus 5.4% for the same planar diode operating at 5 MV when the electrons are relativistic.

Even with the current enhancement due to relativistic voltages as shown in Eq. 2, such ion-beam generators are relatively inefficient. One method of increasing the ion-generation efficiency beyond this level is to use a pinch-reflex-diode geometry as discussed by Goldstein and Lee.[8] Such a diode geometry is shown schematically in Fig. 1. A cylindrical hollow cathode and thin planar anode foil force electrons to travel a longer distance than ions to cross the diode gap. Electrons emitted from the cathode are bent toward the axis by their self magnetic fields and may reflex through the anode foil on their way to the center stalk. For such a diode the relative ion current density to first order is given by

$$\frac{J_i}{J_e} = \left(\frac{M_e}{2M_i}\right)^{1/2} (\gamma + 1)^{1/2} \frac{R}{D} \qquad (3)$$

where R is the cathode radius and D is the diode gap. For large R/D the pinch-reflex geometry can yield an order of magnitude increase in ion efficiency. Diodes with ion efficiency approaching 50% provide useful sources for intense ion beams.

III. Experimental Procedure

These experiments were performed on the Aurora accelerator operated in positive polarity to allow direct diagnostic access to the ion

beam. The Marx generator was charged to +90 kV out of a possible charge of +120 kV. The lower charge level was used to minimize possible damage to the Blumlein in positive polarity and to limit the voltage across the diode insulator. Only one of four vacuum transmission lines on the generator was used. Copper sulphate dummy loads were installed in the oil on the three unused lines.

The output end of the transmission line on the accelerator with the diode is shown in Fig. 2. The Blumlein output breaks down an oil prepulse switch putting the voltage pulse across the cylindrical insulator tube. This pulse propagates 7 meters along a magnetically insulated 50-Ω coaxial transmission line. The 1.2-m outer diam coaxial conductor is reduced to a 25-cm diam vacuum chamber at the front end while the 58-cm inner diam conductor is tapered to 10 cm. The ion diode is mounted one meter into this smaller diam coax. A flashover prepulse switch mounted on the inner conductor, as shown in Fig. 2, lowers the ~200-kV prepulse on the transmission line to less than 50 kV. On some shots a plasma erosion switch (PES) was used to further suppress the prepulse as well as to sharpen the risetime of the main pulse.

A cross sectional view of the PES system is shown in Fig. 3. The plasma guns for this system were supplied by Sandia National Laboratory[9] and similar systems have been used elsewhere.[10] Several microseconds before the main power pulse arrives, the plasma guns inject columns of carbon plasma with electron densities in the 10^{11}-10^{12} cm^{-3} range into the coaxial vacuum transmission line. These columns short the inner and outer conductors by providing a low impedance shunt in parallel with the ion diode located downstream. This protects the ion-diode load from the machine prepulse as well as diverting some fraction of the main voltage

pulse. After the plasma columns have transmitted a certain amount of charge, the ion background density in the columns erodes near the outer injection aperture leading to sheath formation and a rapid decrease in the current diverted through the columns. The columns act as an opening switch, after which the remainder of the power pulse is delivered to the diode load. The prepulse and the leading edge of the main pulse have been shunted, and the voltage risetime across the load becomes the PES opening time which under most circumstances is less than the normal accelerator voltage risetime. The fraction of the main voltage pulse which is diverted through the erosion switch can be controlled by adjusting the injected plasma density. This is done by altering the distance of the plasma guns from the center conductor and the firing time of the guns.

The ion diode used in these experiments is shown in Fig. 4. The anode consists of a 127-μm thick polyethylene (CH_2) foil stretched on a 12-cm diam aluminum ring and supported by a thin-wall (0.17 mm) aluminum tube. The cathode is a 10-cm inner diam, 6.4-mm thick aluminum cylinder with a rounded end. On some shots a 2-μm thick aluminized foil (Kimfol*) is located inside the cathode followed by an aluminum witness plate coated with LiCl for neutron diagnostics. A Rogowski coil is mounted behind the cathode to measure the ion current incident on the Kimfol. This probe remains at ground potential with the generator configured in positive polarity.

The locations of the accelerator electrical diagnostics are shown in Fig. 2. The resistive voltage divider V_T, located in oil near the insulating tube, provides the most reliable voltage monitor. Capacitive

*Available from Kimberly Clark Corp., Lee, Mass. 01238

voltage probes located in the vicinity of V_A in the magnetically-insulated transmission line suffer from electron emission or collection and do not provide useable data. Resistive current shunts located on the outer conductor provide reliable signals but do not measure current due to electrons flowing in the vacuum along the surface of the outer conductor. The magnitude of such electron current is expected to be small at the relatively low electric fields present in the large diam coax region.

The electron and ion-beam diagnostics used in the experiment are shown in Fig. 5. These are similar to the previous negative-polarity experiments.[5] Time integrated x-ray emission from the diode was imaged with a pinhole camera, while a scintillator-photodiode measured the time resolved x-ray signal. The ion diagnostics are based primarily on measurements of neutrons from the $^7Li(p,n)^7Be$ reaction resulting from proton bombardment of the LiCl target. Neutron intensities were measured with a Rh-activation detector[11] and with Mn-activation detectors.[12] Neutron energies were measured with the time-of-flight (TOF) technique for flight paths of 10 to 15.2 meters in the forward direction. These energy measurements were used to determine the ion voltage for the diode.

IV. Results

Approximately 50 shots have been taken with anode-cathode (AK) gaps ranging from 1.5 to 5.5 cm with and without the plasma erosion switches. Pinching of the electron-beam on the anode axis as in negative-polarity experiments[5] was confirmed by x-ray images from the pinhole camera. For a 2.0-cm AK gap, the diode operated at 2.5 MeV and 10 Ω

10 Ω (inferred from neutron TOF and total current measurements), while for a 5-cm AK gap the diode operated at 5 MeV and 35 Ω.

The large variation of the diode load impedance modified the power flow in the accelerator significantly. At low impedance the mismatch between the diode and the accelerator limited the amount of power delivered to the load. In addition the voltage measured across the insulator tube was found to be dependent on the load impedance. Figure 6 shows the behavior of the tube voltage for two shots with AK gaps of 5.5 cm and 3.0 cm. The large-AK-gap shot (No. 3057) ran at a higher tube voltage and impedance than the smaller-AK-gap shot (No. 3509). In general shots with lower peak tube voltage had longer-duration voltage pulses. This trade off between high voltage and pulse duration is demonstrated in Fig. 7 where the peak tube voltage (V_T) is plotted against the full-width-at-half-maximum (FWHM) of the voltage pulse for many shots with different AK gaps. This behavior of the tube voltage may be a consequence of the insulator design. The insulator was built for negative-polarity operation and can withstand 150-ns FWHM, 12-MV peak voltage pulses normally used in the bremsstrahlung mode. Using the same insulator for positive polarity degrades its voltage standoff by about a factor of two.[13] The insulator flashover process is time and voltage dependent with higher voltages giving faster breakdown as indicated by the experimental data in Fig. 7. An attempt to suppress insulator flashover was made by placing a 120-Ω copper sulphate resistor across the insulator stack in parallel with the diode load. Shots with this resistor in place are indicated by open circles in Fig. 7. The resistor did cause the pulse duration to increase, but the dependence of the peak tube voltage on the duration of the tube voltage is still

evident. Thus for low impedance diodes the accelerator coupling limited power flow while at higher impedance the insulator flashover limited power flow. In all cases the peak power was less than 1 TW.

The dependences of the peak shunt current, I_A, (see Fig. 2) and peak Rogowski-coil current, I_R, (see Fig. 3) on the AK gap are displayed in Figs. 8 and 9 respectively. In both cases, an inverse relationship between current and AK gap is observed. The shunt current measures the total diode current except for vacuum electron flow past the shunt. This electron flow is expected to be small in the large diameter vacuum coax region where the shunt resistor is located. The Rogowski coil measures the net ion current passing through the coil and does not record current lost in front of the coil or current shielded by co-moving electrons. Witness plate and surface damage in the diode indicate that ions striking the cathode before the Rogowski coil represent < 10% of the total ion current. Computer simulations[14] of the behavior of electrons and ions in the diode suggest that co-moving electrons could shield as much as 20% of the total ion current.

The PES system was operated on about half of the shots in this experiment. The amount of plasma in the erosion-switch gap differed from shot to shot depending on the plasma-gun timing. The erosion-switch operation did not affect the inverse dependence of the shunt current on the AK gap (see Fig. 8). On some shots the plasma density was increased so that most of the pulse was shunted through the PES system. On these shots the peak shunt-current signal approached 300 kA independent of the AK gap.

The maximum Rogowski current of 65 kA peak value was measured at the smallest AK gap of 2 cm (see Fig. 9). Operation of the PES system

did not seem to affect the inverse dependence of the Rogowski current on the AK gap but did affect the shape of the Rogowski-current signal. With the PES system operating, the onset of the ion-current signal was delayed by ~50 ns, and the signal risetime was sharpened measurably. These observations are consistent with suppression of plasma formation in the diode by the PES system early in the voltage pulse.

The diode voltage was inferred from neutron TOF measurements using the $^{7}Li(p,n)^{7}Be$ reaction. Neutron TOF traces for three different AK gaps are shown in Fig. 10a. As the AK gap is reduced, the neutron signal is delayed in time and is less intense. Measureable neutron traces were observed at small AK gaps by decreasing the neutron flight path. The neutron flight time was determined by measuring from the peak of the x-ray pulse to the leading edge of the neutron signal (50% of the peak) and correcting for the x-ray flight time. This measurement corresponds to the most energetic neutrons and consequently the most energetic protons from the diode. Proton energies extracted from such measurements using the $^{7}Li(p,n)^{7}Be$ reaction kinematics[15] are shown in Fig. 10b. These measurements have an uncertainty of ± 0.2 MeV due to the uncertainty in time between the x-ray and neutron signals. This measurement is difficult below 3 MeV because this reaction has a neutron-production threshold of 1.9 MeV. The dependence of the proton energy on AK gap is not sensitive to the use of the PES system (see Fig. 10b).

The proton intensity may be deduced from the measured neutron yield for comparison with the Rogowski-current measurements. Yields of 1 to 2 x 10^{11} neut/sr at 45^{0} are measured for AK gaps of 2 to 5 cm. This yield is approximately constant as the AK gap is increased because the larger

AD-A111 663 JAYCOR ALEXANDRIA VA F/G 20/7
ION DIODE RESEARCH ON THE AURORA ACCELERATOR.(U)
JAN 82 R A MEGER N00014-81-C-2093
UNCLASSIFIED JAYCOR-J207-82-001FR NL

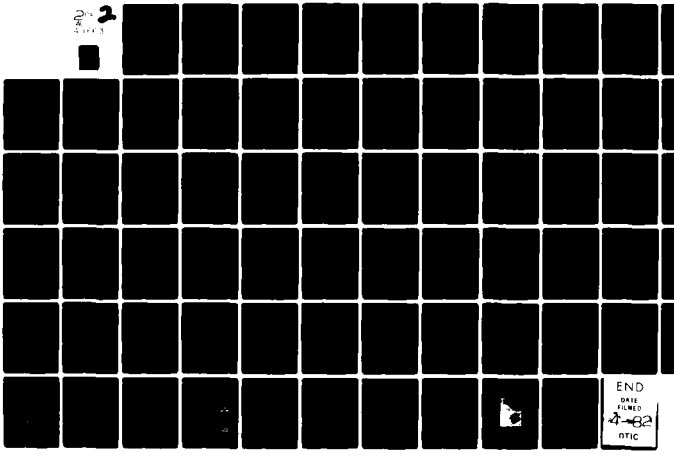

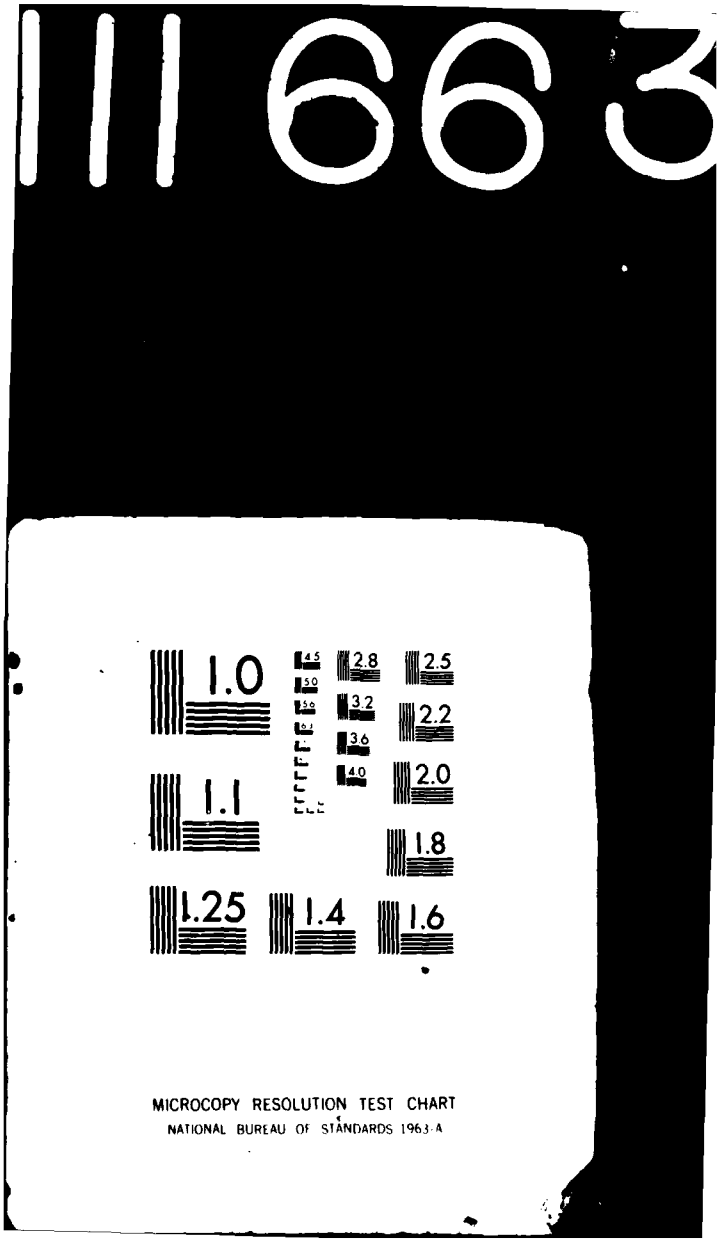
111663
1.0
1.1
1.25
1.4
1.6
2.8
3.2
3.6
4.0
2.5
2.2
2.0
1.8
MICROCOPY RESOLUTION TEST CHART
NATIONAL BUREAU OF STANDARDS 1963-A

yield expected from increasing proton energy is compensated for by a decreasing proton current. The largest yield in these experiments is 2 x 10^{12} neutrons/pulse into 4π, which is only 20% of that obtained in the negative-polarity experiments.[5] Power levels in this experiment were significantly less than in the negative-polarity experiments. The proton intensity is determined from the neutron yield by using thick-target yields[5] at 45^0 for the $^7Li(p,n)^7Be$ reaction and the proton energy determined from neutron TOF. Intensities range from 5 x 10^{15} protons for a 5-cm AK gap to 2 x 10^{16} protons for a 2-cm AK gap. These intensities correspond to proton currents of 8 kA and 30 kA respectively for a pulse duration of 100 ns. These currents are approximately one-half of the Rogowski-current measurements given in Fig. 9. Such a difference is consistent with average currents for neutron measurements compared with peak values from Rogowski-coil measurements.

To provide a representative diode impedance, the diode voltage, derived from a neutron TOF measurement, is divided by the peak diode current, as given by the shunt current (I_A). This impedance increases from about 10 Ω at the smallest AK gap to 35 Ω at the largest AK gap. The ion-generation efficiency is measured by the ratio, I_R/I_A. This ratio is 20% for a 2.5-MV, 10 Ω diode with 2-cm AK gap. If the gap is increased to 5 cm, the ion efficiency is still 20% but the diode operates at 5 MV and 35 Ω. These results are similar to negative-polarity experiments for which the ion efficiency was 20% at 5 MV and25 Ω. [5] However, the negative-polarity experiments were carried out at a higher power level of ~1.2 TW.

In order to test the scaling of the ion-beam-generation efficiency, as described in Sec. II, the peak ion current from the Rogowski coil was

normalized to the electron current ($I_e = I_A - I_R$) and to the relativistic factor $(\gamma + 1)^{1/2}$ where $\gamma = [V_p/(M_e c^2) + 1]$ and V_p is the proton energy derived from neutron TOF. The dependence of these normalized quantities on the AK gap is shown in Fig. 11. Shots with the PES system are consistent with an inverse dependence on the AK gap as would be expected from the theory described in Sec. II. The non-PES shots fall to the right of the PES data in Fig. 11. Comparison of these data suggests that without the PES system, anode and cathode plasmas formed early in time result in a 1-cm greater closure of the AK gap than shots with the PES system. Gap closure of 1 cm without the PES is possible due to anode and cathode plasma formation either from the accelerator prepulse or during the rising portion of the diode voltage pulse. The data shown in Fig. 11 correspond to a value of $\frac{I_R}{I_e}(\gamma + 1)^{-1/2} = 0.09$ for a 2.5-cm AK gap using peak values for the various terms. This value is 2.5 times larger than that predicted for R/D scaling of the pinch-reflex diode. Such enhancement factors are consistent with previous experimental results on the other accelerators.[16]

V. Summary

In these first experiments performed in positive polarity on the Aurora accelerator the Marx generator and Blumlein operated satisfactorily at +90 KV Marx charge. A voltage dependent shortening of the pulse across the diode-insulator stack was observed and may be related to insulator flashover. This behavior is dependent on the diode impedance as determined by the AK gap in the pinch-reflex-diode geometry used in these experiments.

Plasma erosion switches were used in these experiments to eliminate

prepulse at the ion diode. These switches appeared to decrease AK gap closure by 1 cm, thereby allowing smaller AK gaps to be used without gap closure shorting the pulse prematurely.

Ion beams with peak net currents of 65 kA were measured for a 10-Ω, 2.5-MV diode configuration. The ion current appears to scale inversely with the AK gap. The ion efficiency is constant at 20% over the 10 to 35 Ω impedance range of this experiment. This effect may be due to the poor coupling of the low-impedance pinch-reflex diode to the 50-Ω transmission line of the Aurora accelerator which limited peak power levels to less than 1 TW. The ion efficiency of 20% is 2.5 times larger than that expected from pinch-reflex-diode theory and agrees with other pinch-reflex-diode experiments and numerical simulations.

Acknowledgements

The success of this experiment required the support and cooperation of many personnel. The conversion of the Aurora pulser to positive polarity was carried out under the direction of A. Stewart of the Harry Diamond Laboratories (HDL). The modifications to Aurora and the operation of the machine were ably handled by the Operations and Maintenance Staff of HDL under the supervision of A. Pourier or D. Lindsey. J. Shipman of Sachs-Freeman assisted in evaluating power-flow problems in positive polarity. Technical assistance with the experimental setup and data acquisition involved the support of the following personnel: S. Graybill, D. Whittaker, K. Kerris, C. Casaers, T. Cassidy and R. Bixby of HDL; R. Boller, J. Condon and T. Robinson of NRL; and D. Bacon of JAYCOR. Guidance and theoretical support were provided by G. Cooperstein of NRL, Shyke Goldstein of JAYCOR, and A. Drobot of SAI. C.W. Mendel, Jr., of Sandia National Laboratory provided plasma-erosion-switch hardware and technical support for their use. The encouragement and support of R. L. Gullickson of the Defense Nuclear Agency is also gratefully acknowledged. This work was supported by the Defense Nuclear Agency.

References

1. P.A. Miller, D.J. Johnson, T.P. Wright, and G.W. Kuswa, Comments Plasma Phys. 5, 95 (1979).
2. G. Cooperstein, Shyke A. Goldstein, D. Mosher, R.J. Barker, J.R. Boller, D.G. Colombant, A. Drobot, R.A. Meger, W.F. Oliphant, P.F. Ottinger, F.L. Sandel, S.J. Stephanakis, and F.C. Young, in Laser Interaction and Related Plasma Phenomena, edited by H. Schwarz, H. Hora, M. Lubin and B. Yaakobi (Plenum, New York, 1981) Vol. 5, p. 105.
3. S.J. Stephanakis, D. Mosher, G. Cooperstein, J.R. Boller, J. Golden, and Shyke A. Goldstein, Phys. Rev. Lett. 37, 1543 (1976).
4. S.J. Stephanakis, J.R. Boller, G. Cooperstein, Shyke A. Goldstein, D.D. Hinshelwood, D. Mosher, W.F. Oliphant, F.C. Young, R.D. Genuario, and J.E. Maenchen, Bull. Am. Phys. Soc., 24, 1031 (1979); and J. Maenchen, R. Genuario, R. Stringfield, J. Kishi, G. Cooperstein, D. Mosher, S. Stephanakis, F. Young, S. Goldstein and D. Hinshelwood, Bull. Am. Phys. Soc. 25, 945 (1980).
5. R.A. Meger, F.C. Young, A.T. Drobot, G. Cooperstein, Shyke A. Goldstein, D. Mosher, S.E. Graybill, G.A. Huttlin, K.G. Kerris and A.G. Stewart, J. Appl. Phys. 52, 6084 (1981).
6. B. Bernstein and I. Smith, IEEE Trans. Nucl. Sci. NS20, 294 (1973).
7. J.W. Poukey, Appl. Phys. Lett. 26, 145 (1975).
8. Shyke A. Goldstein and Roswell Lee, Phys. Rev. Lett. 35, 1079 (1975).
9. C.W. Mendel, Jr., D.M. Zagar, G.S. Mills, S. Humphries, Jr., and

S.A. Goldstein, Rev. Sci. Instrum. 51, 1641 (1980).

10. C.W. Mendel, Jr., and S.A. Goldstein, J. Appl. Phys. 48, 1004 (1977).

11. F.C. Young, IEEE Trans. Nucl. Sci. NS-22, 718 (1975).

12. R.A. Meger, F.C. Young, A.T. Drobot, G. Cooperstein, Shyke A. Goldstein, D. Mosher, S.E. Graybill, G.A. Huttlin, K.G. Kerris, and A.G. Stewart, NRL Memorandum Report No. 4477, March, 1981 (unpublished).

13. I.D. Smith, Intl. Symposium on High Voltages in Vacuum, MIT, Cambridge, MA, Oct. 19-21, 1966 (unpublished).

14. A.T. Drobot, R.A. Meger, and Shyke A. Goldstein, Bull. Am. Phys. Soc., Ser. II, 25, 900 (1980).

15. H. Liskien and A. Paulsen, At. Nucl. Data Table 15, 57 (1975).

16. S.J. Stephanakis, private communication.

Figure Captions

Fig. 1. Pinch-reflex-diode schematic with conceptual electron and ion trajectories.

Fig. 2. One arm of the Aurora pulser from the oil region to the ion diode. The location of the resistive voltage divider (V_T), the current shunt (I_A), the flashover prepulse switch and the plasma-erosion-switch system are shown.

Fig. 3. Cross-sectional schematic of the plasma-erosion-switch system.

Fig. 4. Details of the ion diode used in positive polarity.

Fig. 5. Schematic arrangement of the x-ray and neutron diagnostics.

Fig. 6. Measured tube voltages (V_T) for a 5.5-cm-AK-gap shot (No. 3057) and for a 3.0-cm-AK-gap shot (No. 3059).

Fig. 7. Dependence of the peak value of the tube voltage (V_T) on the full-width-at-half-maximum (FWHM) of the tube voltage. Shots with a 120-Ω resistor in parallel with the insulator are plotted as open circles.

Fig. 8. Dependence of the peak value of the shunt current (I_A) on the AK gap. Shots with the PES system operating are plotted as open circles.

Fig. 9. Dependence of the peak value of the Rogowski-coil current (I_R) on the AK gap. Shots with the PES system operating are plotted as open circles. The solid curve represents an inverse dependence on the AK gap.

Fig. 10. (a) Neutron TOF signals measured for AK gaps of 5.5, 4.0 and 3.0 cm.

(b) Dependence of the proton energy, determined from neutron TOF, on the AK gap. Shots with the PES system operating are plotted as open circles.

Fig. 11. Dependence of the peak Rogowski-coil current, normalized according to Eq. 2, on the AK gap. Shots with the PES system operating are plotted as open circles. The solid curve represents an inverse dependence on the AK gap.

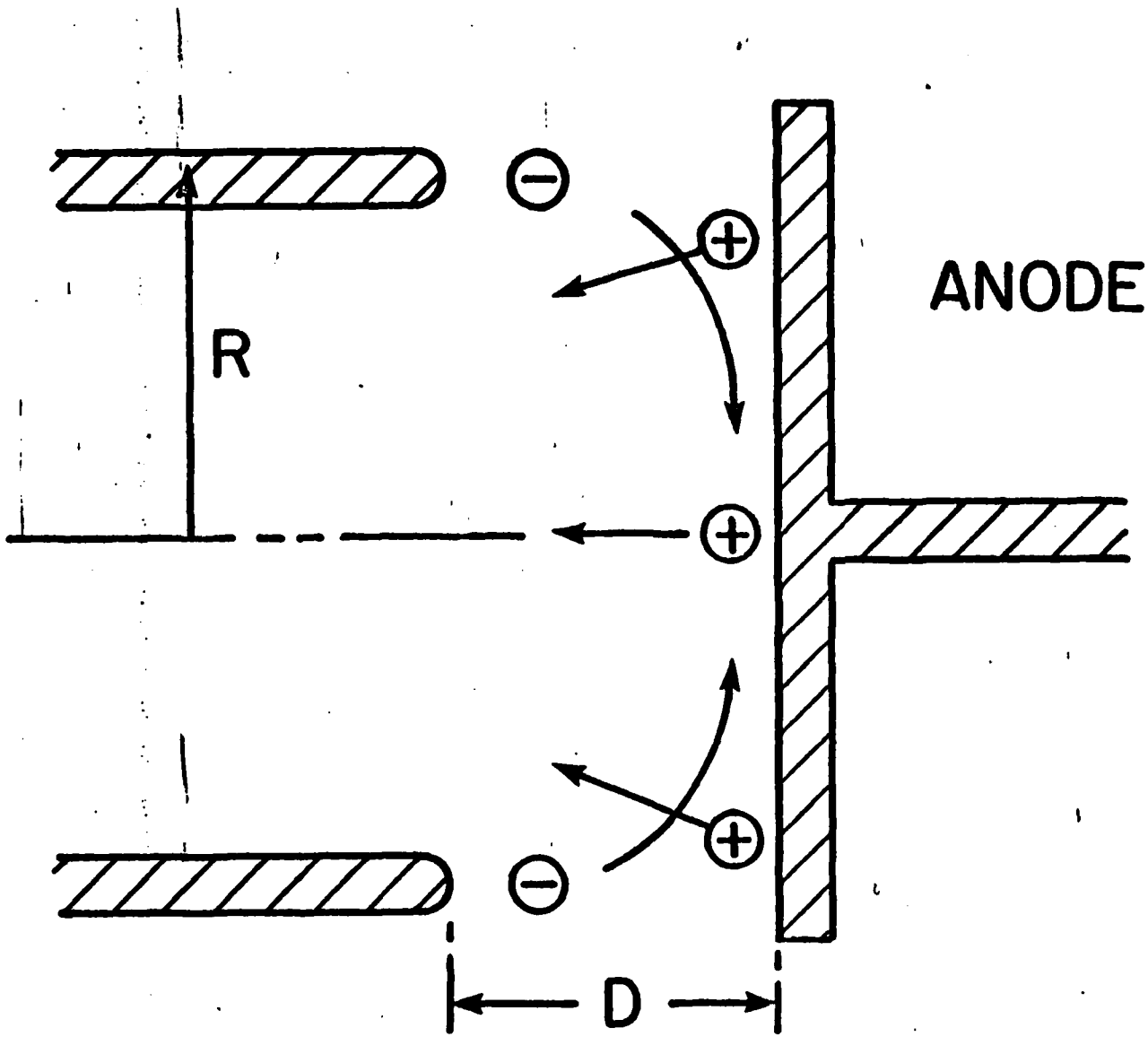
ANODE
R
D

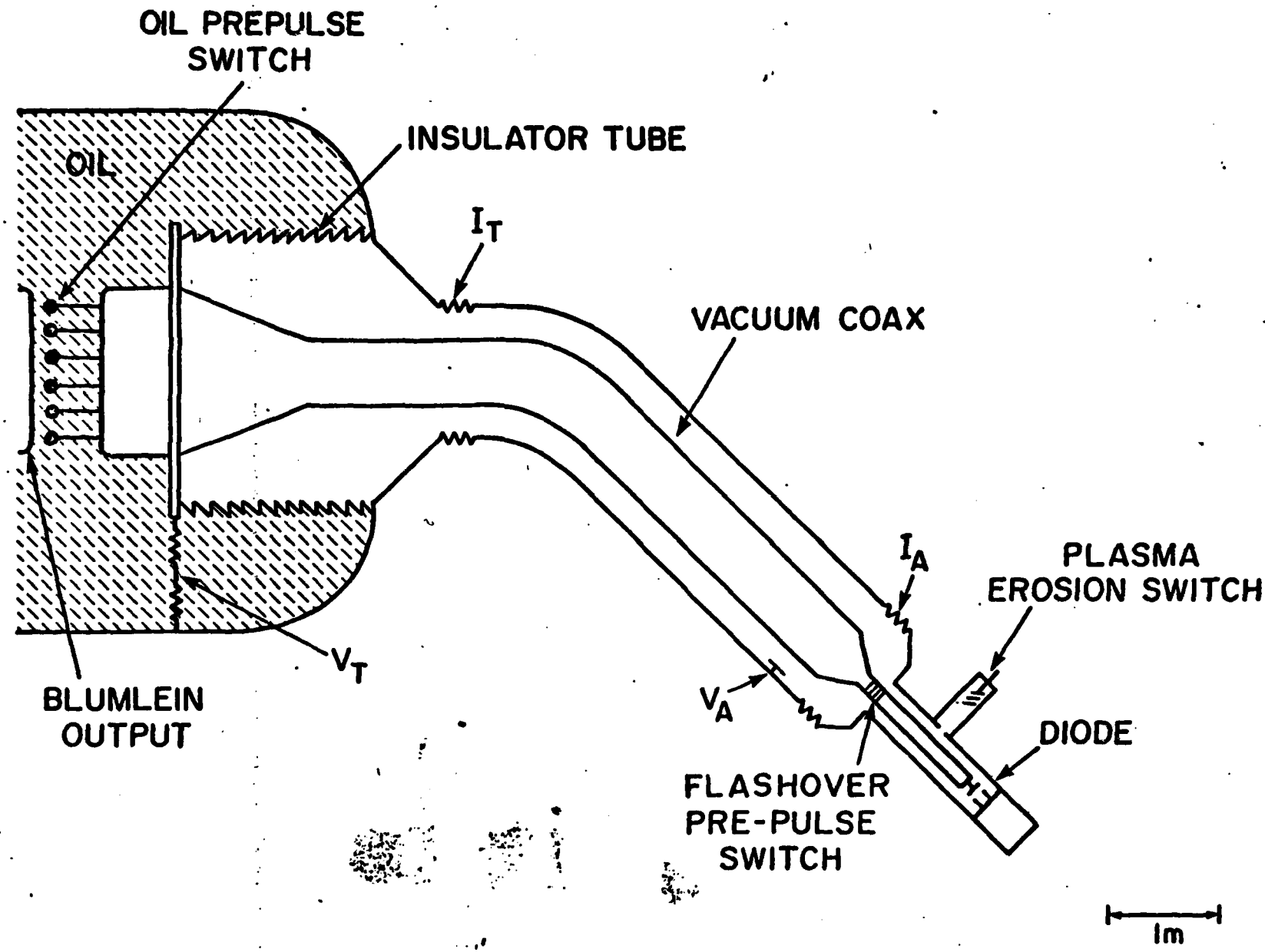
OIL PREPULSE SWITCH
INSULATOR TUBE
OIL
I_T
VACUUM COAX
I_A
PLASMA EROSION SWITCH
V_T
BLUMLEIN OUTPUT
V_A
DIODE
FLASHOVER PRE-PULSE SWITCH
1m

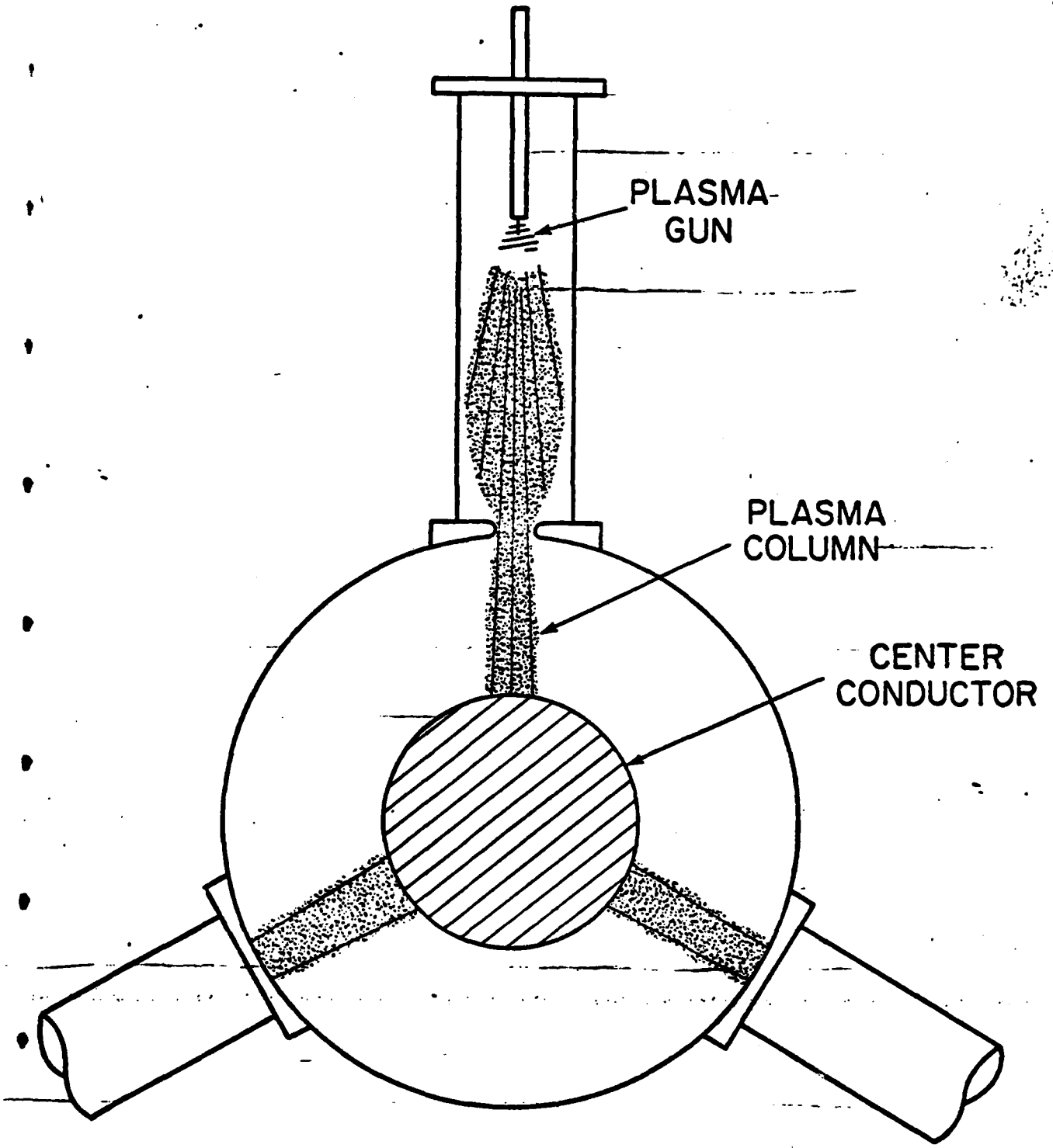
PLASMA-
GUN
PLASMA
COLUMN
CENTER
CONDUCTOR

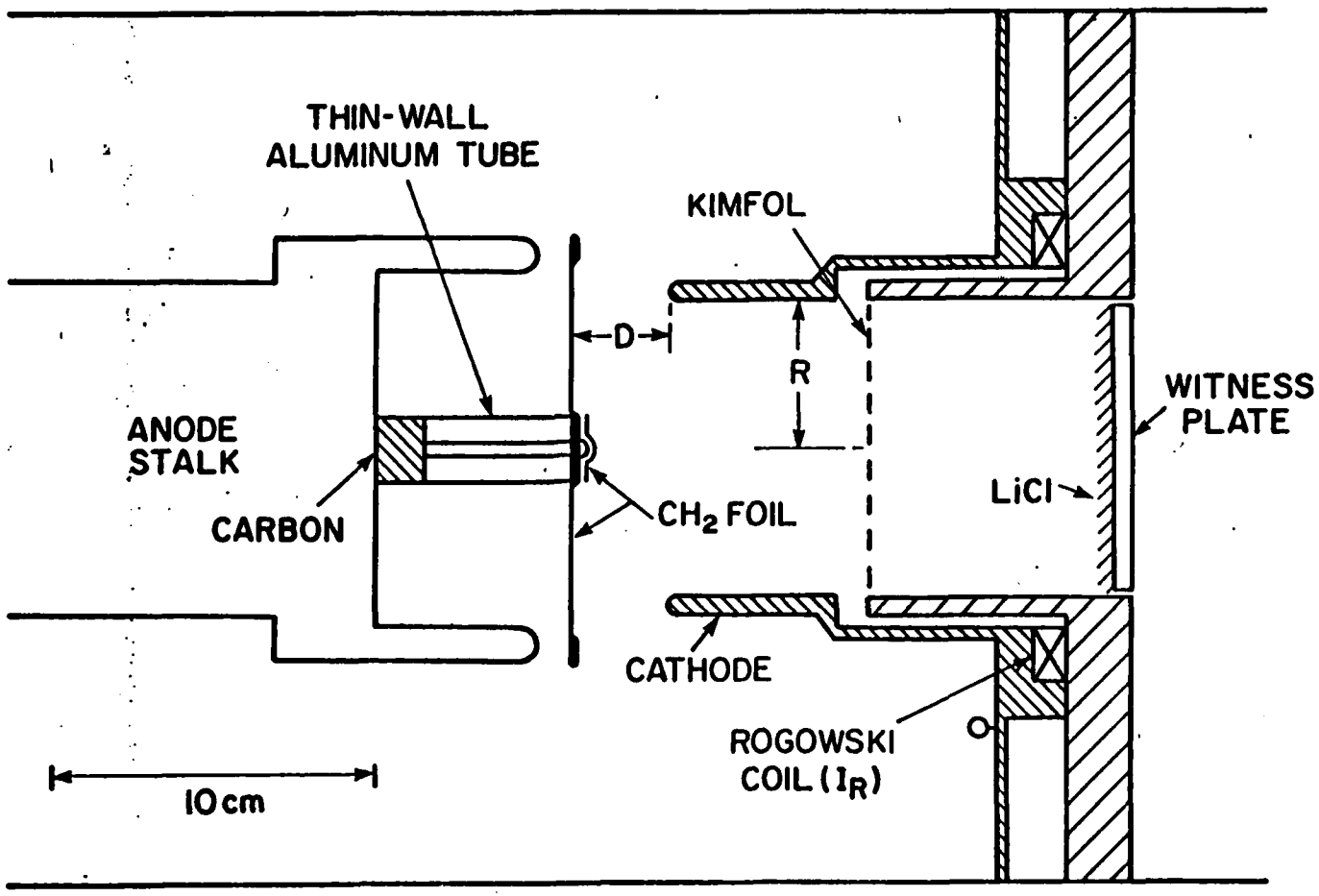
THIN-WALL
ALUMINUM TUBE
KIMFOL
D
R
WITNESS
PLATE
ANODE
STALK
CARBON
CH_2 FOIL
LiCl
CATHODE
ROGOWSKI
COIL (I_R)
10 cm

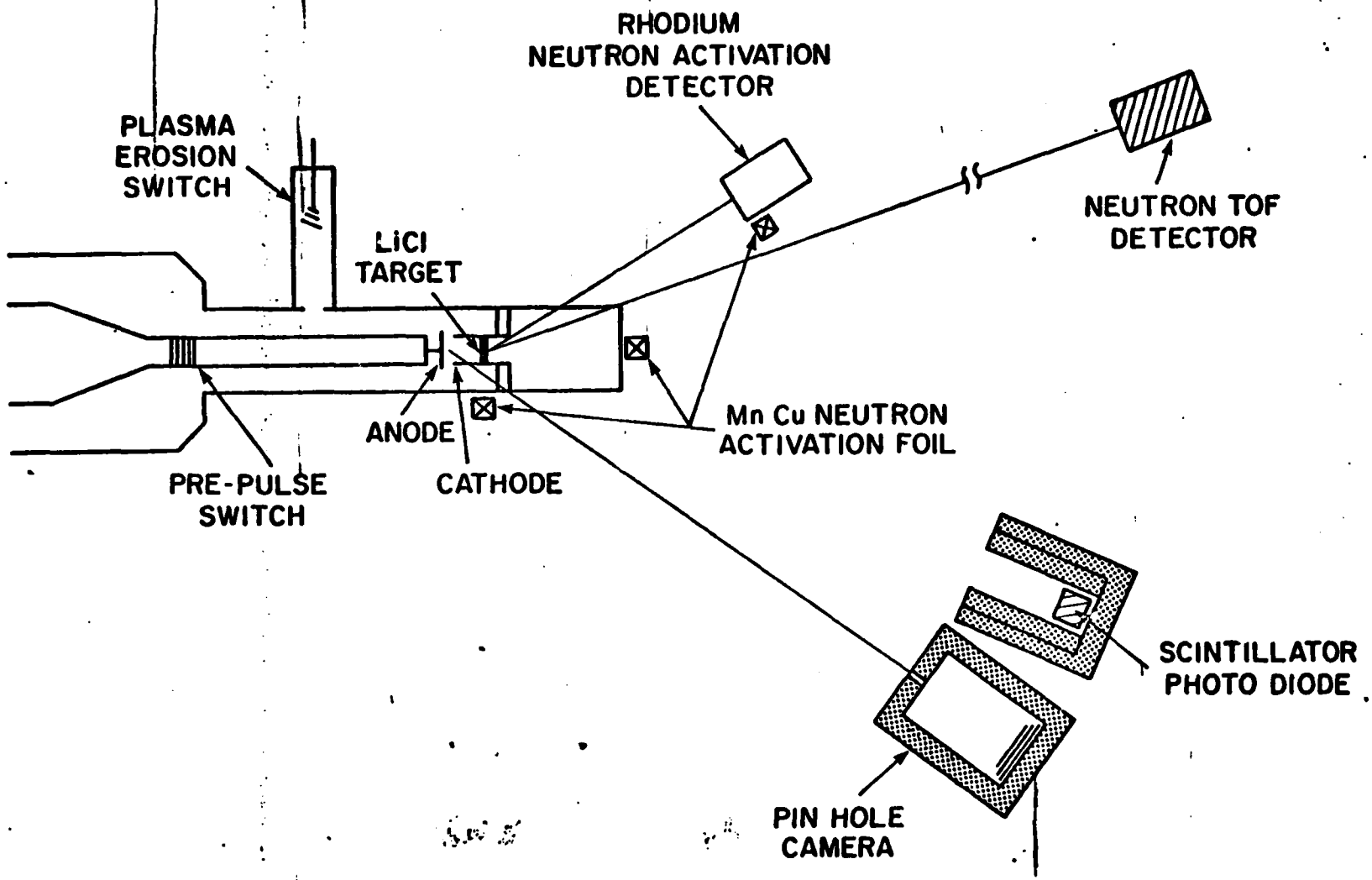
RHODIUM
NEUTRON ACTIVATION
DETECTOR
PLASMA
EROSION
SWITCH
NEUTRON TOF
DETECTOR
LiCl
TARGET
ANODE
Mn Cu NEUTRON
ACTIVATION FOIL
PRE-PULSE
SWITCH
CATHODE
SCINTILLATOR
PHOTO DIODE
PIN HOLE
CAMERA

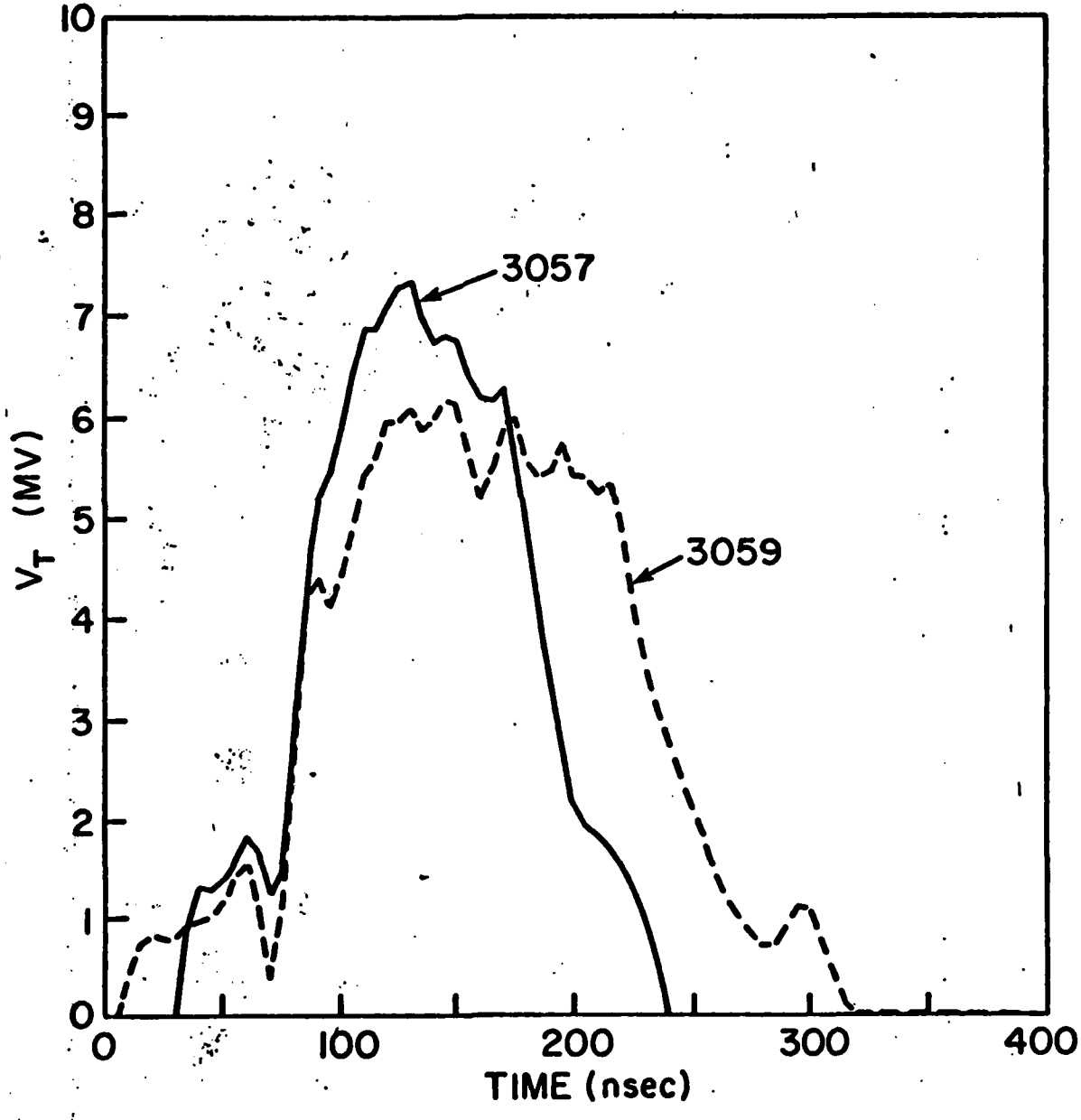
10
9
8
7
6
5
4
3
2
1
0
V_T (MV)
3057
3059
0
100
200
300
400
TIME (nsec)

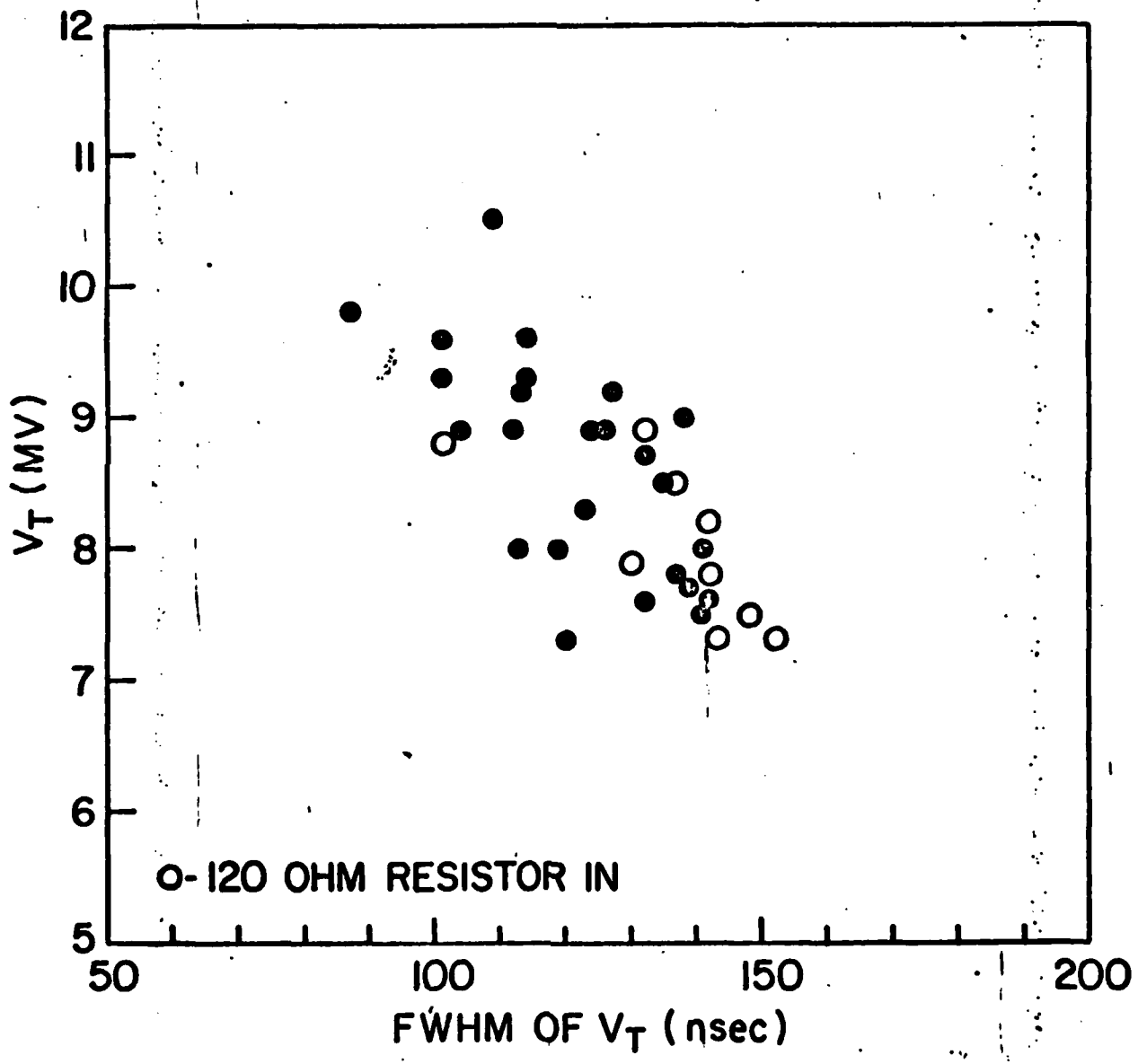
12
11
10
9
8
7
6
5
V_T (MV)
O-120 OHM RESISTOR IN
50
100
150
200
FWHM OF V_T (nsec)

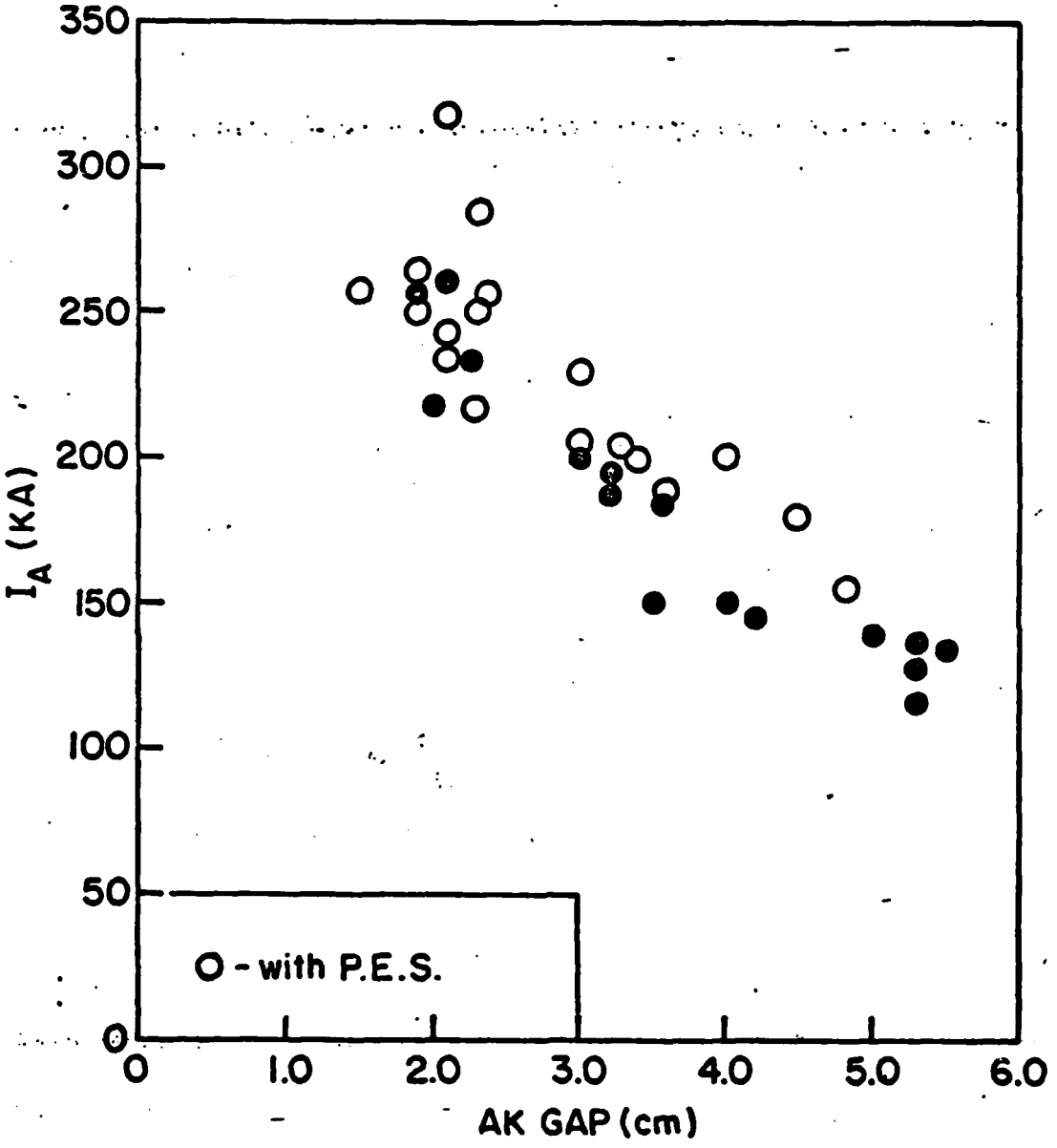
350
300
250
200
150
100
50
0
I_A (KA)
O - with P.E.S.
0
1.0
2.0
3.0
4.0
5.0
6.0
AK GAP (cm)

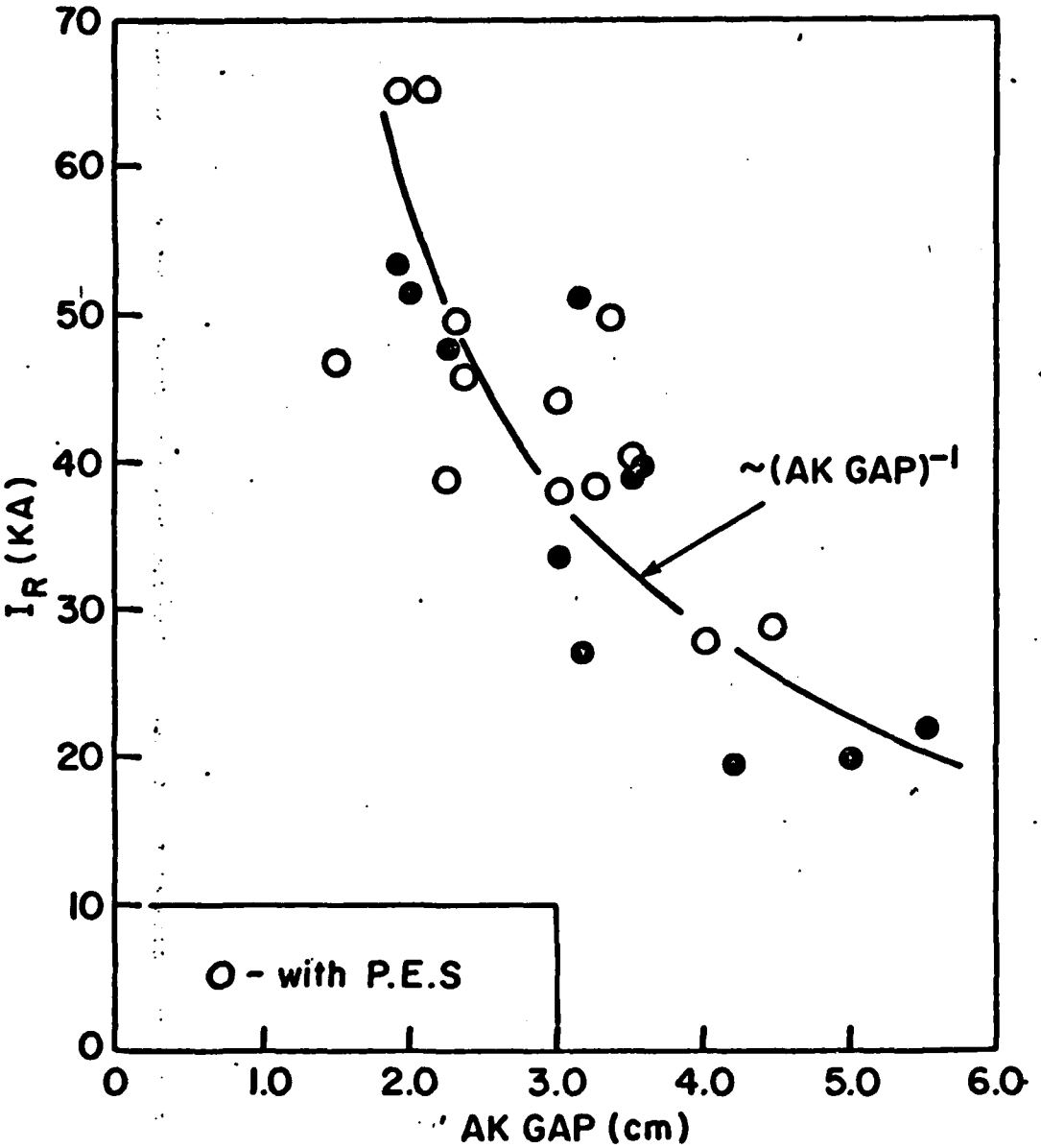
70
60
50
40
30
20
10
0
I_R (KA)
~(AK GAP)$^{-1}$
O - with P.E.S
0
1.0
2.0
3.0
4.0
5.0
6.0
AK GAP (cm)

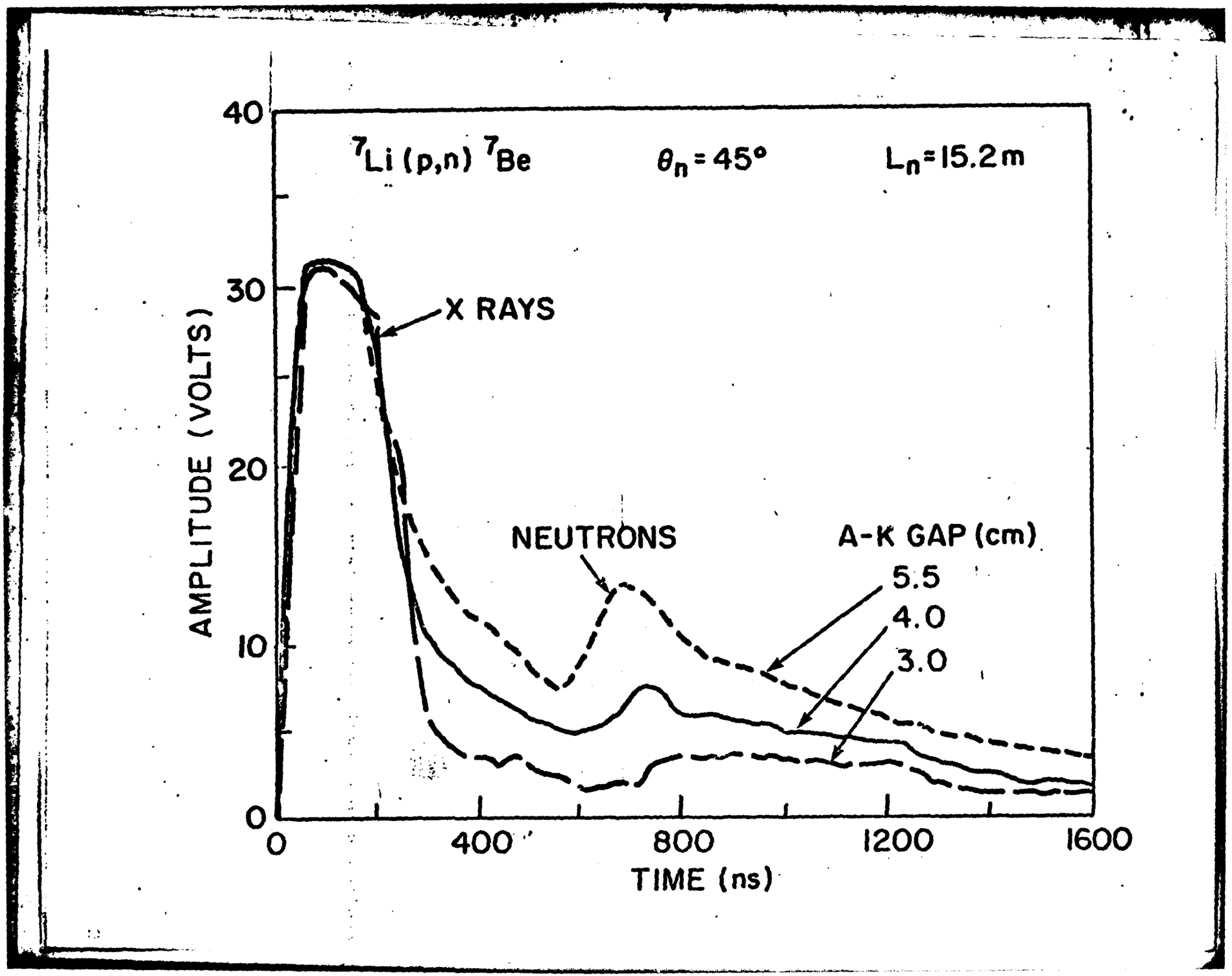
^{7}Li (p,n) ^{7}Be
θ_n = 45°
L_n = 15.2 m
X RAYS
NEUTRONS
A-K GAP (cm)
5.5
4.0
3.0
AMPLITUDE (VOLTS)
TIME (ns)
0
10
20
30
40
0
400
800
1200
1600

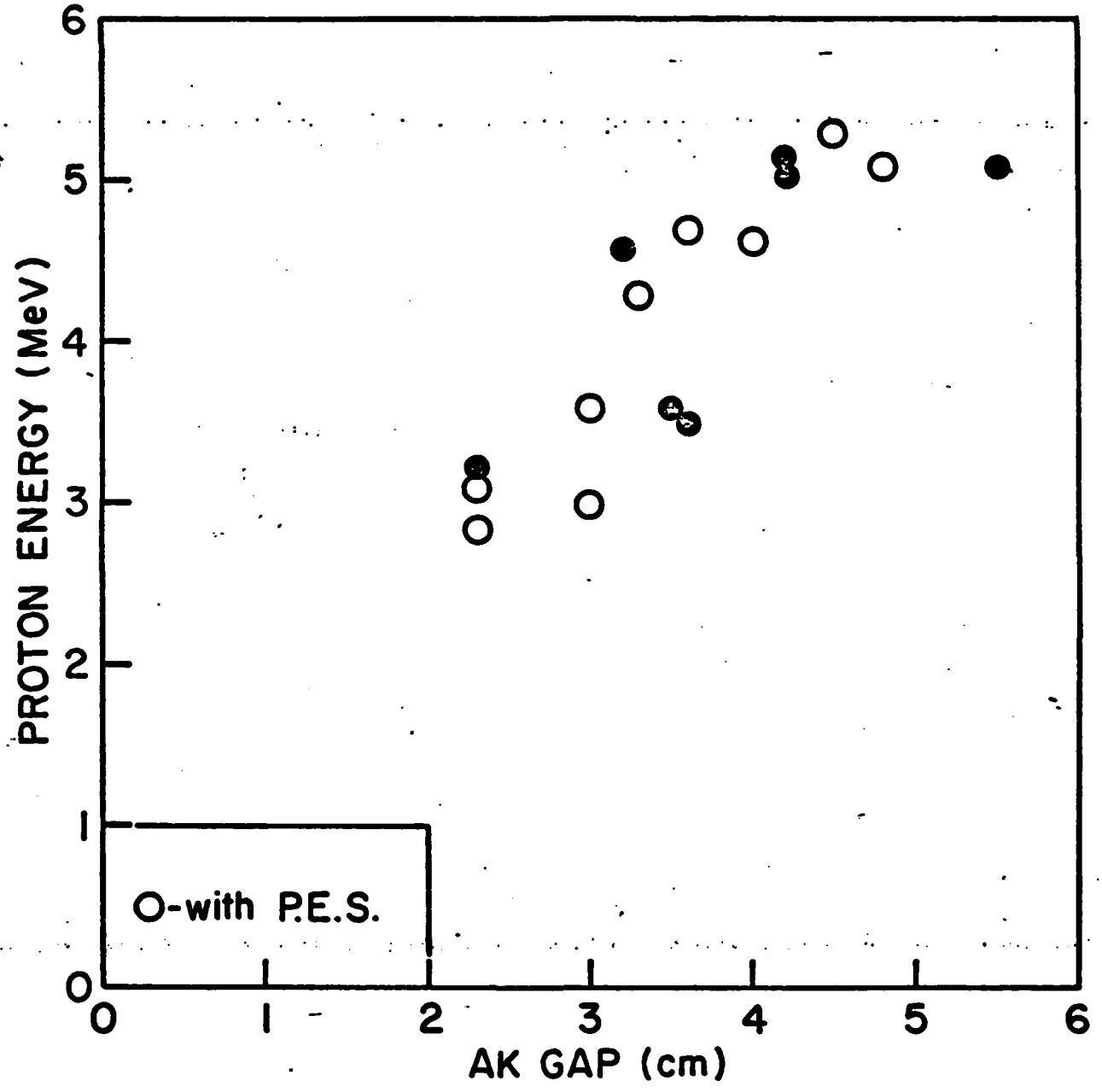
PROTON ENERGY (MeV)
AK GAP (cm)
O-with P.E.S.
0
1
2
3
4
5
6

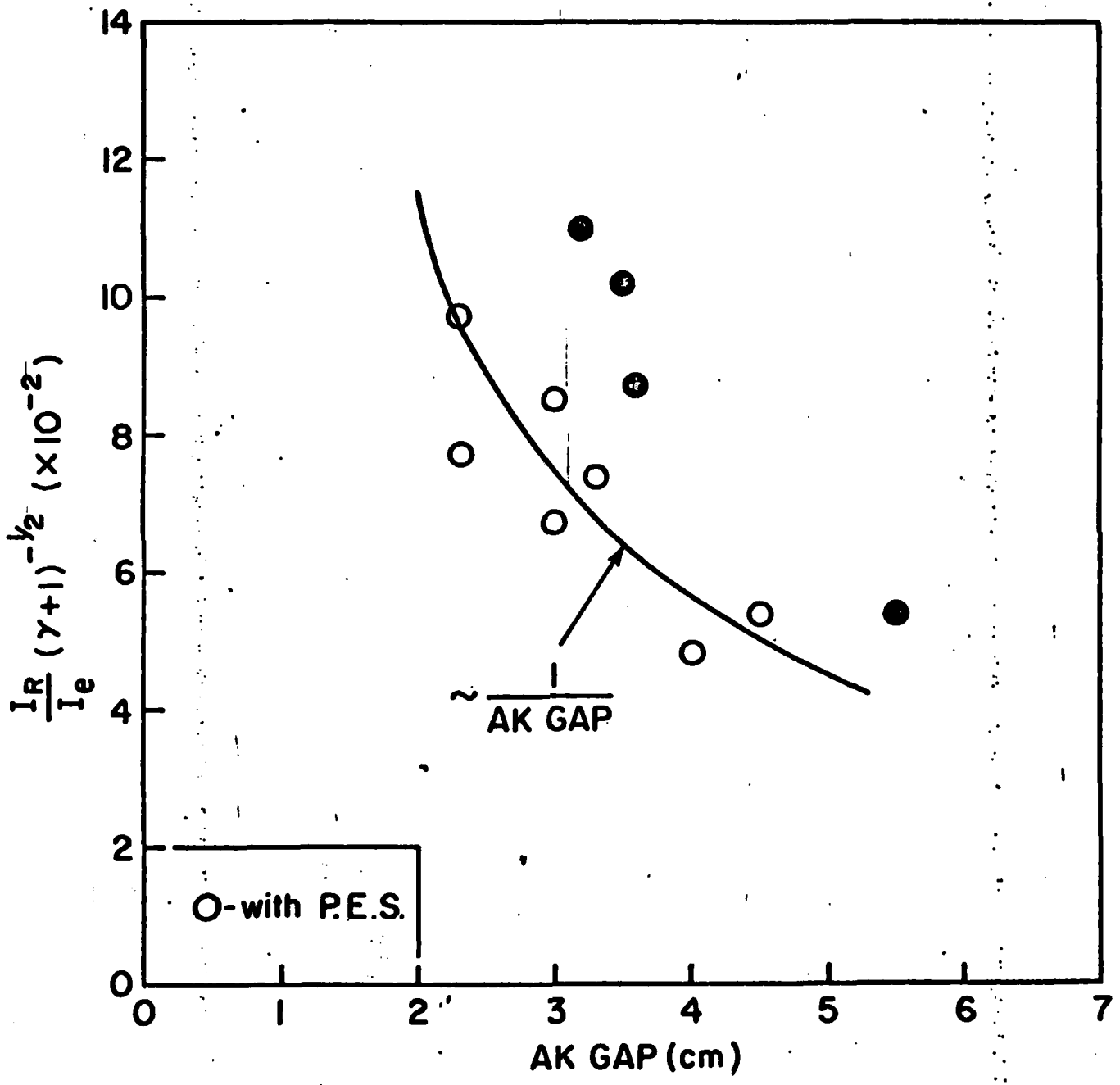
14
12
10
8
6
4
2
0
0
1
2
3
4
5
6
7
$\frac{I_R}{I_e}(\gamma+1)^{-1/2}$ (×10^{-2})
AK GAP (cm)
$\sim \frac{1}{\text{AK GAP}}$
O-with P.E.S.

APPENDIX III

Abstract submitted for the

1981 IEEE INTERNATIONAL CONFERENCE ON PLASMA SCIENCE

May 18-20, 1981

Modified Aurora Ion-Diode Experiments* R. A. MEGER†, P. C. YOUNG, A. T. DROBOT‡, R. J. BARKER†, J. J. CONDON, G. COOPERSTEIN, SHYKE A. GOLDSTEIN†, Naval Research Laboratory and R. BIXBY, G. A. HUTTLIN, K. G. KERRIS, D. A. WHITTAKER, Harry Diamond Laboratories.

The production of intense light-ion beams on the high impedance Aurora accelerator is being studied as a potential driver for inertial confinement fusion. In the past, measurements of proton beams from various ion diodes have been made with the accelerator operating in both negative[1] and positive[2] polarity. Based on the success of these experiments, the transmission line of the accelerator is being modified[3] to increase power delivery to the ion diode in positive polarity.

Positive polarity experiments to date have produced ion beams with net currents of $\leq$ 70 kA out of $\sim$ 300 kA total diode current at proton energies of $\geq$ 2 MeV. The peak proton current has been shown to follow a simple reflex diode scaling[4] of $I_i/I_e \sim [M_e(\gamma+1)/2M_i]^{\frac{1}{2}} R/D_{eff}$ where M_e and M_i are the electron and ion masses, γ is the relativistic factor for electrons, R is the cathode radius and D_{eff} is the effective anode-cathode gap allowing for plasma closure. Experiments have shown that diode operation is sensitive to the presence of a prepulse. Plasma erosion switches and flashover prepulse suppressors have been used to divert the accelerator prepulse from the ion diode and to sharpen the risetime of the main voltage pulse at the diode. In this manner anode-cathode gaps as small as 2 cm have been used without gap closure during the 150 nsec voltage pulse.

In this paper, the new ion-diode geometry will be described; the results of computer simulations of the diode operation based on this geometry will be shown; and preliminary experimental results with the modified accelerator and new diode geometry will be presented.

*Work supported by the Defense Nuclear Agency

†JAYCOR, Inc., Alexandria, VA 22304

‡Science Applications, Inc., McLean, VA 22102

[1] R. A. Meger, et al, IEEE Conference Record-Abstracts, 1980 International Conference on Plasma Science Madison, Wisconsin, p. 58.

[2] P. C. Young, et al, Bull. Am. Phys. Soc. 25, 899 (1980).

[3] See J. R. Boller, et al, these proceedings.

[4] Shyke A. Goldstein and R. Lee, PRL 35, 1079 (1975).

Please refer to "First and Final Call for Papers" announcement for instructions in preparing your abstract.

- Subject category name: Intense Ion Beam
- Subject category number: 3
- (x) Prefer oral session
- ( ) Prefer poster session
- ( ) No preference
- ( ) Special requests for placement of this abstract

THIS PAPER SHOULD IMMEDIATEL FOLLOW "Aurora Modification for Positive Polarity Ion Diode Operation" paper by J.R. Boller et al.

- Submitted by:

(Signature)

R. A. Meger
(same name typewritten)

Code 4770
(full address)

Naval Research Laboratory

Washington, DC 20375

- I am a member of the Committee on Plasma Science and Application

( ) yes (x) no

This form, or a reasonable facsimile, plus two Xerox copies must be received NOT LATER THAN FEBRUARY 16, 1981, at the following address: S. J. Gitomer, Conference Chairman, Group X-1, MS-531, Los Alamos Scientific Laboratory, Los Alamos, NM 87545, USA.

Figure 1: The following represents the paper presented by R. A. Meger at the Santa Fe IEEE Meeting. The paper represents the first data presented on the Modified Aurora Ion Diode (MAID) experiments and is only an interim report of results at the time of the conference.

Figure 2: The removal of the 50-ohm coax from the Aurora accelerator required a complete redesign of the ion diode hardware. A new inner conductor was constructed and installed on the gimballed Aurora mount. The inner conductor was designed to allow changes in its axial length through tubular sections clamped in place or by way of spring loaded thread rod accessible to the outside while the system was under vacuum. Two voltage monitors, a dv/dt monitor designed by J. Shipman and a capacitive voltage divider designed by G. Huttlin, as well as a stainless steel current shunt were installed to take advantage of the diagnostic access provided by the inductive insolator. The anode itself was of a previous design consisting of a 5 mil polyethylene foil stretched on an aluminum ring and supported with a 5cm long cigar tube anode stalk. The anode was mounted on a thin aluminum plate which was backed by an e-beam expansion chamber. A carbon beam dump at the rear of the chamber absorbed the electrons while limiting the debris escaping into the accelerator vacuum region. This chamber can be pressurized for future applications. A TLD array was placed behind the carbon beam dump.

The outer conductor was comprised of an aluminum dish with six radial ports and a counterbalanced front door. The radial ports were designed to allow line of sight access to the anode and cathode region. On the front door were mounted three plasma erosion switch (PES) gun chambers set to inject their plasma columns axially rear the outer edge of the inner conductor. Alternating with the PES tubes were the axial adjustment rods fed in through vacuum quick-connects. A 10 in. i.d. diagnostic chamber was located behind the cathode which was screwed into the door. The cathode was a self contained module with two Rogowski coils to measure net currents before and after a Kimfol used to current neutralize the ion beam. Witness plates or shadow boxes with front surfaces coated with LiCl

were mounted at the rear of the module. Cables were fed out through a window in the diagnostic chamber. Two current measuring loops were located on the door, one radially outside the erosion switches and the other inside.

X-ray dignostics used in the experiment included TLD arrays behind the anode and elsewhere near the diode region, an x-ray photo diode and pinhole camera behind the anode, and a second pinhole camera at 60^{o} to the AK axis. Voltages were measured with the two monitors on the center conductor as well as a resistive divider in the oil behind the insulator. In addition, proton energies were determined indirectly with neutron time-of-flight (TOF) techniques. Currents were measured in the oil with a dB/dt monitor, with resistive shunts on the center conductor and at two positions on the outer conductor, and dB/dt loops on the door of the front end. Ion diagnostics include the two Rogowki coils, witness plates and shadow boxes behind the cathode, and measurements of nuclear reaction products from the aluminum cathode and LiCl targets placed in the ion beam. Neutrons from the $^{7}Li(p,n)^{7}Be$ reaction were measured with a neutron TOF detector located 12.6 meters from the diode and with Rhodium and Manganese neutron activation detectors located near the diode. Aluminum in the cathode structure was actived by the $^{27}Al(^{12}C,\alpha n)^{34m}Cl$ reaction from the carbon component of the beam and the ^{34m}Cl activation was measured after the shot.

Figure 3: In general the results of this run on Aurora with the Modified Aurora Ion Diode (MAID) were quite successful. The run suffered from an off-centering of the electron pinch which limited the amount of useful data taken. The off-centering was evenually traced to the presence of the PES's on the door and a small vacuum leak in one of the switches. Those shots that did center showed the desired increase in power delivery to the diode. Shots with AK gaps of 2-5 cm were taken, all without plasma erosion switches (PES). Smaller than 2-cm Ak gaps shorted out during the pulse. This figure shows the results from a single well-centered shot with a 4-cm Ak gap, no PES's and a +90 kV marx charge. The tube voltage reached 8.7 MV and was $\sim$145 nsec wide which is comparable to negative polarity shots. The power into

the tube was ∿1.5 TW. At the ion load the voltage reached 6.7 MV and 220 kA were measured. The pulse width of ∿180 ns was somewhat longer that in the tube as predicted from computer modeling. The peak power was ∿1.4 TW which represents nearly all the power in the tube. Previous polarity results with the long 50-ohm coax showed <1 TW of power delivered to the diode region. The diode impedance on this shot was ∿25 ohms. The peak Rogowski current was 44 kA and neutron time-of-flight diagnostics confirmed ∿6 MeV proton energies. Results from the ion diagnostics were similar to the previous negative polarity results with the long 50-ohm coax.

The next two figures will give details of the voltage and currents measured on this particular shot.

Figure 4: These drawings show the voltage and current as measured in the tube by the resistive voltage monitors, the oil dB/dt monitor, and the derived impedance, power and energy. At this point in the accelerator the voltage shows a characteristic ∿100 ns rise time to 8.7 MV, sloping downward to ∿6 MV. The current rise time is slower, peaking near the end of the voltage pulse. The impedance shows a gradual decay over the length of the pulse. Computer modeling of the accelerator with resistive, constant impedance loads shows the tail end of the derived impedance to approximate the actual diode impedance. In this case the tail end measures 25-30 ohms before collapsing to zero. The power pulse has a FWHM of ∿150 nsec and a peak of ∿150 nsec and a peak of ∿1.5 TW. Energy delivered to this location is ∿200 kJ.

Figure 5: The inductive isolator permits voltage and current measurements to be taken within 1 meter of the diode load. The voltage from the capacitve monitor and the current from the stainless steel shunt are shown here with the derived impedance, power, and energy. The voltage risetime is slower than the tube monitor with the peak coming near the end. The ramped voltage waveshape was predicted in the computer simulations and may be useful for beam bunching during transport. The dV/dt monitor followed the capacitive monitor for ∿100 nsec before it would

consistently take off due to some collected charge. The current followed the voltage but plateaued eariler. The impedance shows 20-30 ohm operation of the diode. The power pulse is somewhat narrower at the load than at the tube showing a ∿120 ns FWHM. Due to the voltage and current the energy never plateaus but shows ∿150 kJ at the end of the pulse.

Figure 6: One consistency check on the measured voltage and current at the load is to use a transmission line code developed by G. Huttlin at HDL. This code takes the voltage and current waveforms at a given position for a known transmission line and calculates the waveform at any other position. The voltage and current waveform at the tube location were run through the program to calculate the voltage and current at the load. These are compared with the measured voltage and current at the load in the figure. Reasonable agreement is obtained in peak and FWHM. The largest difference is the double peaked signal of the voltage predicted by the computer but not measured.

Figure 7: The shot being analyzed has a LiCL target in place 20 cm downstream from the anode. Neutrons from the $^{7}Li(p,n)^{7}Be$ reaction were measured by a neutron TOF detector consisting of a sintillator-photo multiplier in a 7.6 cm thick lead sheild. The dashed line is the signal measured by a scintillator-photo diode (SPD) placed alongside this TOF detector. The SPD is sensitive to x-rays but does not have enough gain to see the neutron flux. Both detectors show the main bremsstrahlung signal followed by a second signal ∿250 ns later. The orgin of the second is unknown but the SPD indicates the signal is from x-rays rather than neutrons. The TOF detector shows a large neutron signal above the background which in the absence of neutrons looks more like the PD trace. A time interval T is marked on the drawing to illustrate the neutron flight time used to determine the proton energy. The measurement is usually taken from the peak of the x-ray signal to a point halfway up the leading edge of the neutron signal. This signal corresponds to the most energetic neutrons. The 400 nsec time interval corresponds to 6.0 MeV proton energy when the x-ray flight time is added and the neutron energy

is computed from the $^{7}Li(p,n)^{7}Be$ reaction kinematics. The uncertainty in the time of emission of the protons during the x-ray pulse leads to an uncertainty of ±1 MeV in the proton energy. The agreement between the measured proton and measured diode voltage is very good.

Figure 8: Another consistency check on the ion voltage and current is shown in this figure. The measured voltage and ion current with the proper relative timing are used in a computer code developed by F. Young to calculate the relative timing and shape of the expected neutron signal. The upper drawing shows the voltage and ion current waveforms used as input to the code. The lower drawing compares the measured TOF signal with the calculated signal. The peaks of the neutron signals have been normalized but no time shifts were made. The two neutron signals agree surprisingly well in shape and time. This agreement confirms the shape and magnitude of the ion voltage and the ion current wave shape. The lack of agreement late in the neutron signal is attributed to neutron scattering in the lead shield and the surrounding room. The computer code also yields the total neutron flux which should be measured by the detector. This can be compared with the measured neutron flux at the detector. The two numbers appear in figure 3. The measured flux of 2.5(11) neutrons/steradian is 30% higher than the calculated value of 1.7(11) neutrons/steradian. This could be due to the Rogowski coil crowbaring early and missing a sizeable fraction of the ion current or due to a large neutralizing electron component in the ion beam.

Figure 9: The final figure summarizes the data presented. The main results were the successful firing of the new geometry hardware, the functioning of the inductive isolator and the markedly improved power flow to the diode load. The shots to date were made without plasma erosion switches (PES) to limit prepulse, and as a result the AK gaps were limited to >2 cm. The best shots produced beams of <50 kA ion current at ∿6 MeV from diodes operating at 20-30 ohms. An offcentering of the electron beam was observed and was traced to the PES ports where a leak caused an asymmetry in power flow to the diode.

Future plans include correcting the power flow asymmetry and for use of the PES's. When these goals are met the marx charge will be increased beyond + 90 kV and new diode geometries to improve focusing and ion generation efficiency will be investigated.

1981 IEEE INTERNATIONAL CONFERENCE ON PLASMA SCIENCE

IC2 MODIFIED AURORA ION-DIODE EXPERIMENTS*

R. A. MEGER†, F. C. YOUNG, A. T. DROBOT‡

R. J. BARKER†, J. J. CONDON, G. COOPERSTEIN,

SHYKE A. GOLDSTEIN†

NAVAL RESEARCH LABORATORY

AND

R. BIXBY, G. A. HUTTLIN, K. G. KERRIS,

D. A. WHITTAKER

HARRY DIAMOND LABORATORY

*WORK SUPPORTED BY THE DEFENSE NUCLEAR AGENCY

†JAYCOR, INC., ALEXANDRIA, VA

‡S.A.I., McLEAN, VA

FIGURE 1.

MODIFIED AURORA ION DIODE

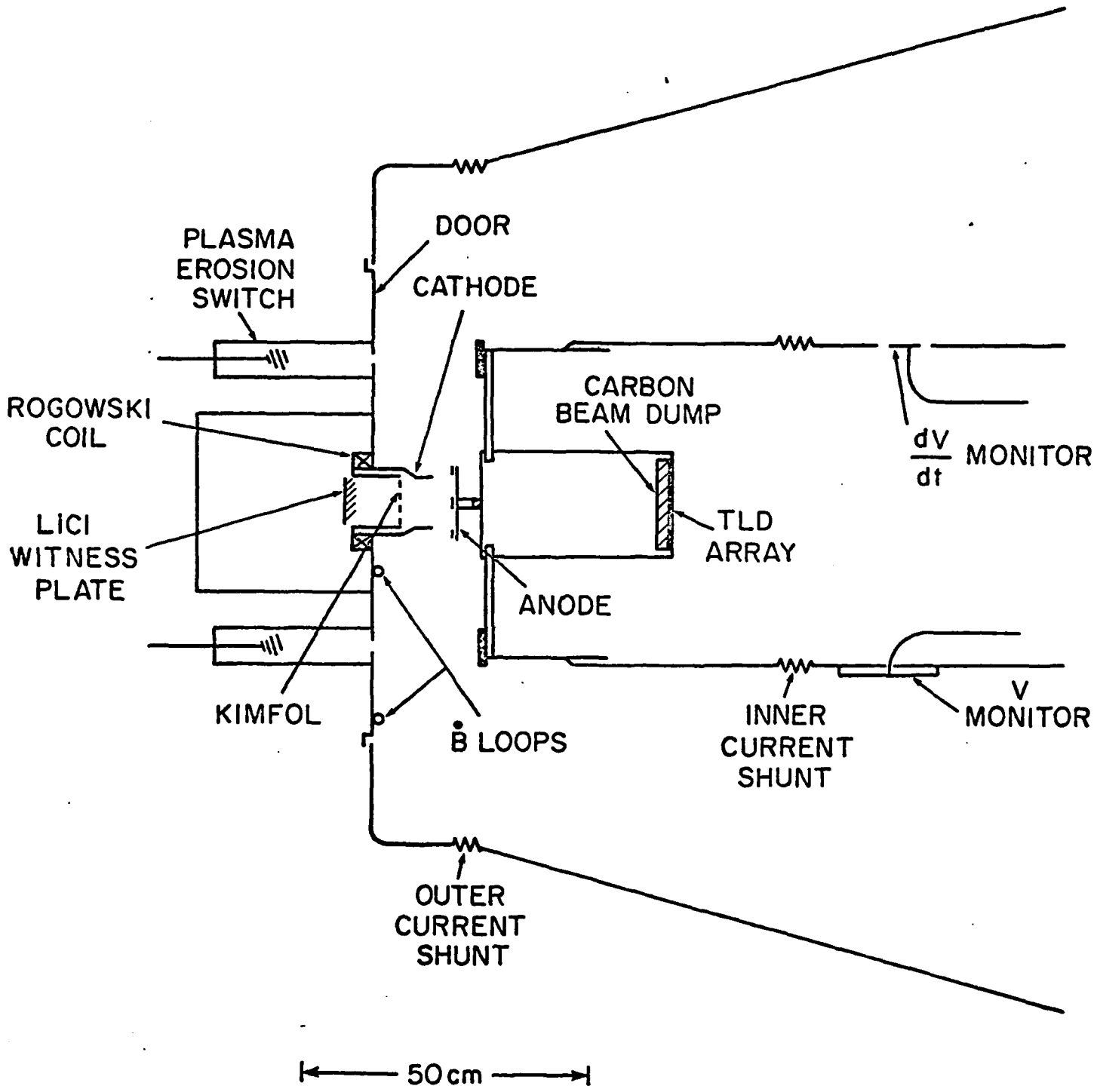

FIGURE 2.

MODIFIED AURORA ION DIODE EXPERIMENT

SHOT	3372 (6 MAY 81)
ANODE CATHODE	4.0 CM
MARX CHARGE	+90 KV
PEAK TUBE VOLTAGE	8.7 MV
FWHM TUBE VOLTAGE	145 NSEC
PEAK TUBE CURRENT	237 KAMP
PEAK TUBE POWER	1.5 TW
PEAK DIODE VOLTAGE	6.7 MV
PEAK DIODE CURRENT	220 KA
PEAK DIODE POWER	1.4 TW
AVERAGE DIODE IMPEDANCE	25 OHMS
PEAK ROGOWSKI COIL NET CURRENT	44 KAMP
MEASURED NEUTRON FLUX AT 45°	2.5×10^{11} NEUTRONS/SR
CALCULATED NEUTRON FLUX AT 45°	1.7×10^{11} NEUTRONS/SR
PROTON ENERGY FROM TOF	6 MEV

FIGURE 3

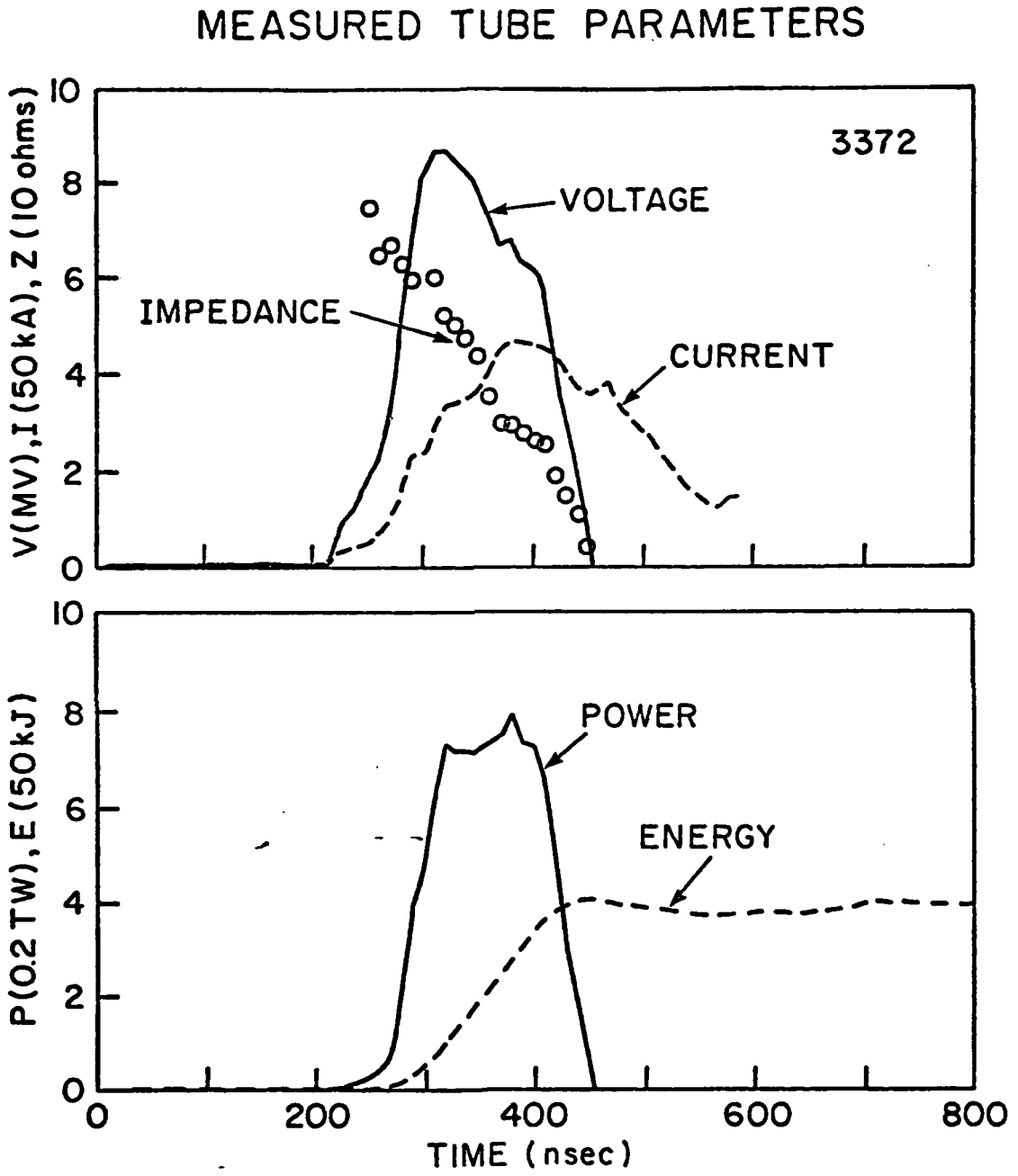
MEASURED TUBE PARAMETERS
3372
VOLTAGE
IMPEDANCE
CURRENT
V(MV), I(50kA), Z(10 ohms)
P(0.2 TW), E(50kJ)
POWER
ENERGY
TIME (nsec)
0
200
400
600
800
2
4
6
8
10

FIGURE 4

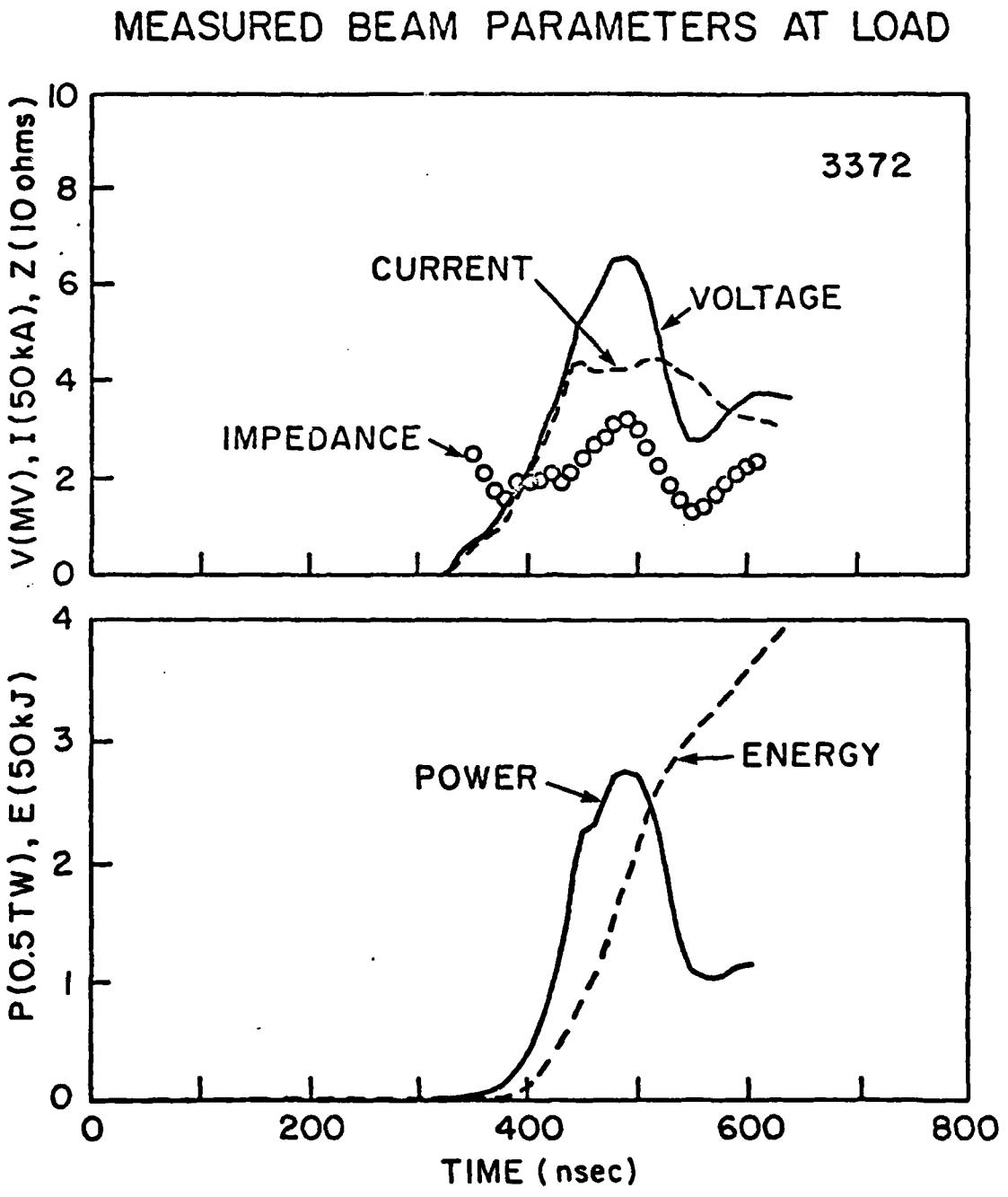
MEASURED BEAM PARAMETERS AT LOAD
3372
CURRENT
VOLTAGE
IMPEDANCE
V(MV), I(50kA), Z(10ohms)
P(0.5TW), E(50kJ)
POWER
ENERGY
TIME (nsec)
0
200
400
600
800

FIGURE 5

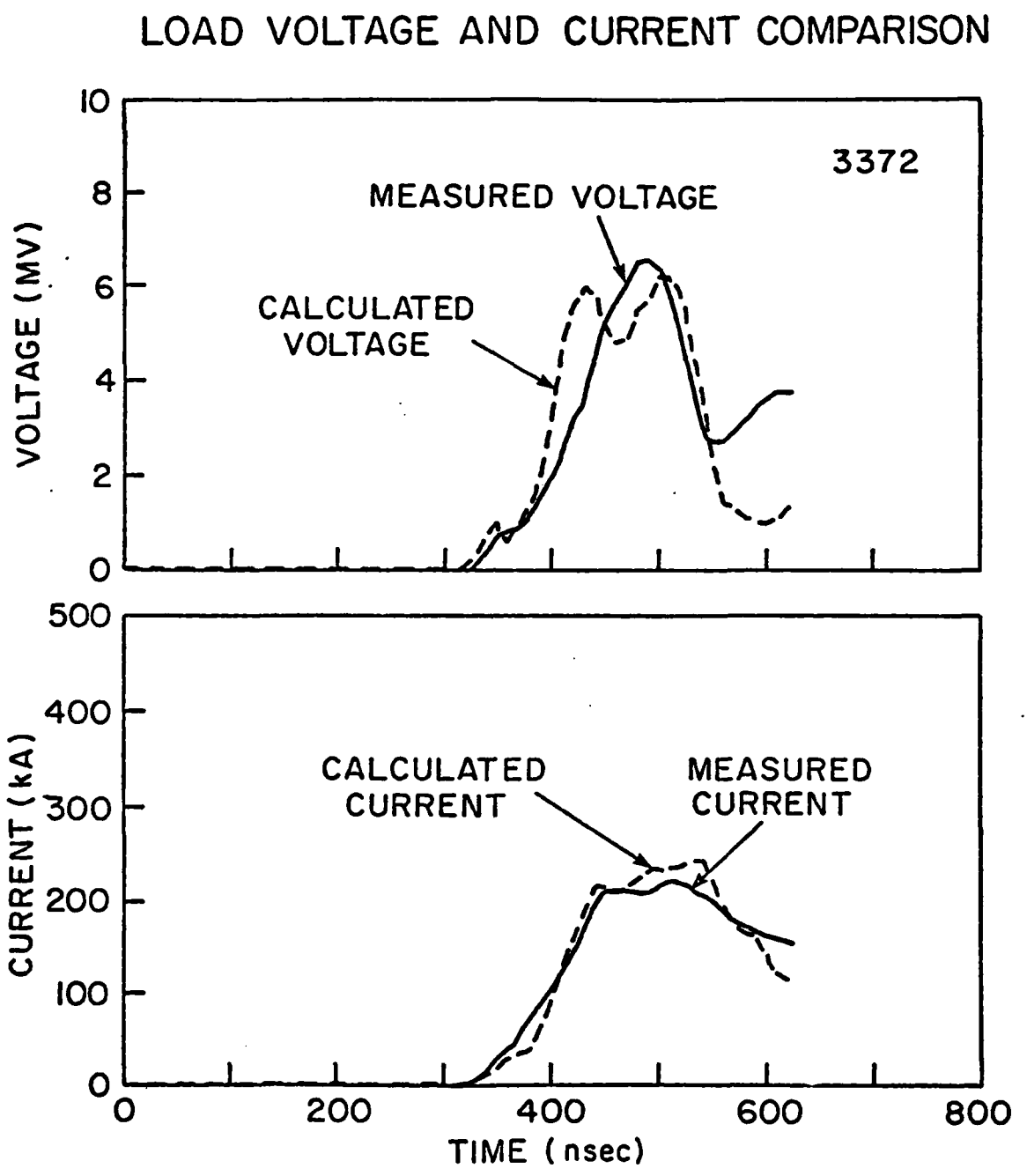
LOAD VOLTAGE AND CURRENT COMPARISON
3372
MEASURED VOLTAGE
CALCULATED VOLTAGE
VOLTAGE (MV)
10
8
6
4
2
0
CALCULATED CURRENT
MEASURED CURRENT
CURRENT (kA)
500
400
300
200
100
0
0
200
400
600
800
TIME (nsec)

FIGURE 6

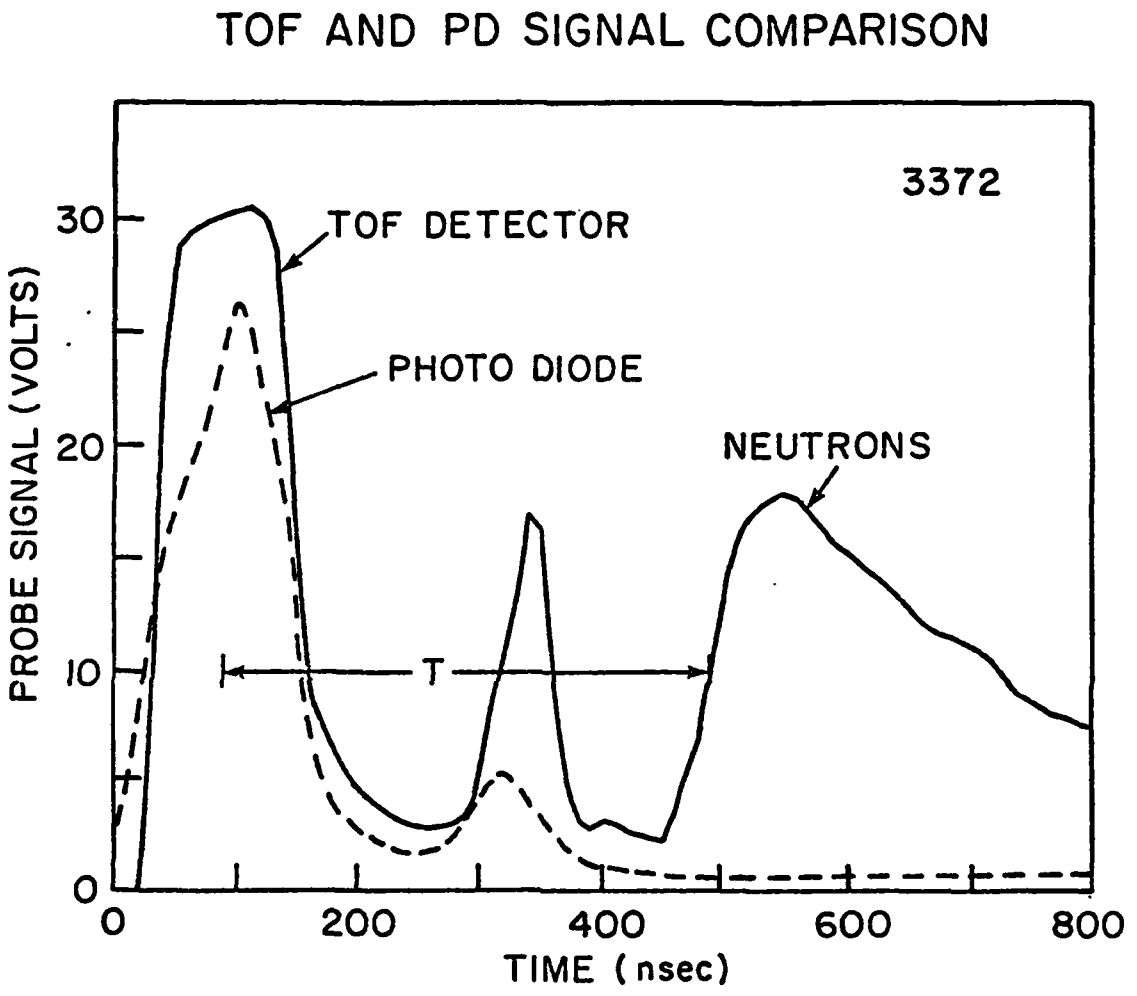
TOF AND PD SIGNAL COMPARISON
3372
TOF DETECTOR
PHOTO DIODE
NEUTRONS
T
PROBE SIGNAL (VOLTS)
TIME (nsec)
0
10
20
30
0
200
400
600
800

FIGURE 7

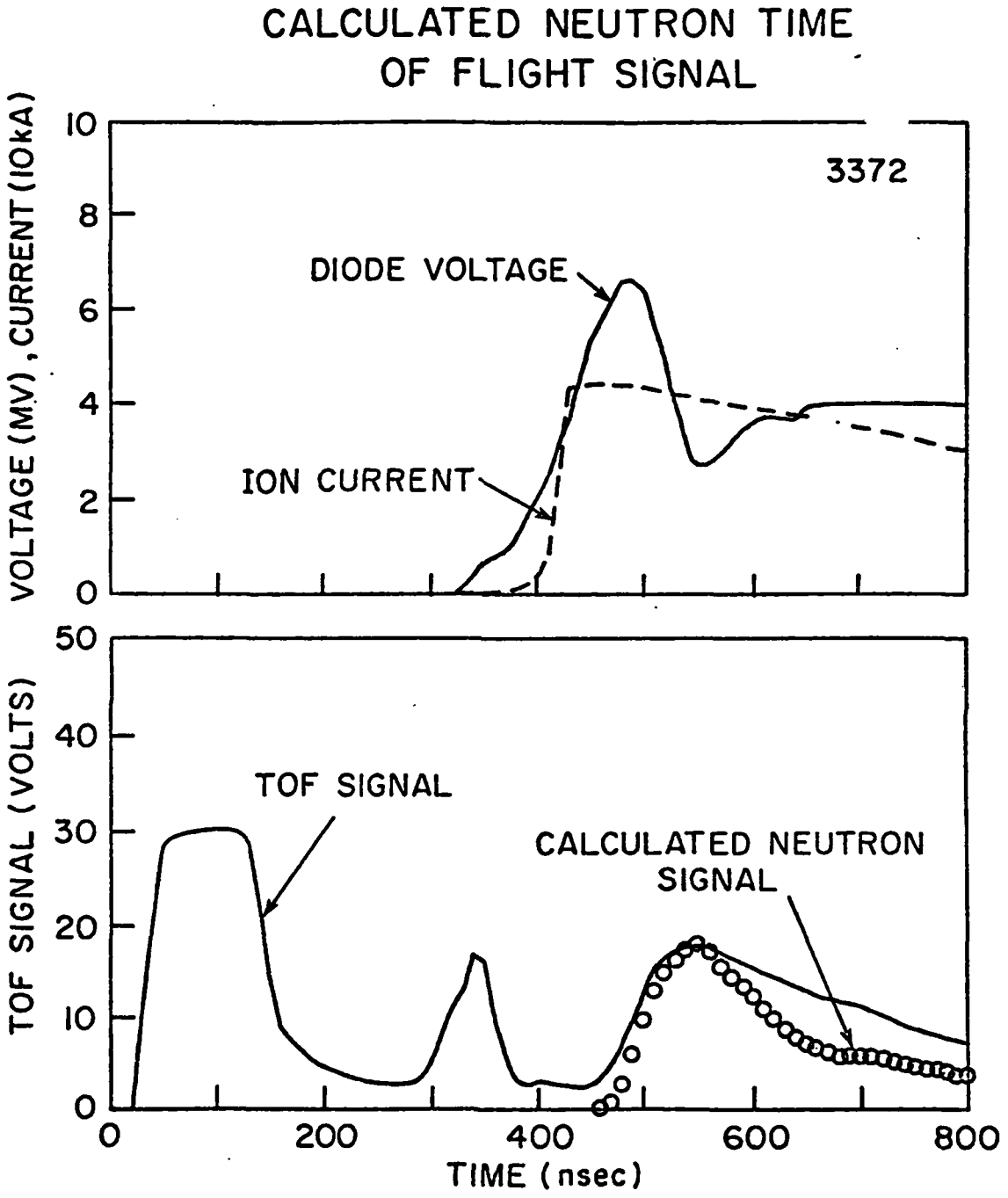
CALCULATED NEUTRON TIME
OF FLIGHT SIGNAL
3372
DIODE VOLTAGE
ION CURRENT
VOLTAGE (MV), CURRENT (10kA)
10
8
6
4
2
0
TOF SIGNAL
CALCULATED NEUTRON
SIGNAL
TOF SIGNAL (VOLTS)
50
40
30
20
10
0
0
200
400
600
800
TIME (nsec)

FIGURE 8

MODIFIED AURORA ION DIODE

PRESENT

NEW HARDWARE — 45 kA P^+ AT 6 MeV

DIAGNOSTIC ON ANODE

POWER FLOW TO THE LOAD IMPROVED

AK GAP LIMITED BY PREPULSE

A SYMMETRIC POWER FEED IN DIODE REGION

FUTURE

PREPULSE SUPPRESSION WITH PLASMA EROSION SWITCHES

SYMMETRIC POWER FLOW

ADVANCED DIODE DESIGNS

INCREASE ACCELERATOR POWER

FIGURE 9

APPENDIX IV

NRL Memorandum Report
0000

The Use of Finite J_θ for Increasing the Ion Efficiency of High Impedance Diodes

ROBERT J. BARKER AND SHYKE A. GOLDSTEIN

JAYCOR, Inc.
Alexandria, VA 22304

This research was sponsored in part by the Defense Nuclear Agency under Subtask T99QAXLA014, work unit 46 and work unit title "Ion Beam Generation" and by the Department of Energy, Washington, D.C.

FINAL DRAFT

CONTENTS

I. INTRODUCTION 00

II. THEORY AND NUMERICAL IMPLEMENTATION 00

II. RESULTS 00

1. Aurora 00
2. PBFA-I 00

IV. CONCLUSIONS 00

ACKNOWLEDGMENTS 00

REFERENCES 00

The Use of Finite J_θ for Increasing the Ion Efficiency of High Impedence Diodes

Abstract

Numerical simulations predict that the ratio of the effective ion current to total diode current can be significantly increased by introducing a small but finite azimuthal current into the tip of the cathode shank of a high impedance (4Ω) axial pinch-reflex diode. Such a current generates large tangential magnetic fields along the electron-emitting cathode surfaces. These fields, in turn, impart a finite angular momentum to the electrons as they are injected into the anode-cathode gap. The resultant particle self-fields alter electron trajectories in such a way as to boost electron space charge near certain portions of the ion-emitting anode surface. The net consequence is a modification of the radial profile of ion emission which enhances the net ion current transmitted through the interior of the hollow cathode shank.

November 12, 1981

I. INTRODUCTION

The efficient generation of intense beams of energetic light ions is a central objective of the NRL Light Ion Fusion Research Program.[1] Over the past several years, focused ion current densities of over 100 kA/cm^2 from terrawatt-level beams have been achieved with magnetically insulated radial diodes at Sandia National Laboratories[2] as well as with pinch-reflex axial diodes at the Naval Research Laboratory.[3] Using diodes of below 2 ohm impedance, ion beam efficiencies of over 70% were achieved in both of the above configurations[4,5] (i.e., — over 70% of the power travelling through the diodes was carried by the light ions generated therein). The question of ion efficiency is critical to the goal of a practical light ion driven inertial confinement fusion (ICF) reactor. As much as possible of a given pulsed power generator's energy must be imparted to the ion beam exiting the diode in order to minimize the number of beam sources necessary for successful pellet ignition as well as to maximize the overall reactor efficiency. These efficiency considerations are well met by the low impedance diodes.

Unfortunately, the high current densities of the ion beams produced by low impedance diodes are not compatible with the focusing and transport systems presently under study for bringing the beams to bear on the proposed fusion targets.[6] In addition, there are strong arguments in favor of the use of high impedance generators in present reactor scenarios.[7] High impedance diodes must be matched to such generators to ensure efficient power transmission but these diodes are plagued by relatively low ion production efficiencies. These low efficiencies are a direct consequence of established diode theory. It has been found semiempirically[8] that the total current flowing through a pinched-beam diode may be approximated by

$$I = I_e + I_i \approx 9(\gamma^2-1)^{1/2}\,\frac{R}{D}\left[1+\left(\frac{eV}{2m_ic^2}\right)^{1/2}\frac{R}{D}\right] \tag{1}$$

where $\gamma = 1 + \frac{V(\text{in } MV)}{0.511}$, R = cathode radius, D = axial anode-cathode ($A-K$) gap, V = diode voltage, and m_i = ion (proton) mass. Implicit in this formula is an ion-to-electron current ratio given by

$$\frac{I_i}{I_e} \geq 0.5\,\frac{v_i}{c}\,\frac{R}{D} \tag{2}$$

where v_i is the mean ion velocity.[9] Thus, for a fixed voltage, increasing the diode impedance translates to decreasing the aspect ratio, R/D. That, in turn, results in a decrease of the current ratio I_i/I_e and a lowering of the ion production efficiency, $I_i/(I_e + I_i)$. This is the crux of the problem addressed by this research. Stated in other terms, Eq. (2) expresses the inverse dependence of the specie current ratio on the ratio of respective species lifetimes in the $A-K$ gap. By increasing the relative electron lifetime over the standard parapotential flow model[10,11] through some modification of the diode field structures, one can hope to significantly beat the R/D limit. The modification studied herein involves the introduction of finite azimuthal current flow in the cathode shank which gives rise to strong tangential magnetic fields along the electron-emitting shank surface. For the J_θ values tested, this technique produced positive results in increasing the effective ion efficiency, η_i, of a 4Ω diode. The same J_θ values tested in a 25Ω diode did not substantially effect its η_i but did modify the density profile of the resultant ion beam. The rationale underlying the finite J_θ techniques as well as the results of the cases tested are presented below.

II. THEORY AND NUMERICAL IMPLEMENTATION

The theories quoted in the previous section assume a predominantly radial flow of electrons cascading from the cathode face at radius, R, down toward the center of the anode. For diode potentials in excess of 1 MV, electrons are quickly accelerated to very near the speed of light, c. Their gap lifetimes, τ_e, are thus on the order of R/c. On the other hand, due to their much greater mass, protons experience little deflection from an axial trajectory across the $A-K$ gap of width, D. They have lifetimes, τ_i, of about $D/\bar{v}_i$ where $\bar{v}_i$ is the average ion velocity. Allowing for oscillations in the electron flow yields a pessimistic electron-to-ion τ ratio equal to the current ratio of Eq. (2). In order to increase this ratio, a thin hydrogen-rich foil may be substituted in place of a solid anode. The thickness of the foil is such as to allow an electron to pass through it without excessive energy loss. Behind the foil, a virtual cathode and/or a strong B_θ acts to reflect the electrons back into the $A-K$ gap.[12,13] In such a case, τ_e increases with N, the number of reflections through the foil experienced by a typical electron. That is the essence of the pinch reflex diode (PRD) (see Figure 1) pioneered by NRL.

Alternately, the entire diode may be reconfigured from an axial to a radial $A-K$ gap geometry as in Figure 2. In such a diode a combination of imposed B_z and self-generated B_θ magnetic fields constrain electron flow to form an azimuthally symmetric negative space-charge cloud stretching some distance from the cathode into the radial gap. Given the proper choice of operating voltage and other parameters, few electrons will reach the anode ($\tau_e \rightarrow \infty$) and virtually all of the current in this "radial diode" will be carried by the ions in their near-radial trajectories across the gap.[14,15]

With reference to the previously mentioned problem of low ion production efficiency in high impedance diodes, it was reasoned that a possible solution might be to combine the τ_e enhancement created by the electron reflexing anode foil with that arising from the electron flow constraints imposed by the magnetic fields such as those found in a radial diode. Specifically, the standard axial pinch-reflex geometry of Figure 1 might be retained while imposing an azimuthal current density, J_θ, in the tip of the cathode shank.[16] Experimentally, this could be achieved by cutting an azimuthally symmetric pattern of spiral gaps into the shank tip.[17] Increasing the pitch and/or the density of the spirals would increase the effective I_θ component of the net cathode current. This I_θ would give rise to a strong B_r along the intense electron emission region at the tip of the cathode which field would impart a finite angular momentum to those electrons. Several consequences can be expected. First of all, depending upon the strength of $(B_r)_{CATHODE}$, net electron emission along the cathode tip will be reduced due to tangential magnetic field effects (longer electron space-charge retention near the emitting surface).[18] If the impedance remains fixed, this would demand an increase in the ion efficiency. Secondly, finite angular momentum will prohibit electrons from reaching $R = 0$ and thus will inhibit the formation of large electron space-charge accumulations along the diode's central axis. (Such a charge build-up is common in pinch-reflex diodes).[19] This should depress the ion emission peak at the center of the anode and likewise limit the growth of the anode plasma "pimple" at zero radius,[20] thus lowering the average divergence of the ion beam. Thirdly, the additional degree of freedom in the electron motion necessarily complicates the particle's trajectory through the $A-K$ gap. Convoluted figure-eight electron orbits have been observed to increase τ_e in conventional PRD's;[21] the effect should be much more pronounced here. Finally, there is a possibility of noticable magnetic insulation of the electron flow near

the anode plasma surface due a combination of electron diamagnetic effects and foil flux exclusion. The resultant formation of an electron charge layer near the ion-emitting surface is a key mechanism for efficient ion production in radial diodes.[22] There are thus four reasons for optimism over this proposed modification for high impedance axial diode design.

NRL's DIODE2D computer code was employed to numerically simulate the steady-state operating conditions for such a J_w-diode (JTD) for various sets of parameters. The details of the code may be found elsewhere.[23] It is sufficient here to point out that DIODE2D calculates equilibrium electric and magnetic field strengths over an $NZ \times NR$ mesh of discrete data points on a pre-determined computational region corresponding to an arbitrary $R-Z$ planar cross-section passing through the diode's centerline. Complete azimuthal symmetry is assumed. A finite number of macro-electrons and macro-protons having correct, physical charge-to-mass ratios are advanced timestep-by-timestep across the mesh in a relativistically covariant manner. A steady-state solution is sought both for field structures as well as for particle flows. No time-dependent phenomena are actually treated.

The dimensions of the diode numerically modeled here come from actual experimental apparatus designed by NRL personnel for light ion beam research on the AURORA and PBFA-I pulsed power generators. At the U.S. Army's Harry Diamond Laboratories (HDL), one of the four 50-ohm lines of the AURORA machine was fitted with a custom designed PRD.[24] The experimental arrangement is depicted in Figure 3. Details of the diode structure at the tip of the device are shown in Figure 4. All radial dimensions are given in centimeters. Of the three, variable axial dimensions indicated, the most significant is D_0, the anode-cathode $(A-K)$ gap. For a fixed cathode radius of five centimeters, the value of D_0 essentially determines the diode impedance and efficiency for a given applied voltage via Eqs. (1) and (2). It may be further noted that the diode of Figure 4 is in a "negative polarity" configuration corresponding to the early experimental runs on AURORA. The cathode is the central conductor of the coaxial line and the resultant ion beam is accelerated toward the machine, making beam diagnostics very difficult and beam transport impossible. In more recent experiments, the central conductor was switched to positive polarity[25] and the anode foil and cathode appropriately reversed.

Such a change in polarity can be expected to significantly modify the source-free electric field structure only at large radii and probably have little impact on the dynamics of particle flows in the active $A-K$ gap below five centimeters radius. This relative isolation of the active particle flow region from the large radius field structure similarly encouraged the use of the same diode structure of Figure 4 to model the 4-6 ohm PRD being designed by NRL for use on the individual lines of PBFA-I at Sandia Labs. Only the diode voltage and axial dimensions were changed. Specifically, the AURORA simulations were conducted with $D_0 = 3.3$ cm at 5.0 MV while those for PBFA-I were with $D_0 = 0.66$ cm at 2.0 MV.

The volume that must be simulated using the DIODE 2D code extends radially from the central axis to the inner radius of the anode shell and axially from the plane corresponding to the recessed foil face of the cathode out to the inner plane surface of the vacuum vessel, anode shell. Since it presumes azimuthal symmetry, the computer code only deals with a single $R-Z$ planar cross-section extending out from the centerline. This computational region is presented in Figure 5. The grid points are shown as dots and correspond to the center of their respective rectangular data cells. Given the monolayer of guard cells completely surrounding the entire region in which particles are "allowed," a total of $(NZ + 2) \times (NR + 2) = 66 \times 52 = 3{,}432$ mesh points are used. The bottom boundary corresponds to the central axis ($R = 0$) of the diode. The right and upper boundaries represent the anode shell and are maintained at the full anode potential. The left boundary is kept at zero voltage up to cell 22 and then increased logarithmically up to the anode voltage. Perfectly conducting cathode and anode surfaces are included in the computational region as shown in Figure 5. They are treated numerically via a capacitance matrix technique described elsewhere (see Ref. 26). On the order of 10^4 macroelectrons and 10^4 macroprotons participate in the simulation at steady state. These macroparticles are emitted at their respective electrodes along the heavy-lined surfaces. Axial currents in the cathode shank and in the anode stalk are treated rigorously as a function of z in order to ensure an accurate distribution of B_θ throughout the diode. The results of these numerical simulations as well as a summary of the conclusions which could be drawn from them are presented in the following two sections.

III. RESULTS

1. AURORA

The first diode modeled was one appropriate for use on the AURORA machine. The diode voltage was fixed at 5 MV. The axial spacing between grid points was set to $\Delta Z = 0.15$ cm, yielding an $A-K$ gap, D_0, of 3.3 cm (see Figure 4). For a cathode radius of 5.0 cm, Eq. (1) predicts a diode current of 156.7 kA yielding an impedance of 32 ohms. Equation (2) predicts an ion efficiency, η_i, of only 0.0725 $\left[= \frac{I_i}{I_e + I_i}\right]$. These predictions fall far short of observed results. A diode with the above geometry and voltage was tested experimentally and computationally by NRL and the results were just recently published.[27] The numerical simulation quoted in that paper found a steady-state diode current of 205 kA of which 40 kA were carried by protons. This amounts to a diode impedance of 24 ohms and an ion efficiency, η_i, of about 0.195. The average experimental results reported in the same paper were $I_{diode} \approx 250$ kA (20 ohms) and $\eta_i \approx 0.20$. It should be noted that the experiment started with an $A-K$ gap of 4.9 cm but that gap closure due to electrode plasma expansion was expected to have narrowed that to about 3.3 cm by the time of peak current in the power pulse. Those findings clearly contradict Eqs. (1) and (2). High impedance operation gives rise to new diode phenomena not properly treated in that earlier analysis. The need for a more complete theoretical treatment still exists. Until one is found, numerical simulation is the best nonexperimental tool available for analysis.

As an additional "benchmark" for the results to be reported here, a numerical simulation was carried out on the same diode but in positive polarity. The results were: $I_e = 182$ kA, $I_i = 56$ kA, $I_{diode} = 238$ kA, $Z = 21$ ohms, and $\eta_i = 0.235$. This is in agreement with the negative polarity experiment indicating that changes in the electric field configuration along the far boundaries of the diode have little effect on the physics of the $A-K$ gap. Higher currents were achieved here than in the negative polarity simulation probably because no electron emission along the cathode shank had been permitted in that earlier run. The electron particle plot of Figure 6 shows very significant electron flow from the shank. To test the effects of J_e in the shank, a negative polarity was again assumed in the diode to

conform to the quoted experiments.

The azimuthal current was imposed in the cathode shank in a very straightforward manner. Referring back to Figure 5, a constant, predetermined value of J_θ was assumed in each of the data cells in the rectangular region stretching from $IZ = 6$ through $IZ = 21$ and from $IR = 18$ through $IR = 21$ (i.e., —a cross-sectional area of 2.4 cm^2). As a first test for the idea, a value of $J_\theta = 1$ kA/cm^2 was arbitrarily chosen giving 2.4 kA of azimuthal current flowing through the shank. The effect of this small I_θ was quite pronounced. In a simulation of electron-only flow, a net current of 209 kA was achieved (diode impedance of 24 ohms). A sampling of electron positions in the steady state for that case is presented in Figure 7. The shaping of the electron flow by the shank's B-field is clearly discernable. Notice, in particular the intense stream of electrons from the top rear of the shank arcing up and across the gap along the field lines. There also seem to be electrons that are emitted from the inside shank surface and then flung upward behind the foil. The net effect is an increase in the mean radius of electron impact on the anode foil. Thereafter in the simulation, proton emission was turned on along the entire front face of the anode foil. The new equilibrium with both species present yielded the following: $I_e = 244$ kA, $I_i = 41$ kA, $I_{net} = 285$ kA, $Z = 17.5$ ohms, and $\eta_i = 0.144$. Thus, the ion production efficiency decreased by 0.091 or almost 40% while the impedance dropped by about 17% compared to the $J_\theta = 0$, "benchmark" case. This was unexpected but an examination of the sample particle plots of Figure 8 suggests two causes. First of all, the electron stream is illuminating only a relatively small area of the anode. This is lowering η_i. Secondly, the shank magnetic field is still enhancing the net shank electron emission by keeping large numbers of electrons emitted in the rear of the shank from hitting the forward portions of the shank and lowering emission there as is normally the case. This "layering" of the shank electron flow can be seen in Figure 8.

In order to remedy this situation, a better choice for J_θ was sought. The simulation code was reset to the electrons only equilibrium and J_θ was set to 10 kA/cm^2 or a total azimuthal shank current of about 24 kA. The results can be seen in Figure 9. This case was not run to equilibrium. The net effects were in a beneficial direction albeit to an extreme. The mean radius of electron impact on the

anode foil was indeed increased. In addition, although emission on the outer surface of the shank was again enhanced, emission on both the inner surface as well as along the cathode tip was greatly curtailed due to direct magnetic insulation. The net electron current fell to about 60 kA.

As a reasonable intermediate choice J_θ was taken as 4 kA/cm^2 yielding I_θ = 4.8 kA. This case was run and again both the impedance and the efficiency dropped. Specifically, the observed steady-state currents were I_e = 257 kA, I_i = 34 kA, and I_{diode} = 291 kA giving an impedance of 17.2 ohms and an ion efficiency of 0.117. As shown in Figure 10, the cause of the problem seems to be very similar to that for the J_θ = 1 kA/cm^2 case. Once again although the shank B-field is reducing emission at the shank tip, it is also preventing much of the normal self-suppression of electron emission over the bulk of the outer shank surface. One improvement is the larger average radius of electron impact on the anode foil. This confirms the ability of the shank J_θ to radially direct the $A-K$ gap electron flow. Still, the anode foil area illuminated by the electrons is rather narrow and most electrons appear to transit immediately to the solid anode surface in the rear without reflexing again through the foil. This tightly restricted nature of the electron flow and resultant ion flow is illustrated by the plots in Figure 11. These radial profiles of ion current density collected at the cathode show distinct regions of enhancement. All three curves show peaks near the central axis due to the strong flow of tightly pinched electrons emitted from the rear cathode foil surface inside the shank. All three likewise have peaks between R = 4 cm and R = 5 cm corresponding to ions collected by the protruding cathode shank. However, in terms of net ion current collected at the various radii, the J_θ = 4 kA/cm^2 profile indicates that most of the ion current is flowing in a hollow cylindrical shell. This capability to shape the ion current density emerging from the diode may prove useful for future applications. Unfortunately it is clear that whatever other benefits $(J_\theta)_{shank}$ may offer for the AURORA diode, an improvement in ion production efficiency does not appear to be among them.

2. PBFA-I

Much of the on-site experimental effort of the NRL Light Ion Fusion Group has been dedicated to the design of an ion-efficient, 3-5 Ω diode for use on individual modules of the PBFA-I pulse power

generator at Sandia National Laboratories. This work has been conducted on the GAMBLE-II machine at NRL.[28] A typical diode configuration used in that research is illustrated in Figure 12. The outer radius of the cathode shank was 3 cm while its thickness varied between 4 and 8 mm. An $A-K$ gap of approximately 5 mm was maintained although electrode plasma expansion gap closure at a normal rate of 3 cm/μsec over the 40 ns power pulse probably created an effective $A-K$ gap of 3.8 mm. The effective diode voltage was about 1.8 MV. For these parameters and a gap of 5 mm, Eqs. (1) and (2) predict an impedance of 7.1 ohms and an ion efficiency, η_i, of 0.186. An effective gap of 3.8 mm changes these to 5.1 ohms and $\eta_i = 0.245$ respectively. Experimentally, the diode ran at from 3 to 5 ohms and achieved 0.25 to 0.35 ion efficiencies in 40% of the shots (see Figure 13). The theoretical predictions using $D_0 = 3.8$ mm were quite close. Numerical simulations were conducted for a similar 4 ohm diode at 1.8 MV and a η_i of about 0.40 was observed.[29] Therefore, theory, experiment, and numerical simulation all call for between 0.25 and 0.40 ion efficiency.

To numerically test the effects of a shank J_θ on diode performance in this lower impedance regime of 3-5 ohms, the same model diode as that used for the AURORA simulations (see Figure 4) was employed except that the voltage was lowered to 2 MV and D_K, D_0, and D_A were set equal to 0.60., 0.66, and 0.57 cm respectively. For those parameters, theory predicts 4.9-ohm operation and an η_i of at least 0.247. The experimental and numerical results from the actual GAMBLE-II diode would indicate that those predictions are pessimistic. The computational results which follow will use the numerical run cited in the previous paragraph as a $J_\theta = 0$ "benchmark."

The total simulation was run in such a way as to sequentially test the following cases: (a) $J_\theta = 0$ with only electrons, (b) $J_\theta = 2$ kA/cm^2 with only electrons, (c) $J_\theta = 2$ kA/cm^2 with ions and electrons, and (d) $J_\theta = 4$ kA/cm^2 with ions and electrons. The traces of the electron and ion currents collected by the opposing electrodes during this run are plotted in Figure 14. The near-steady state at $T = 400$ for electron flow in the $J_\theta = 0$ case was used as the starting point for the imposed J_θ tests. This azimuthal current density was again imposed on the numerical mesh points in the rectangular cathode shank cross-section extending from $IZ = 6$ through $IZ = 21$ and from $IR = 18$ through $IR = 21$.

With the new axial grid spacing of $\Delta Z = 0.03$ cm, this amounts to an area of 0.48 cm^2. The first test case, with $J_w = 2$ kA/cm^2, therefore amounts to a net azimuthal current of 0.96 kA. This shank current component was "turned on" at $T = 400$. At $T = 600$, ion emission was initiated along the front anode surface. The test for this particular value of J_w was terminated at $T = 1200$, well before a steady state had been achieved. The reason for the early termination was the poor development of the electron flow pattern in the diode. This is illustrated by the sequence of sample electron position snapshots shown in Figure 15. The first shot depicts the electrons-only flow for $J_a = 0$ at $T = 400$. A substantial amount of reflexing through the anode foil is apparent as is a significant loss of electrons directly to the solid anode surface behind the foil. A stream of electrons emitted from the recessed cathode foil inside the shank can also be seen. Note that the electron mainstream initially impacts the anode foil almost exactly opposite the cathode shank face (i.e.-between 4.0 and 5.0 cm in radius). The electrons-only flow with $J_a = 2$ kA/cm^2 in the second shot of the series embodies the same electron flow characteristics as the $J_a = 0$ case but with significantly more radial pinching. Few electrons are impacting the anode foil opposite the shank face. In fact, a distinct gap has opened in the flow above a radius of 4.2 cm within a millimeter of the foil surface. Finally, in the last of the three segments of Figure 15, the electron flow is shown at a time when the main ion flow has traveled about halfway toward the recessed cathode foil. Only the anode foil below 3.0 cm in radius is being illuminated by electron impacts. This translates to no enhancement of ion emission over the large anode foil areas at larger radii.

In order to remedy the electron flow pattern problem, the beneficial effects of elevated J_a are recalled (see Figure 9). At $T = 1200$, the azimuthal shank current density was doubled to 4.0 kA/cm^2. When equilibrium was reached at $T = 2600$, the sample electron and ion flow appeared as shown in Figure 16. There is a definite improvement of anode illumination by electrons compared with the $J_a = 2$ kA/cm^2 case as indicated by Figure 17 which provides radial profiles of accumulated numbers of electron hits (not necessarily absorptions) across the face of the anode foil. The numbers given are relative and may be normalized to the total electron current in each case if so desired. For the purposes of this comparison, take I_e to be the same for each case. The $J_a = 4$ kA/cm^2 profile yields the most sharply

peaked hollow electron beam at the highest mean radius. The sharpness of the profile is not unlike that observed in hollow cathode diodes having strong applied axial magnetic fields.[30] The equilibrium total currents were I_e = 322 kA and I_i = 232 kA yielding an impedance of 3.6 ohms and an ion production efficiency of 0.42 compared to the J_θ = 0 benchmark of 4.0 ohms and η_i = 0.40.

The observed gain in net ion efficiency of 0.02 is insignificant, especially when taken in combination with the 0.4 ohm drop in diode impedance. There is a difference, however, between the total ion current flowing in a diode and the net ion current which can be extracted from a diode through the hollow cathode shank. Only the latter is useful from a practical, experimental standpoint. This distinction is crucial in judging the merits of the *J*-theta diode. Plotted in Figure 18 are the radial profiles of ion current density striking the cathode for both the J_θ = 0 case (a $1/r$ profile with a central plateau corresponding to the location of the anode foil support button) and for the J_θ = 4 kA/cm^2 case. For J_θ = 0, a full 22% of the total ion current is lost to the cathode shank. This reduces the *effective* ratio of useful (extractable) ion current to total diode current to 0.31, in good agreement with the previously mentioned experimental observation of 0.25 to 0.35 ion efficiencies in 40% of the 4Ω shots actually conducted on GAMBLE-II. In comparison, for J_θ = 4 kA/cm^2, only 11% of the total ion current is lost to the shank, leaving an *effective* ion efficiency of 0.374. This amounts to an improvement of over 20% in $(\eta_i)_{\text{effective}}$ and thereby recommends this J_θ-diode for experimental testing on GAMBLE-II for possible use on PBFA.

In addition to this favorable result regarding enhanced effective ion production, several other results merit mention. Comparison of Figure 18 to the corresponding AURORA J_i profiles of Figure 11 show a hollowing of the ion beam. The central axis current density peak dissappears. Since shank electrons with their finite angular momentum cannot reach R = 0, this indicates that significantly more electrons are being emitted from the recessed cathode foil on the AURORA diode. These *can* reach R = 0 and enhance ion emission there. Another difference between the two impedance regimes is the nature of the cathode shank electron flow. On AURORA, the imposition of J_θ actually enhanced electron emission on the shank by lifting the flow away from the surface. This phenomenon does not man-

ifest itself in the 4Ω runs. Finally, there was some question whether any actual magnetic insulation of the electron flow from the anode foil was taking place. The answer was obtained by measuring the strength of the radial component of the magnetic field one-half data cell (0.015 cm) from the magnetic-flux-excluding surface of the anode foil. Figure 19 shows that, as expected, very high fields are to be found over large areas of the foil. This is typical of the diamagnetic field enhancement observed in magnetically insulated radial diodes.[31]

IV. CONCLUSIONS

The major results of all of the above computer simulations are summarized in Table 1. The imposition of a relatively small azimuthal current in the hollow cathode shank of a 4-ohm axial diode has been numerically shown to increase the *effective* ion production efficiency of the diode by over 20%. This positive result recommends the further study of the new concept both theoretically and experimentally. Additional simulations should be conducted to examine diode equilibria for other values of J_θ. Experimentally, an actual J_θ-diode has been constructed as shown in Figure 20. Its cathode shank is approximately six centimeters in diameter with 48 slots 3/8 inch deep, 0.045 inch wide, and angled at 20° cut around its periphery in order to generate a J_θ by spiraling the current flowing through the shank. Three shots were conducted using this diode on GAMBLE-II but diagnostic difficulties prevented the gathering of enough useful information for proper evaluation. Additional shots will be attempted as circumstances permit.

For diodes with impedances in the neighborhood of twenty ohms, no evidence of ion efficiency boosting via a shank J_θ has been obtained. However, even for that case the azimuthal current component does significantly modify the radial profile of the extractable ion current density. Such a capability to change the shape of the ion beam which emerges from the diode may prove useful in the future for optimizing this beam for transport away from the diode through plasma channels.

ACKNOWLEDGMENTS

THe authors are indebted to R.A. Meger and S.J. Stephanakis for their valuable assistance in the preparation of this report.

JDT REFERENCES

1. G. Cooperstein, S.A. Goldstein, D. Mosher, and R.J. Barker, et al., NRL Memo Report 4387 (1980).

2. D.J. Johnson, G.W. Kuswa, A.V. Farnsworth, Jr., and J.P. Quinteny, et al., Phys. Rev. Lett. 42, 610 (1979).

3. G. Cooperstein, S.A. Goldstein, and D. Mosher, et al., in Proceedings 3rd International Topical Conference on High Power Electron and Ion Beam Research and Technology, Novosibirsk, USSR (1979).

4. D.J. Johnson, Bull. Am. Phys. Soc. 24, 925 (1979).

5. S.J. Stephanakis, J.R. Boller, G. Cooperstein, S.A. Goldstein, D.D. Himshelwood, D. Mosher, W.F. Oliphant, F. Sandel, and F.C. Young, Bull. Am. Phys. Soc. 23, 907 (1978).

6. D.G. Colombant, S.A. Goldstein, and D. Mosher, Phys. Rev. Lett. 45, 1253 (1980).

7. R.A. Meger, F.C. Young, G. Cooperstein, S.A. Goldstein, and D. Mosher, NRL Memo Report 4477 (1981).

8. D.J. Johnson, S.A. Goldstein, R. Lee, and W.F. Oliphant, J. Appl. Phys. 49, 4634 (1978).

9. S.A. Goldstein and R. Lee, Phys Rev. Lett. 35, 1079 (1975).

10. S.A. Goldstein, R.C. Davidson, J.G. Siambis, and R. Lee, Phys. Rev. Lett. 33, 1471 (1974).

11. D.P. Bacon, S.A. Goldstein, R. Lee, and G. Cooperstein, NRL Memo Report 4326 (1980).

12. M.M. Widner, J.W. Poukey, and J.A. Halbleib, Sr., Phys. Rev. Lett. 38, 548 (1977).

13. J.W. Shearer, Lawrence Livermore Lab Report UCRL-52129 (1976).

14. R.J. Barker and P.F. Ottinger, NRL Memo Report 4654 (1981).

15. R.J. Barker and S.A. Goldstein, to appear as an NRL Memo Report (1981).

16. R.J. Barker and S.A. Goldstein, Bull. Am. Phys. Soc. 25, 900 (1980).

17 Suggested independently for other applications by F. Sandel in 1978.

18. S.A. Goldstein, J. Appl. Phys. 47, 894 (1976).

19. A.E. Blaugrund, G. Cooperstein, and S.A. Goldstein, Phys. Fluids 20, 1185 (1977).

20. D. Mosher, Bull. Am. Phys. Soc. 25, No. 8 (1980).

21. J.W. Poukey, J.R. Freeman, and G. Yonas, J. Vac. Sci. Technol. 10, 954 (1973).

22. S. Humphries, Jr., Plasma Physics 19, 399 (1977).

23. R.J. Barker, A.T. Drobot, R. Lee, and S.A. Goldstein, Proc. 9th Conf. on the Numerical Simulation of Plasmas, Evanston, Ill. (1980).

24. R.A. Meger, A.T. Drobot, S.A. Goldstein, and F.C. Young, Bull. Am. Phys. Soc. 25, 900 (1980).

25. F.C. Young and R.A. Meger, et al., Bull. Am. Phys. Soc. 25, 899 (1980).

26. R.J. Barker, Banach Center Publications 3, 255, Warsaw, Poland (1975).

27. R.A. Meger, F.C. Young, and A.T. Drobot, et al., NRL Memo Report 4477 (1981) and J. Appl. Phys. 52, 6084 (1981).

28. S.J. Stephanakis, S.A. Goldstein, D. Mosher, and W.F. Oliphant, Bull. Am. Phys. Soc. 25, 900 (1980).

29. A.T. Drobot, private communication.

30. R.J. Barker, S.A. Goldstein, and R.E. Lee, NRL Memo Report 4279 (1980).

31. R.J. Barker, S.A. Goldstein, and A.T. Drobot, Proc. IEEE Conf. on Plasma Science, Madison, Wisc. (1980).

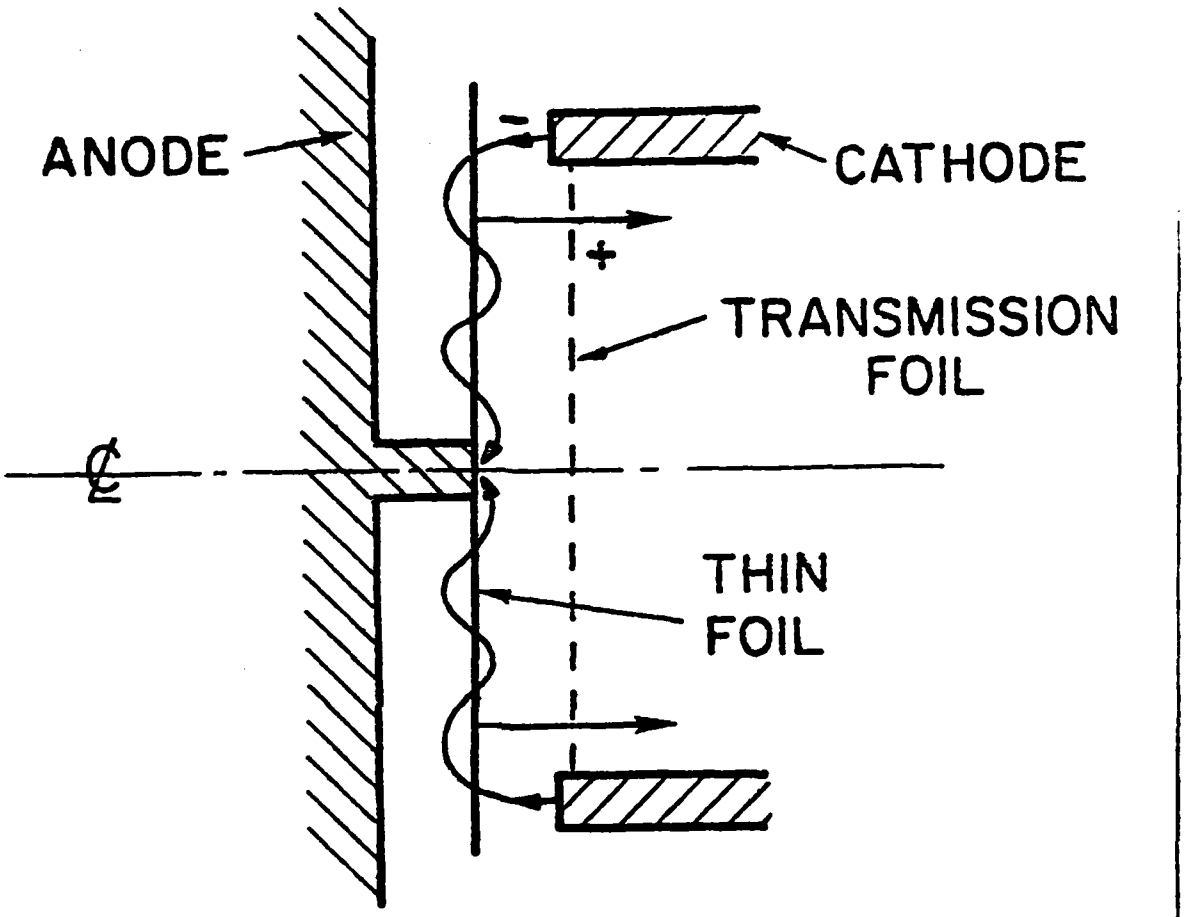

Figure 1. The Pinch-Reflex Diode.

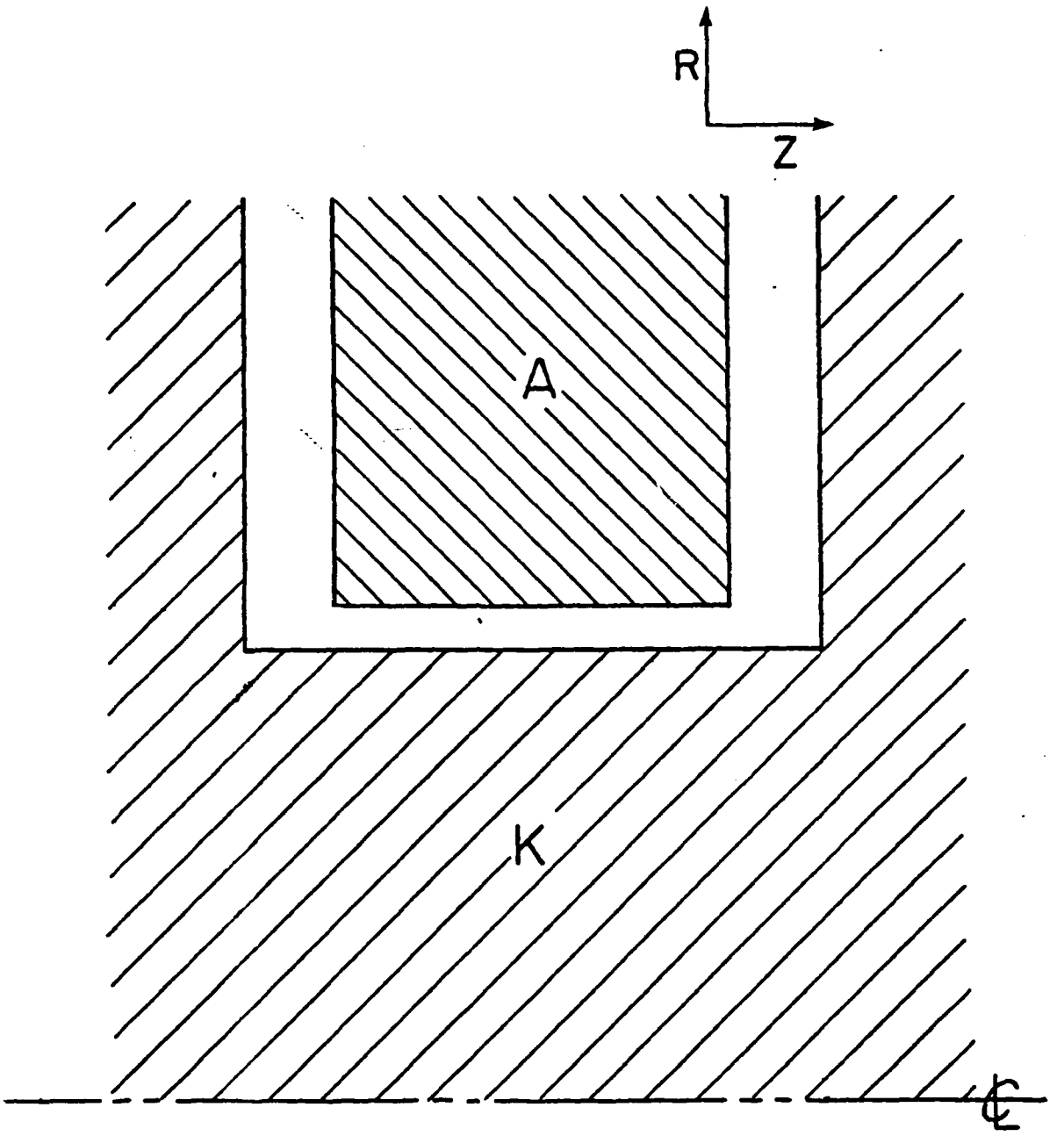

Figure 2. Schematic of a Radial Diode.

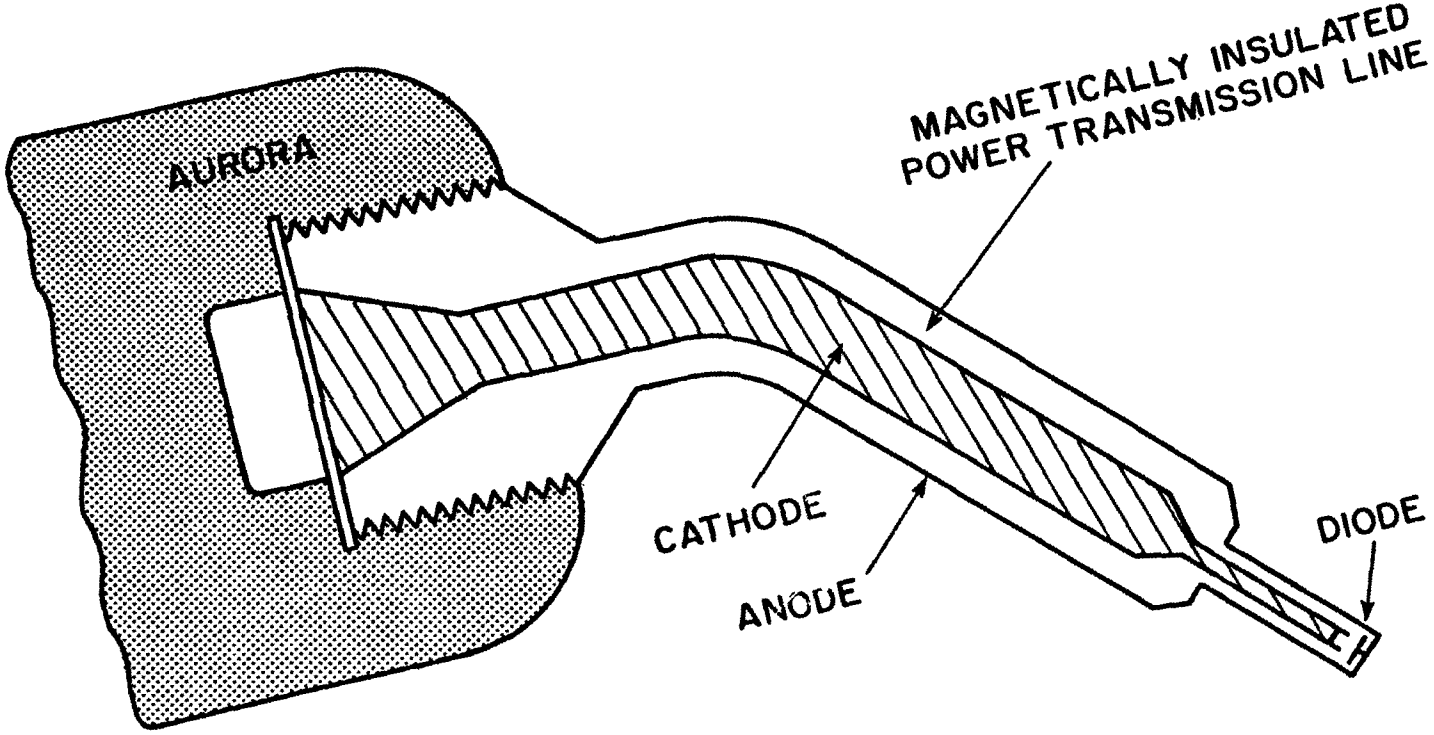

Figure 3. The NRL-AURORA Ion Diode Experiment.

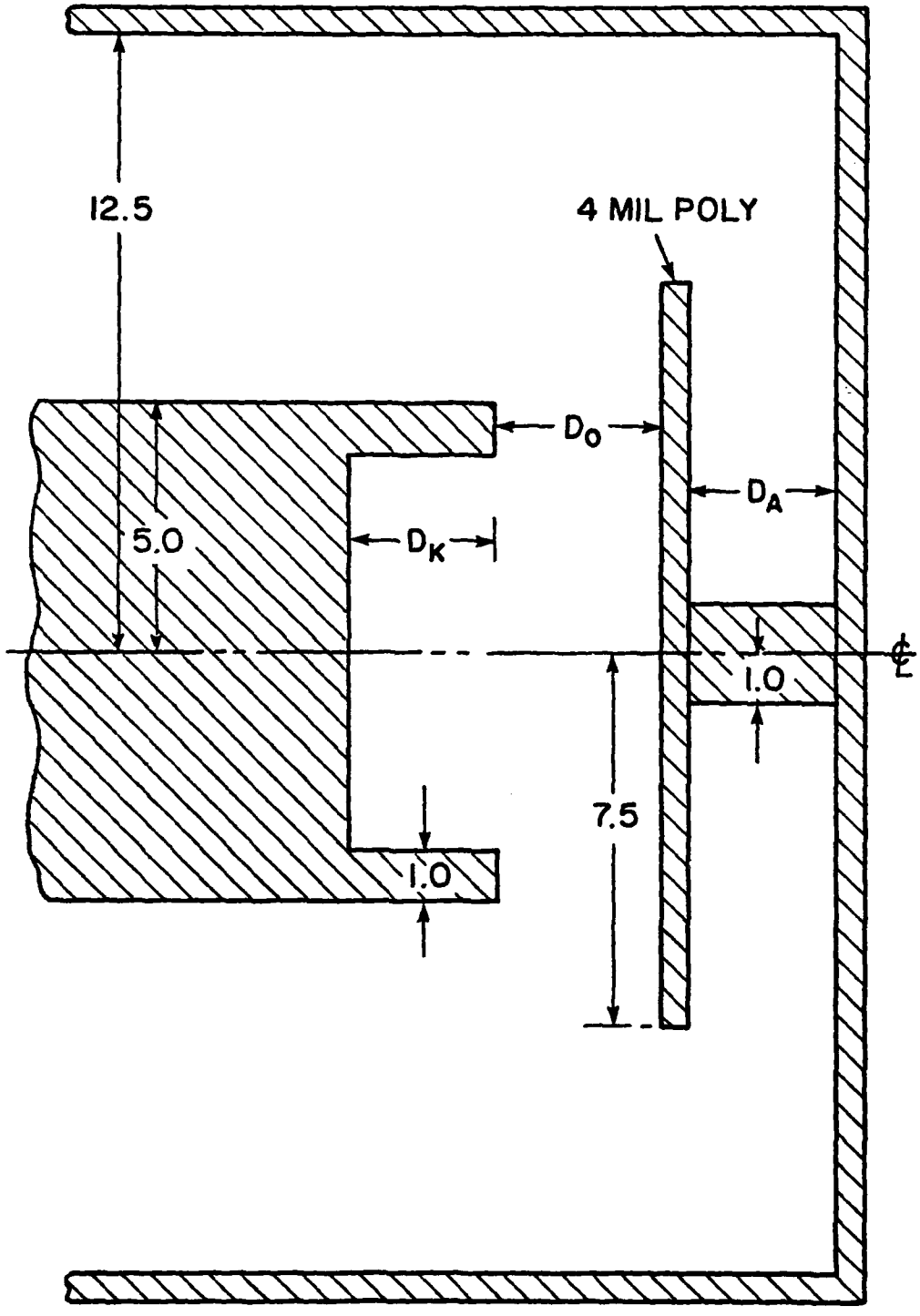

Figure 4. The Diode to be Modeled.

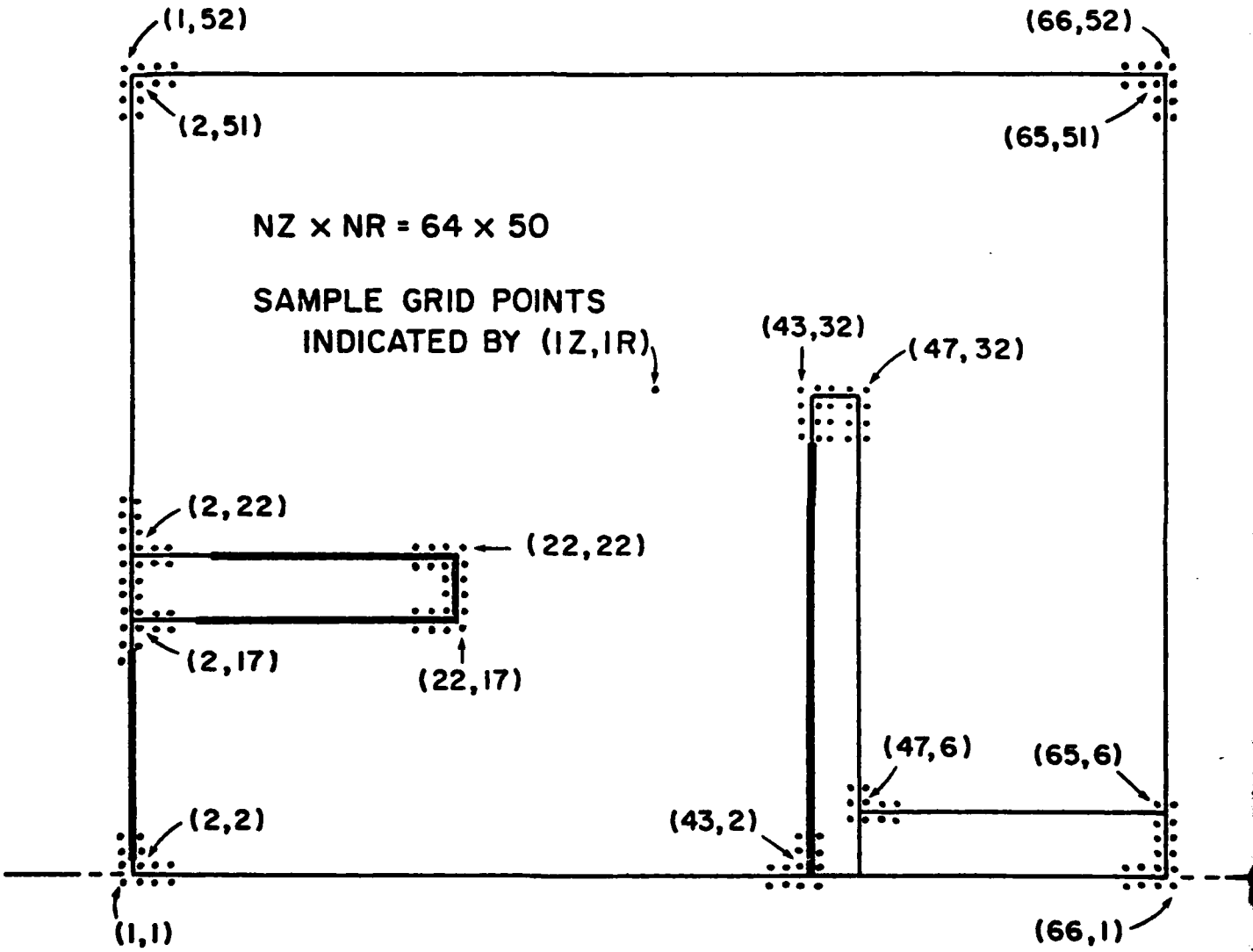

Figure 5. Set-up of the Numerical Simulation Region.

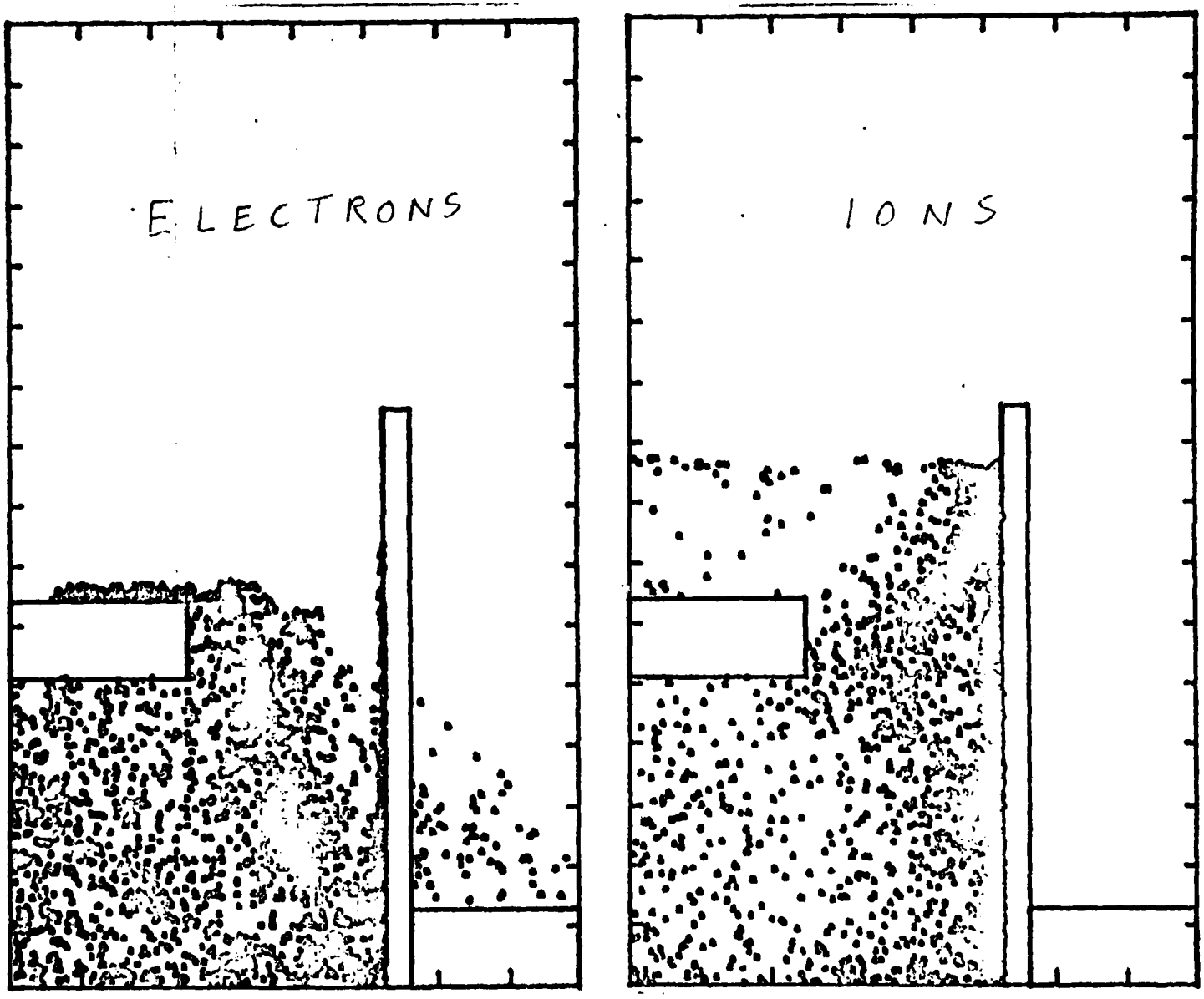

Figure 6. AURORA Electron and Ion Flow for $J_\theta = 0$.

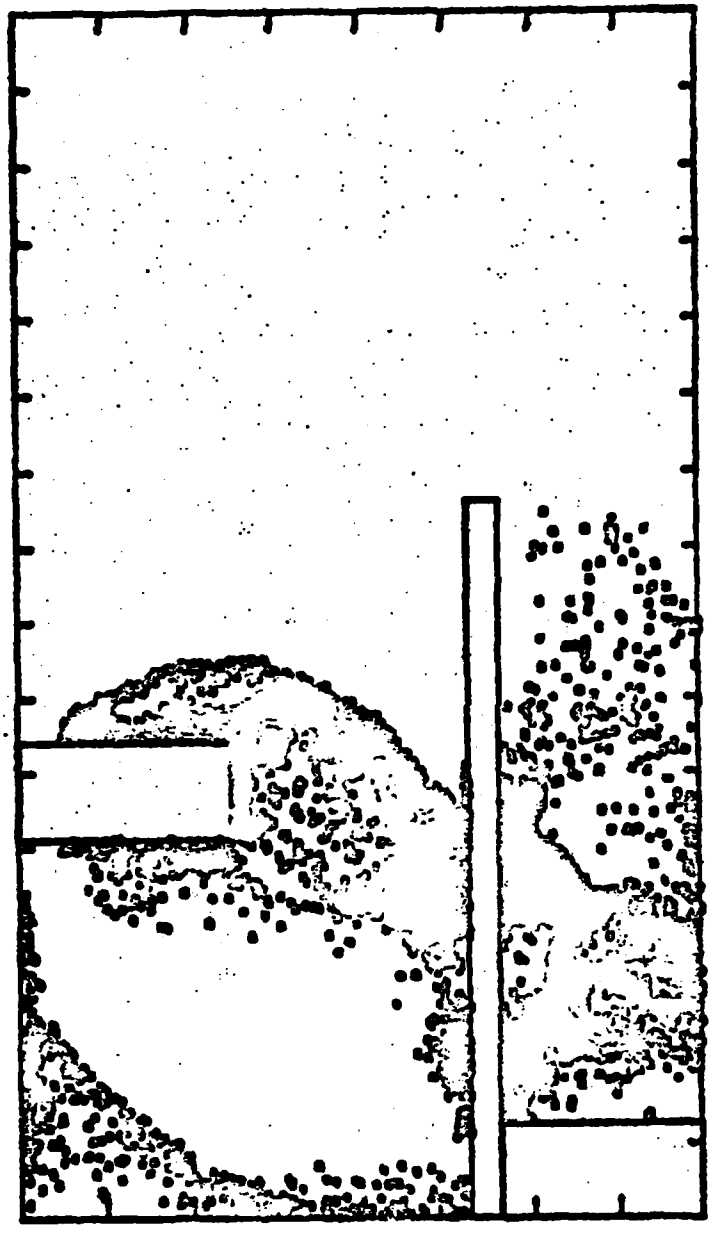

Figure 7. AURORA Electrons-only Flow for J_θ= 1 kA/cm^2.

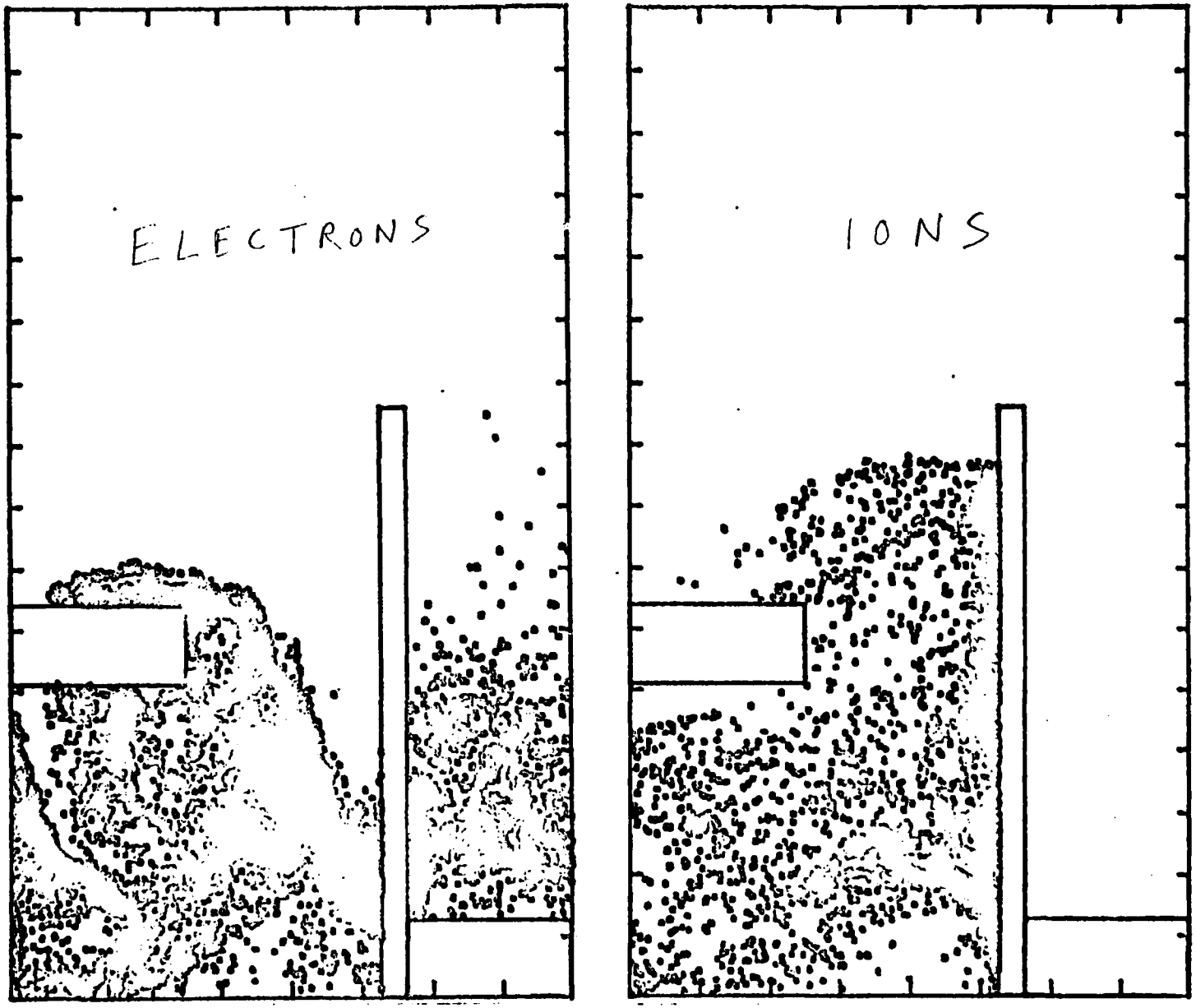

Figure 8. AURORA Electron and Ion Flow for J_θ= 1 kA/cm^2.

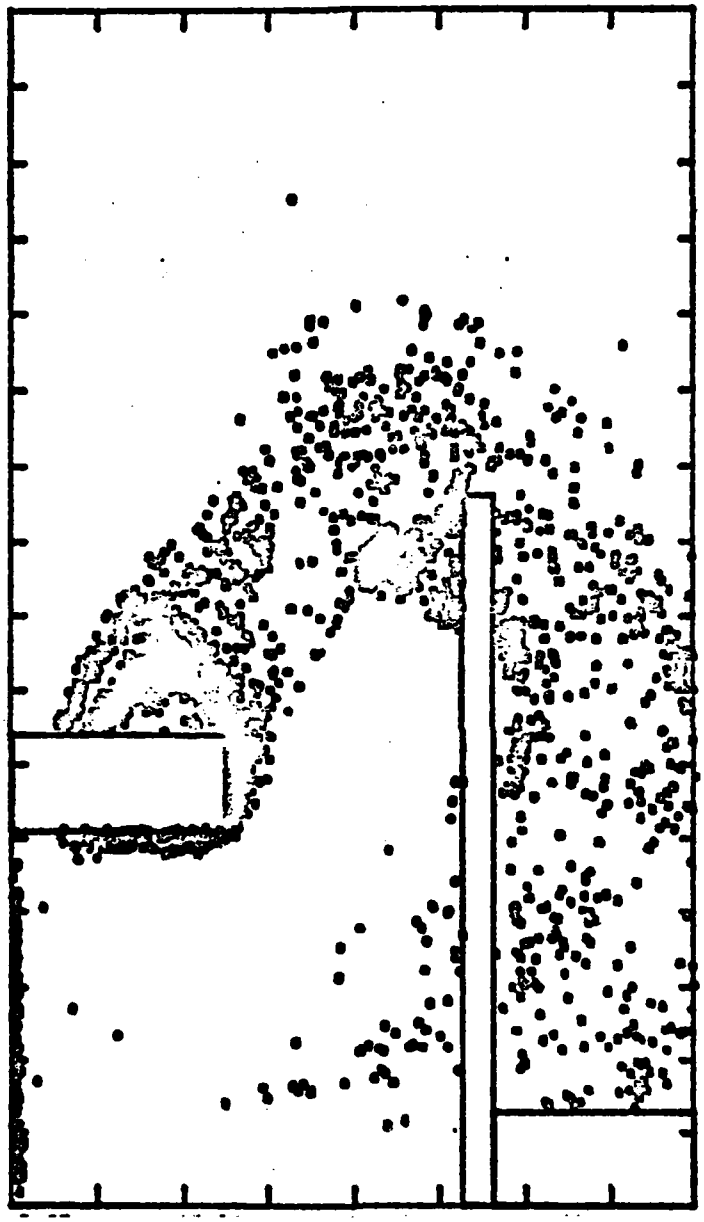

Figure 9. AURORA Electrons-only Flow for J_θ= 10 kA/cm^2.

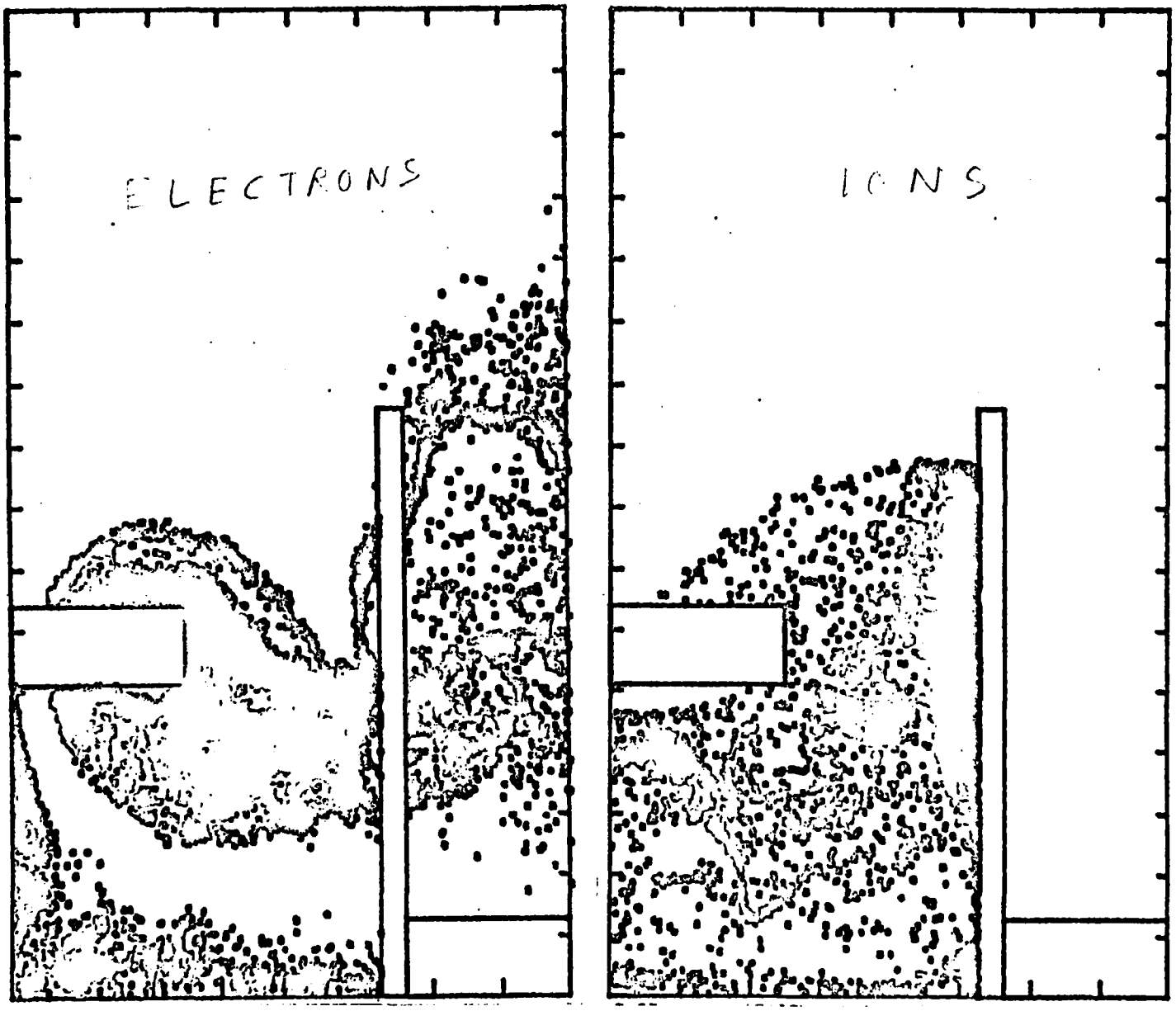

Figure 10. AURORA Electron and Ion Flow for J_θ= 4 kA/cm^2.

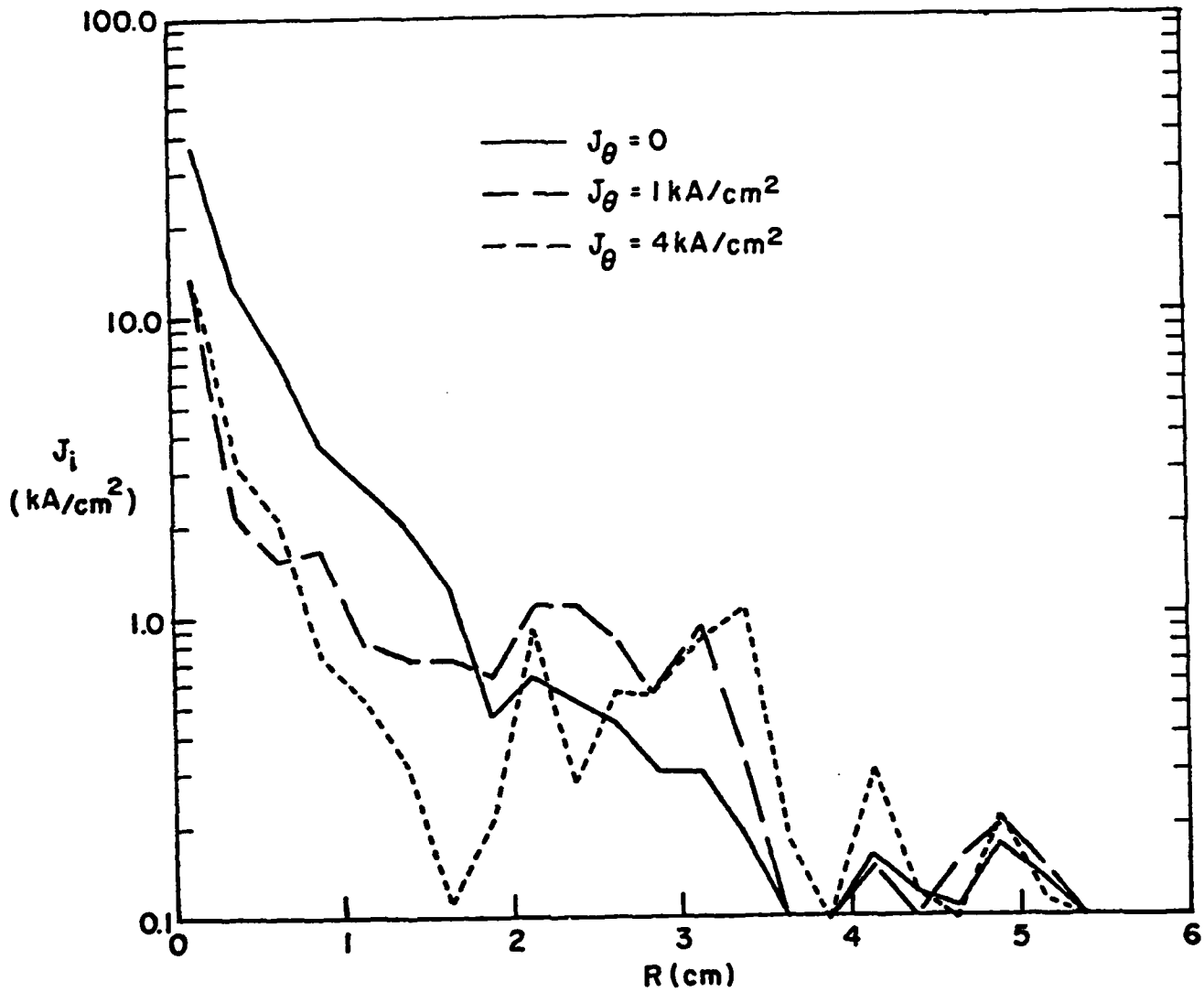

Figure 11. Radial Profiles of AURORA Ion Current Density Collected at the Cathode.

HIGH-Z DIODE

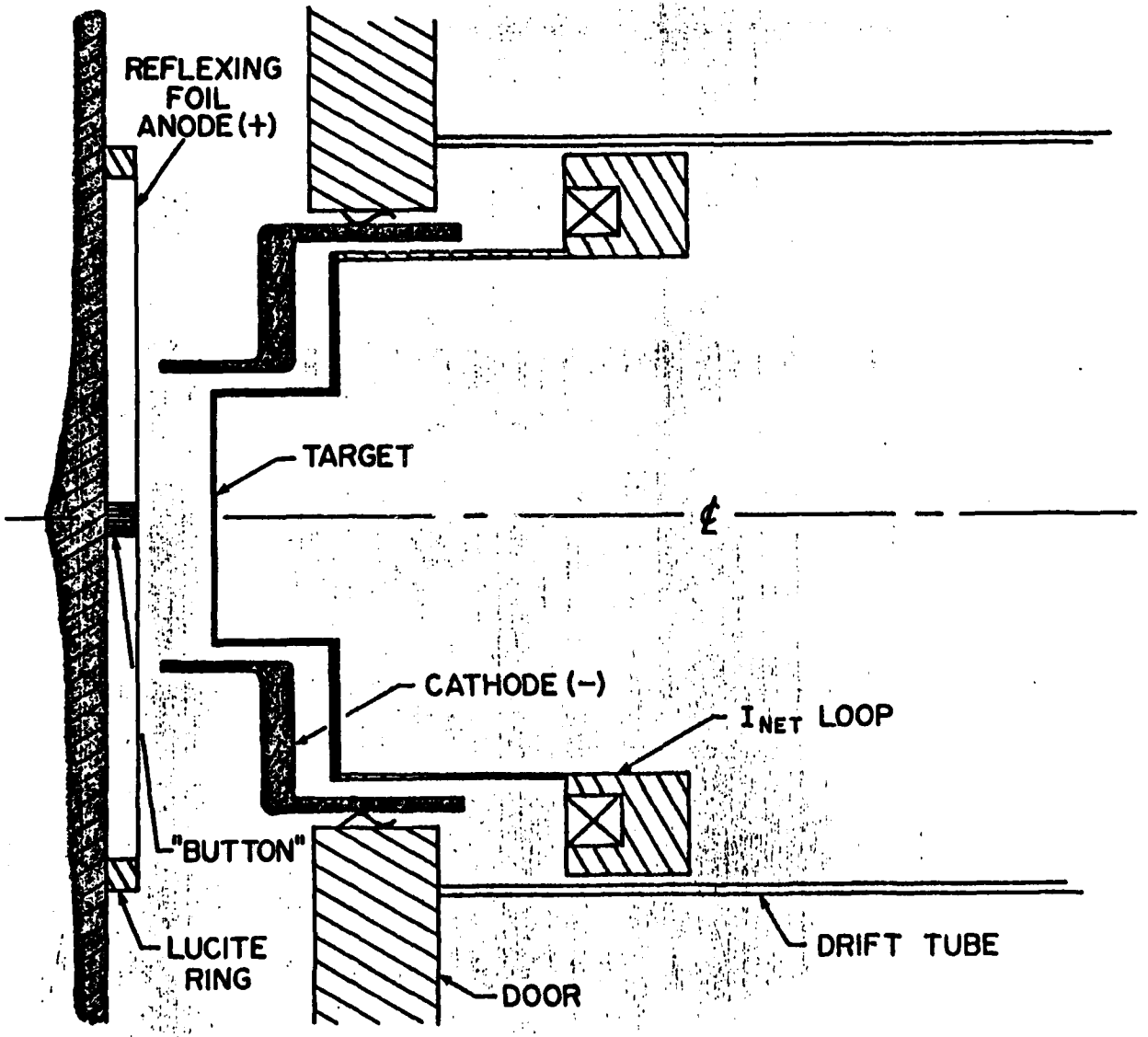

Figure 12. The High Impedance Gamble II Test Diode for PBFA-I (Courtesy of S.J. Stefanakis and D. Mosher).

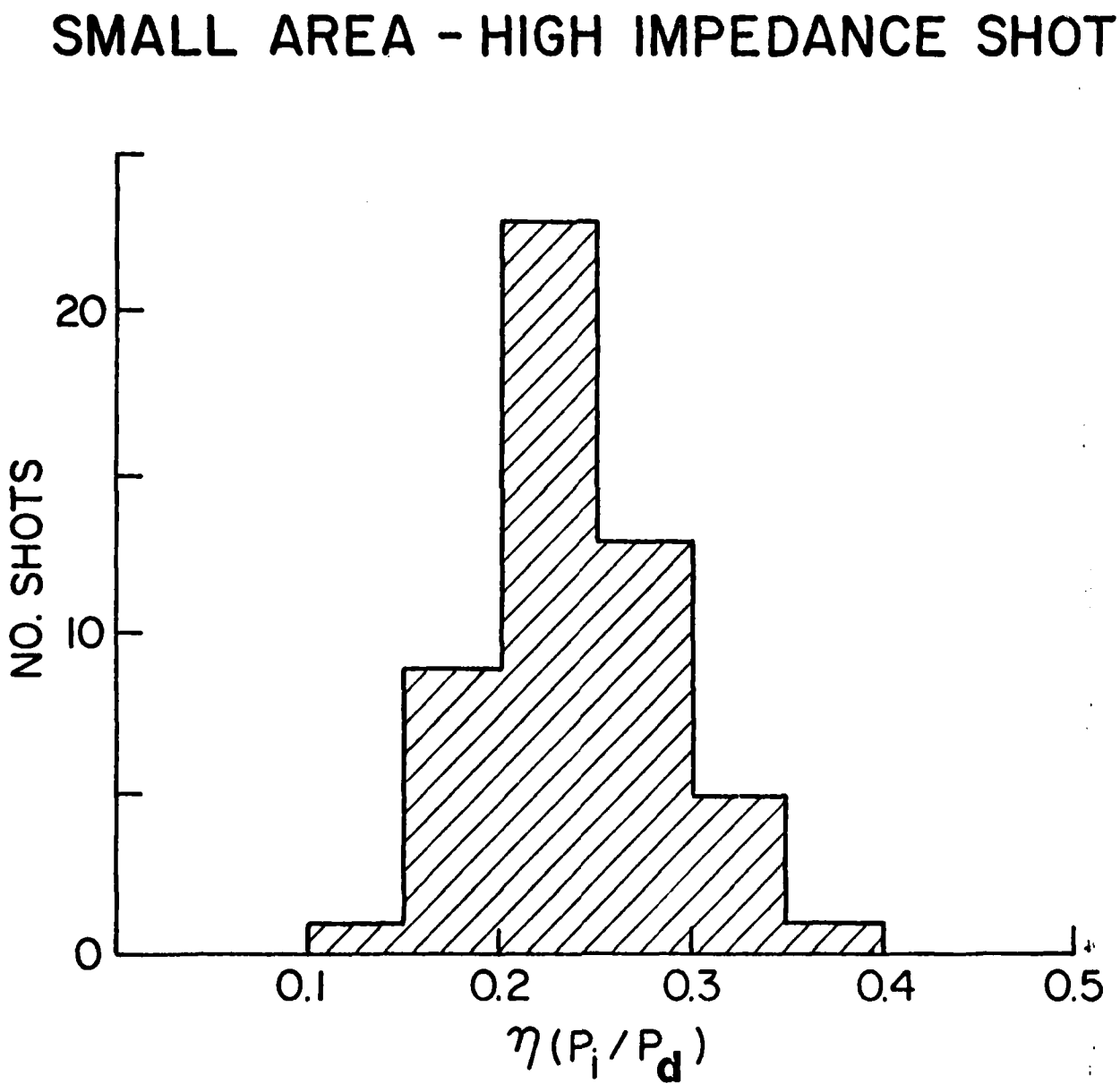

Figure 13. Statistical Distribution of η_i for the 4 Diode. (Courtesy of S.J. Stefanakis).

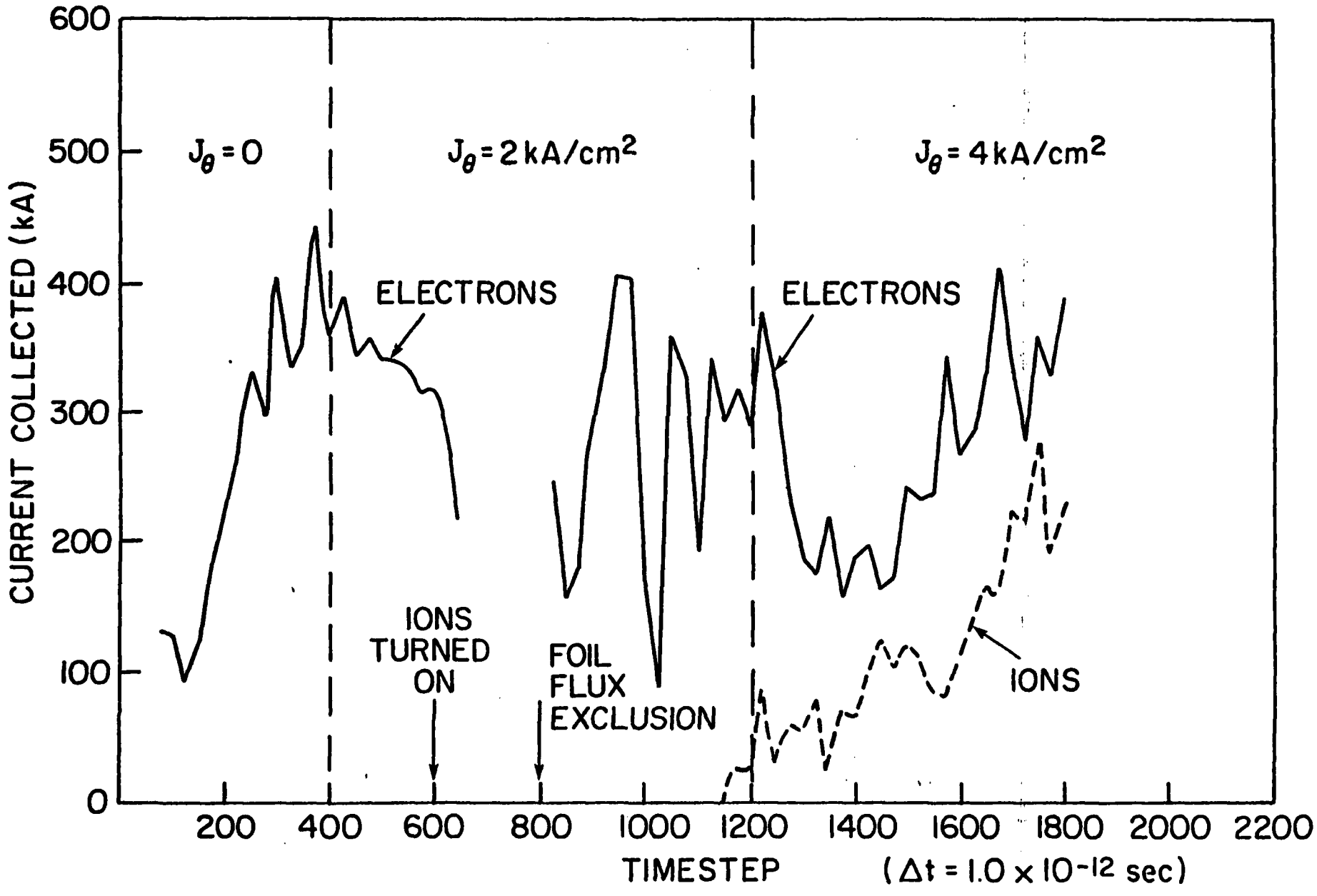

Figure 14. Temporal Traces of Collected Electron and Ion Currents from the PBFA-I Diode Simulation.

Figure 15. Comparison of PBFA-I Electron Flow Patterns.

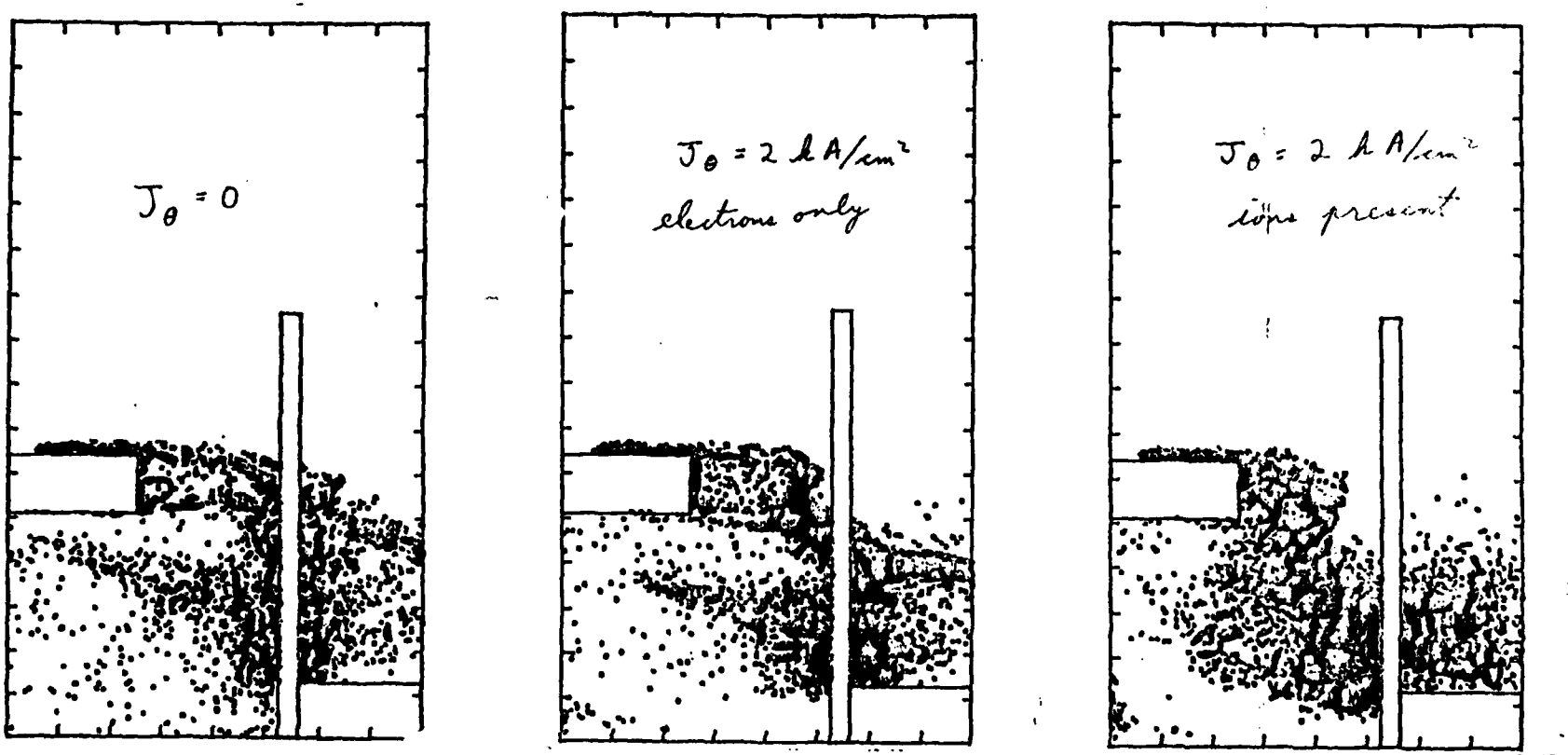

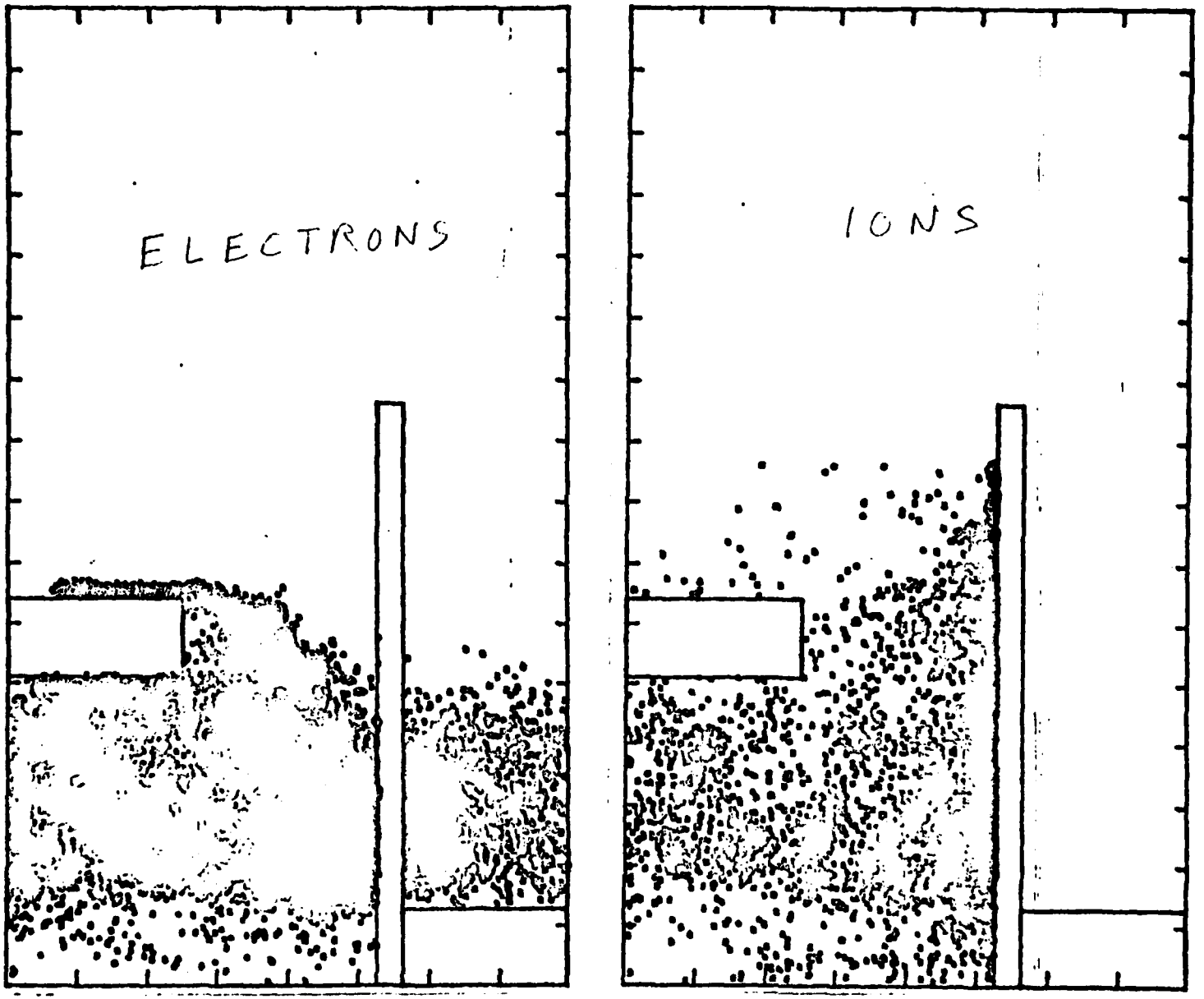

Figure 16. PBFA-I Electron and Ion Flow for J_θ= 4 kA/cm^2.

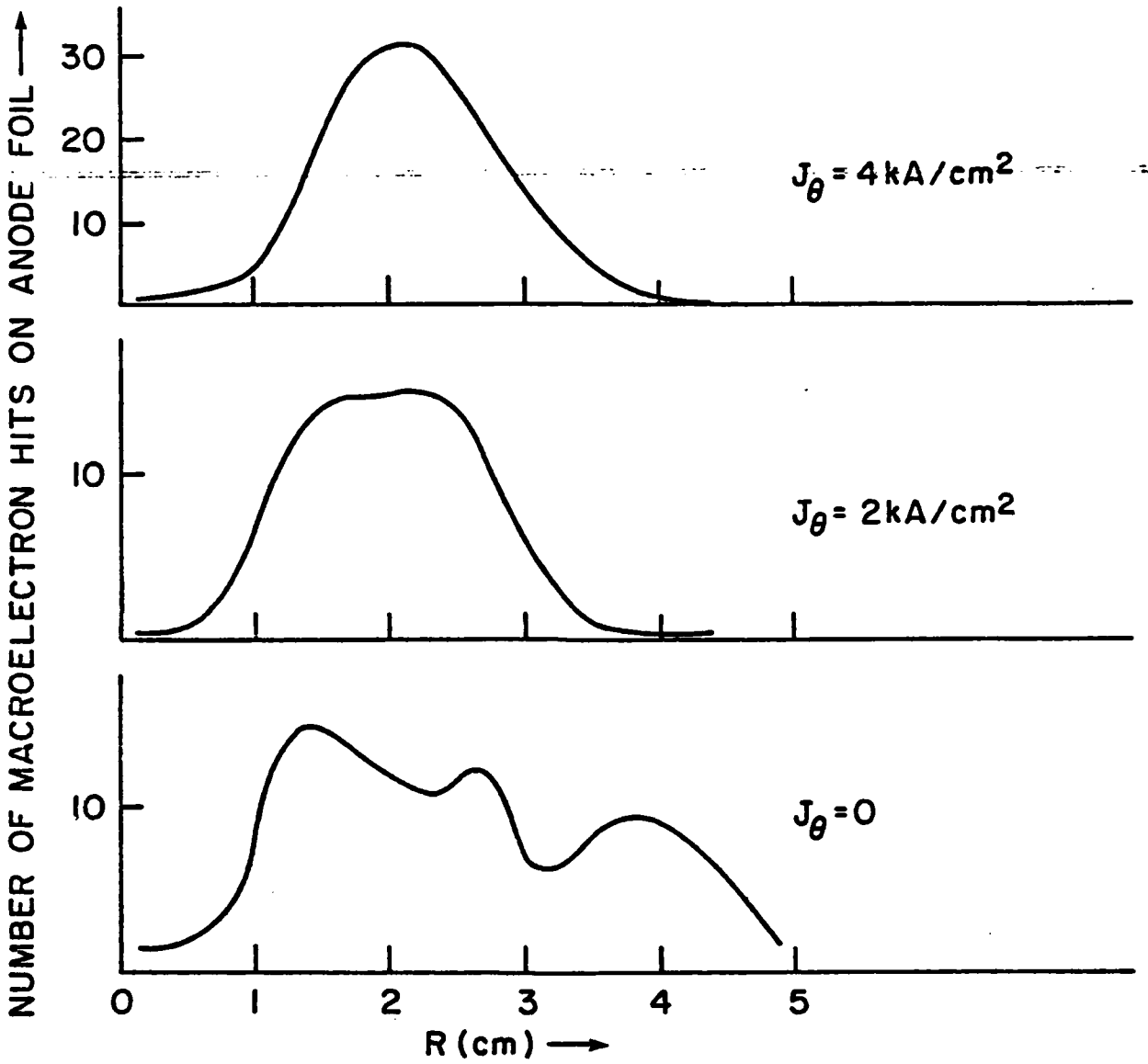

Figure 17. Comparitive Radial Profiles of Electron Impacts on PBFA-I Anode Foil.

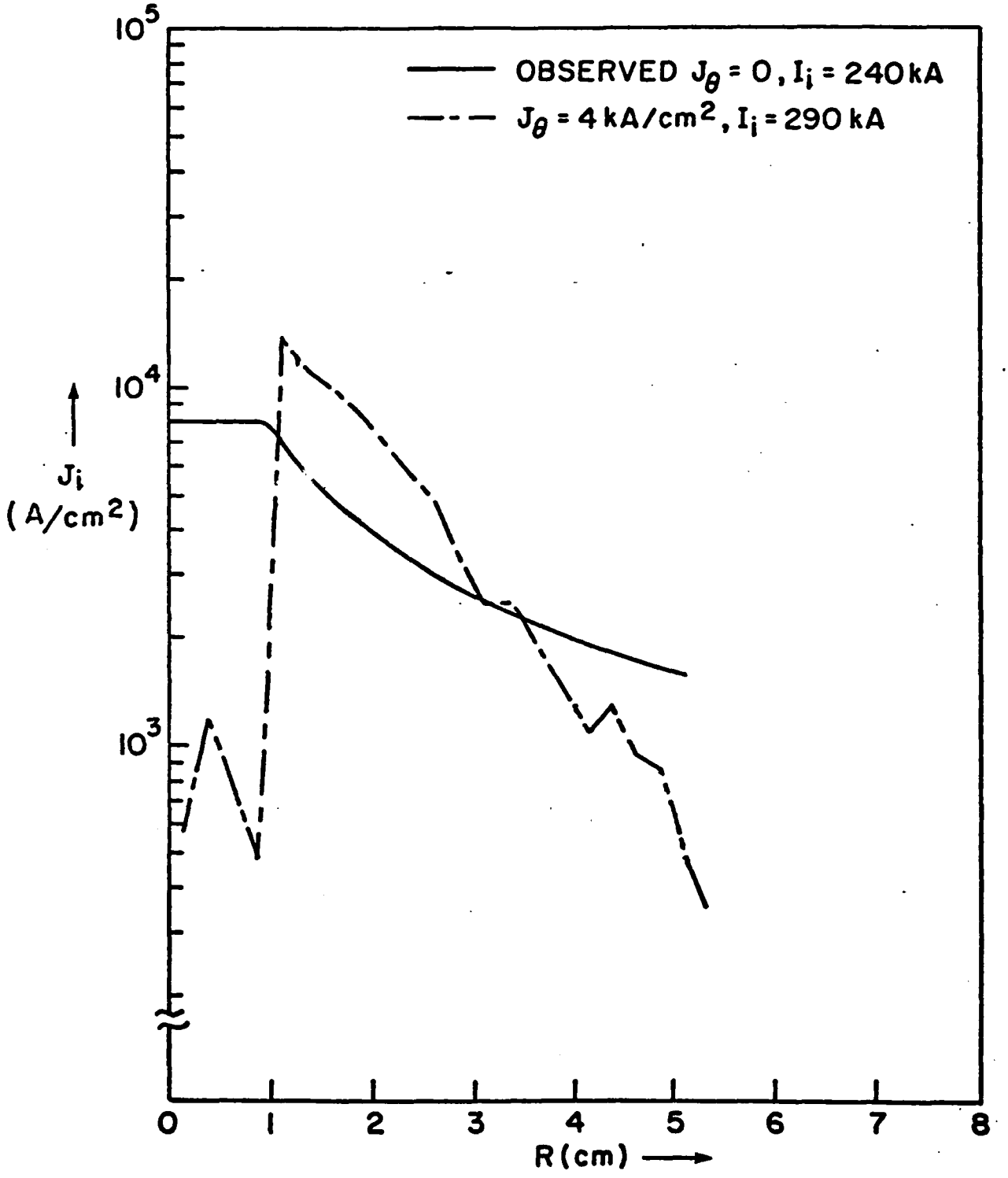

Figure 18. Radial Profiles of PBFA-I Ion Current Density.

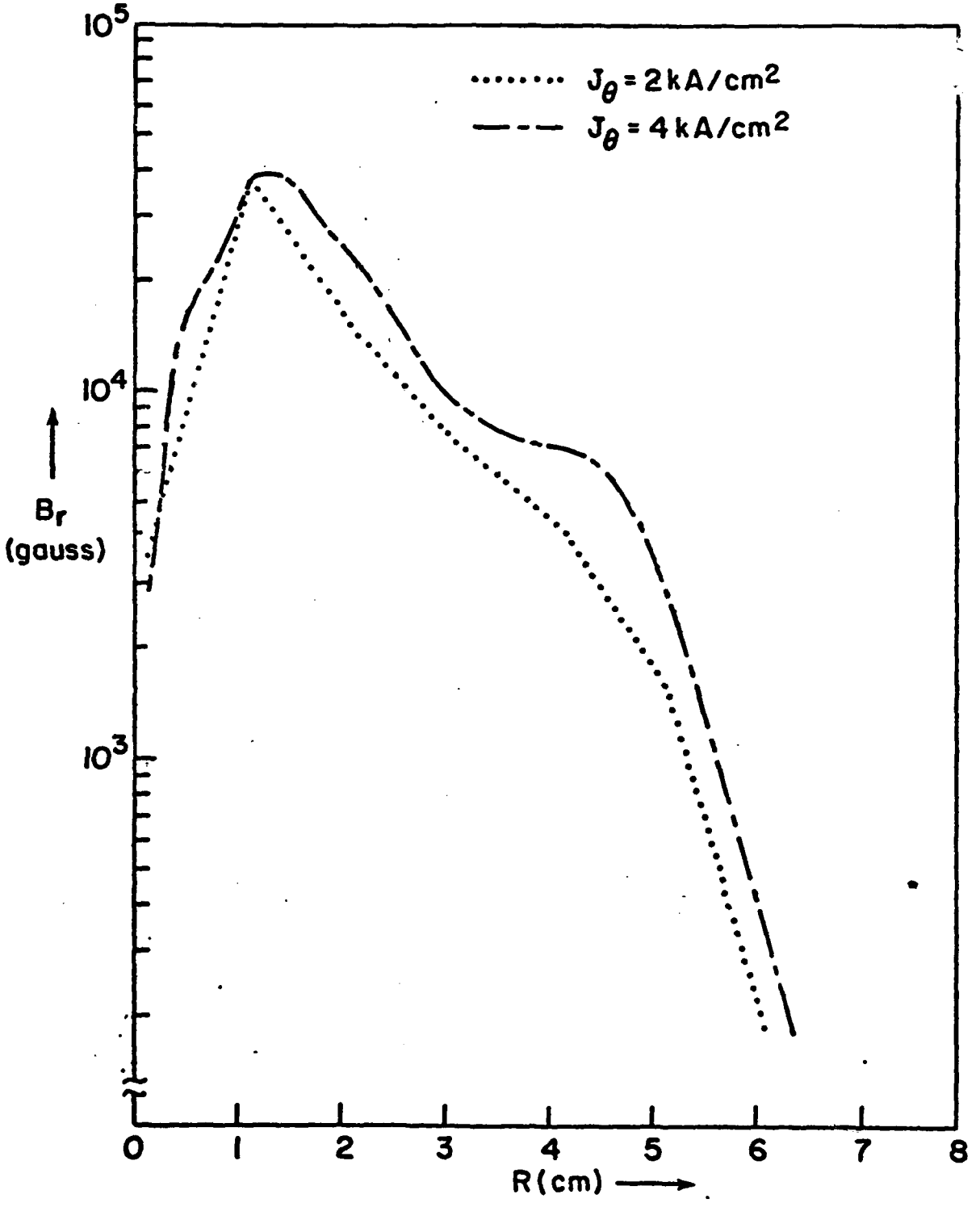

Figure 19. Radial Profiles of B_r near PBFA-I Anode Foil.

Figure 20. The Experimental J-Theta Diode (JTD) for Testing on Gamble-II.

	AURORA (5 MV)				PBFA (2 MV)	
J_θ (kA/cm^2)	0 ($^{neg.}_{pol.}$)	0 ($^{pos.}_{pol.}$)	1	4	0	4
I_e (kA)	165	182	244	257	300	322
I_i (kA)	40	56	41	34	200	232
$(I_i)_{eff}$ (kA)	35	50	35	30	150	207
I_{diode} (kA)	205	238	285	291	500	555
Z (ohms)	24.4	21.0	17.5	17.2	4.0	3.6
η_i	0.195	0.235	0.144	0.117	0.40	0.42
$(\eta_i)_{eff}$	0.171	0.210	0.123	0.103	0.30	0.37

Table 1. Summary of Major Results.

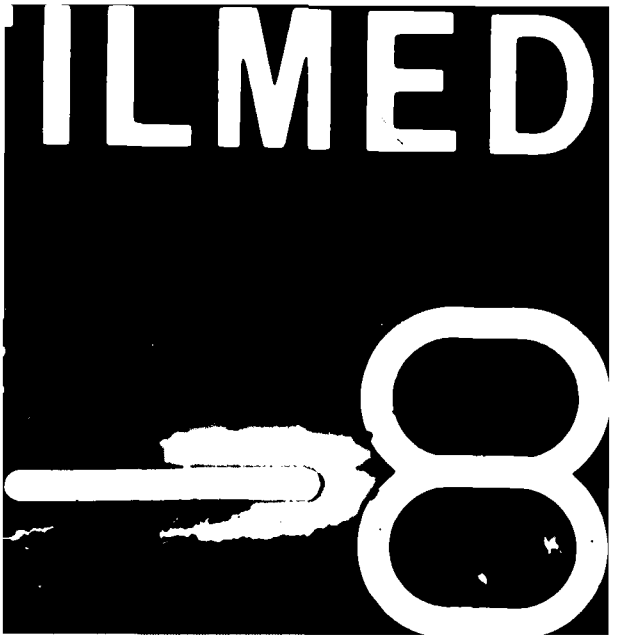
ILMED
8